Aalto University
School of Electrical Engineering

Aalto University
School of Electrical Engineering
Doctoral Programme in Electrical Engineering

Sari Sirviö

Characterization of Atomic Layer Deposited Thin Films: Conformality in High Aspect Ratio Pores and the Electrical Properties of Capacitors

Thesis for the degree of Licentiate of Science in Technology submitted for inspection, Espoo, 20th of September, 2014.

Supervising professor Professor Pekka Kuivalainen

Thesis advisor Professor Sami Franssila

Aalto University

AALTO UNIVERSITY SCHOOLS OF TECHNOLOGY PO Box 11000, FI-00076 AALTO http://www.aalto.fi	ABSTRACT OF THE LICENTIATE THESIS	
Author: Sari Sirviö		
Title: Characterization of Atomic Layer Deposited Thin Films: Conformality in High Aspect Ratio Pores and the Electrical Properties of Capacitors		
School: School of Electrical Engineering	Department: Department of Micro- and nanotechnology	
Research field: Semiconductor technology		Code: S-69
Supervisor: Professor Pekka Kuivalainen	Instructor(s): Professor Sami Franssila Assistant Professor Hele Savin	
Examiner(s): D. Sc. (Tech) Matti Putkonen (VTT) Dos. Timo Sajavaara (University of Jyväskylä)		

Abstract:

In this work the characterization of atomic layer deposited (ALD) Al_2O_3, TiO_2 and ZnO thin films is presented by introducing their conformality in high-aspect ratio pores and their electrical properties in capacitors, followed by the experimental results. In addition, a literature survey on thin films and ALD technology is presented. Trimethyl aluminium (TMA), titanium tetrachloride ($TiCl_4$), diethyl zinc (DEZ) and water vapor (H_2O) were used as precursors. The conformality of high aspect ratio pores was studied by deposition of Al_2O_3, TiO_2 and ZnO films in closed and open end pores and analysis by using scanning electron microscope (SEM). The ALD deposition process was confirmed conformal in closed pores, but in open end pores the conformal deposition process was non-ideal. The electrical properties of Al_2O_3 and Al_2O_3-TiO_2 laminates in planar capacitors were studied by deposition of the thin films as the dielectric layer in capacitors with varying deposition temperature, film thickness, surface area and TiO_2 content in the laminate films. The results were analyzed by measuring the capacitance value, leakage current and breakdown strength of the planar capacitors. The higher deposition temperature increases growth rate and produces thicker films, which have lower capacitance values than thinner films. However, higher deposition temperature resulted in low leakage current. The smaller surface area of the capacitor resulted in low leakage current density. Laminates with low TiO_2 content resulted in low leakage current. The key finding was that capacitors prepared with TiO_2 in the dielectric thin film layer exhibited ability to short energetic peaks without irreversible failure. Also, low leakage current in ALD Al_2O_3 dielectric capacitors was achieved with use of relatively low deposition temperature.

Date: 20th of September, 2014	Language: English	Number of pages: 87

Keywords: ALD-Al_2O_3, -TiO_2, -ZnO Thin Films, Nanolaminates, High Aspect Ratio Pores, Planar Capacitors, 3D Capacitors

Aalto-yliopisto

AALTO-YLIOPISTO TEKNIIKAN KORKEAKOULUT PL 11000, 00076 AALTO http://www.aalto.fi	LISENSIAATINTUTKIMUKSEN TIIVISTELMÄ
Tekijä: Sari Sirviö	
Työn nimi: Characterization of Atomic Layer Deposited Thin Films: Conformality in High Aspect Ratio Pores and the Electrical Properties of Capacitors	
Korkeakoulu: Sähkötekniikan korkeakoulu	Laitos: Mikro- ja nanotekniikan laitos
Tutkimusala: Puolijodetekniikka	Koodi: S-69
Työn vastuuprofessori: TkT Pekka Kuivalainen	Työn ohjaaja(t): TkT Sami Franssila
Työn ulkopuolinen tarkastaja(t): TkT Matti Putkonen, Dos. Timo Sajavaara	

Tiivistelmä:

Tässä työssä esitetään atomikerros ohutkalvokasvatus tekniikalla kasvatettujen Al_2O_3, TiO_2 ja ZnO kalvojen kasvun karakterisointi tutkimalla kokeellisesti konformaalista kalvon kasvua korkean aspektisuhteen huokosissa sekä kalvojen sähköiset ominaisuudet tasokondensaattoreissa. Lisäksi esitetään kirjallisuuskatsaus ohutkalvoista ja ALD tekniikasta. Tuloksissa esitetään kokeellisen osuuden havainnot. Lähtöaineina käytettiin trimetyyli alumiinia (TMA), titaani tetrakloridia ($TiCl_4$), dietyyli sinkkiä (DEZ) ja vesihöyryä (H_2O). Konformaalista kalvon kasvua tutkittiin kasvattamalla suljettujen ja avoimien korkean aspektisuhteen huokosten sisään Al_2O_3, TiO_2 ja ZnO ohutkalvoja. Tuloksia tutkittiin skannaavalla elektronimikroskoopilla (SEM). Huomattiin, että suljettuissa huokosissa kalvon kasvu oli konformaalista, mutta avoimissa huokosissa kalvon kasvu oli epäideaalista. Tasokondensaattoreiden, joissa käytettiin Al_2O_3 ja Al_2O_3-TiO_2 laminaatti ohutkalvoja sähköisiä ominaisuuksia tutkittiin kasvattamalla ohutkalvoja varioimalla prosessiparametreissa lämpötilaa ja kalvon paksuutta, kondensaattorin pinta-alaa sekä laminaattikalvoissa varioimalla TiO_2 pitoisuutta. Tuloksia analysoitiin mittaamalla kondensaattorien kapasitanssi, vuotovirta sekä läpilyöntijännite. Korkea kasvatuslämpötila johti korkeampaan kasvunopeuteen ja siten paksumpaan kalvoon. Paksujen kalvojen kapasitanssi on pienempi kuin ohuilla kalvoilla. Kuitenkin, korkeampi kasvatuslämpötila johti alhaisempaan vuotovirran tiheyteen. Laminaattikalvot pienempi TiO_2 pitoisuus johti alhaisempaan vuotovirran arvoon. Keskeinen havainto oli, että Al_2O_3-TiO_2 laminaatilla valmistetut kondensaattorit kestivät peruuttamattomasti hajoamatta korkeita virran arvoja sekä alhaisen vuotovirran Al_2O_3 kondensaattoreita saavutettiin suhteellisen alhaisessa kasvatuslämpötilassa.

Päivämäärä: 20.9.2014	Kieli: Englanti	Sivumäärä: 87

Avainsanat: ALD-Al_2O_3, -TiO_2, -ZnO ohutkalvot, Nanolaminaatit, Korkean aspektisuhteen huokoset, Tasokondensaattorit, 3D kondensaattorit

Acknowledgements

This work was started in the Microelectronic centre at the Helsinki University of Technology (now known as AALTO University Foundation) in the beginning 2007 and the experimental work continued in the Microfabrication group at the Technical Research Centre of Finland (VTT) to the middle of 2008. The writing of the licentiate thesis started in autumn of 2008 and has continued periodically at every opportunity alongside of work

I wish to thank professors Pekka Kuivalainen, Sami Franssila and assistant professor Hele Savin for giving me the opportunity and support to write this thesis while working outside of the university. I am grateful to the external evaluators Matti Putkonen and Timo Sajavaara for the eye opening comments and advice to help me become a better writer. I wish to thank colleagues and friends who have offered fruitful advice and comments and/or fruitless discussions to keep my spirits up. An unexpected journey begun during taking vacation from work to concentrate on writing the thesis in 2012. I asked Sami Franssila for a writing place at AALTO University and he put me in a room of three researchers. One of them offered me more help and support than the others - and longer. In 2013 he proposed to me and in 2014 we got married. I wish to thank my husband Osku for the non-stop support and love.

Helsinki 20.09.2104

Sari Sirviö

Table of Contents

List Of Abbreviations 7

List Of Abstracts 9

1. Introduction 10

2. Thin Film Technology 12

2.1. What Are Thin Films 12

2.2. Applications Of Thin Films 13

2.3. Thin Film Deposition Technologies 14

2.3.1. Chemical Gas Phase Deposition Processes 15

2.3.2. Physical Gas Phase Deposition Processes 16

2.3.3. Comparison Of ALD, CVD And PVD Technologies 16

2.4. Properties, Characterization And Material Features Of Thin Films 17

2.4.1. Crystallinity 18

2.4.2. Mechanical Properties 21

2.4.3. Electrical Properties 23

2.4.4. Surface And Interface Properties 24

2.4.5. Physical And Chemical Properties 25

2.5. Conformality 27

2.5.1. Conformality Of Low Aspect Ratio And High Aspect Ratio Structures 27

2.5.2. Conformality Using Templates 29

3. Atomic Layer Deposition (ALD) 30

3.1. History Of ALD 30

3.2. Film Growth And Surface Chemistry Of ALD 30

3.2.1. Film Growth 30

3.2.2. The Surface Chemistry Of ALD 32

3.3. Precursor Requirements And Process Windows 39

3.4. Materials And Reaction Mechanisms 42

3.4.1. Al_2O_3: TMA + H_2O Process 43

3.4.2. Al_2O_3: TMA + Ozone (O_3) Process 43

3.4.3. Tio_2: $Ticl_4$ + H_2O Process 44

3.4.4. Zno: DEZ + H_2O Process 45

3.5. Limitations Of ALD 45

4. Thin Film Capacitors 47

4.1. Capacitors 47

4.2. Characteristics Of Capacitors 48
4.3. ALD Capacitors 50
5. Materials And Methods 52
5.1. Materials And Reaction Mechanisms 52
5.2. Methods 52
6. Results And Discussion 54
6.1. ALD Thin Film Conformality In High Aspect Ratio Pores 54
6.2. ALD Thin Film Capacitors 58
6.2.1. ALD Capacitor Characteristics 58
6.2.2. Leakage Characteristics Of Capacitors 63
6.3. Discussion 66
7. Conclusions And Future Studies 68
8. Bibliography 71
Appendix I 78
Appendix II 83
Appendix III 85

List of Abbreviations

Abbreviation	Meaning
σ	Sigma, standard deviation
3D	Three dimensional
$AlCl_3$	Aluminium trichloride
ALD	Atomic Layer Deposition
ALE	Atomic Layer Epitaxy
$AlMe_3$	Trimethyl Aluminum
Al_2O_3	Aluminum oxide, Alumina
CMOS	Complementary Metal Oxide Semiconductor
CSD	Chemical Solution Deposition
CVD	Chemical Vapor Deposition
DC	Direct Current
DEZ	Diethyl Zinc [$Zn(C_2H_5)_2$]
DRAM	Dynamic Random Access Memory
EL	Electroluminescent
GaP	Gallium phosphide
$GeCl_4$	Germanium tetrachloride
GPC	Growth per Cycle
H_2	Hydrogen
H_2O	Water
H_2S	Hydrogen sulfide
HCl	Hydrochloric acid
IC	Integrated Circuit
ICP	Inductively Coupled Plasma
k	Dielectric Constant
LPD	Liquid Phase Deposition
LPCVD	Low-Pressure Chemical Vapor Deposition
P	Phosphorus
Pa	Pascal, Measurement unit for pressure
PEALD	Plasma-enhanced ALD
PECVD	Plasma-enhanced Chemical Vapor Deposition
PVD	Physical Vapor Deposition
MBE	Molecular-beam Epitaxy
MIM	Metal-Insulator-Metal
MLD	Molecular Layer Deposition
Mo	Molybdenum
MOALD	Metal-Organic Atomic Layer Deposition
MOCVD	Metal-Organic Chemical Vapor Deposition
O_2	Oxygen
O_3	Ozone
OFET	Organic Field Effect Transistor
RF	Radio Frequency
S	Sulphur
SiO_2	Silicon dioxide
SiN	Silicon nitrdie
Sn	Tin
SOG	Spin-On-Glass
$TaCl_5$	Tantalum(V)chloride, Tantalum pentachloride
$TiCl_4$	Titanium tetrachloride

TiO_2	Titanium oxide, Titania
TMA	Trimethyl Aluminum $[Al(CH_3)_3]$
Zn	Zinc

List of Abstracts

I S. Sirviö, L. Sainiemi, S. Franssila, K. Grigoras. Atomic layer deposition of Al_2O_3, TiO_2 and ZnO into high aspect ratio pores. Transducers 2007. Conference on solid-state sensors, actuators and microsystems. June 10-14, 2007. Lyon, France. Abstract and poster presentation.

II S. Sirviö, L. Sainiemi, K. Grigoras, S. Franssila, V-M. Airaksinen. ALD layers for passivation and functionalization of micro- and nanopores and membranes. Nanotech Northern Europe Conference March 27-29, 2007. Helsinki, Finland. Abstract and poster presentation.

III S. Sirvö, R.L. Puurunen, H. Kattelus. Electrical properties of capacitors with ALD-grown Al_2O_3 and Al_2O_3-TiO_2 nanolaminate thin film dielectric layers. 8th International Conference on Atomic Layer Deposition-ALD 2008. June 29-July 2 2008. Bruges, Belgium. Abstract and poster presentation.

The author of this thesis was responsible of all the ALD depositions and all characterization of the thin films (1-III) including: ellipsometry, optical microscopy, scanning electron microscopy (SEM) and profilometry.

1. INTRODUCTION

Thin films are thin layers of materials that are deposited on a substrate. Their thickness can vary from few nanometers to micrometer [1]. The benefit of thin films is in the possibility of tailoring the material properties. The surface functionality can, for example, be an electronically conducting or insulating layer [2]. There are multiple thin film deposition methods, of which ALD is a method that enables surface controlled deposition that is pin-hole free and the film is able to cover 3D structures evenly. The commonly used materials in ALD are metals and metal oxides [2].

The goals of this thesis are to understand the background and details of the ALD process and the behavior of the process in deposition of demanding topographies. ALD technology is beneficial for this study due to the surface controlled deposition process and due to the non-line-of-sight deposition property to coat topographies behind corners. Also, a goal is to understand the electrical properties of the ALD thin films and how they can be manipulated. ALD deposited films are pinhole free, which increases the electrical quality of the film by decreasing the leakage current.

There are two research questions in this thesis:
1. The conformality of ALD thin films. How good is the conformality of ALD thin films on 3D structures, such as high aspect-ratio pores or spherical objects? What factors have effect on the conformality?
2. Using ALD thin films as dielectric layer in planar capacitors. How does the deposition temperature, film thickness, surface area of the capacitor, and reactor configuration affect the capacitance? Considering both single layer and multilayer laminates, how will the chosen materials affect the leakage current characteristics of the capacitor?

The research question no. 1 was studied in laboratory tests by preparing multiple samples of high aspect-ratio pores and varying the ALD deposition parameters. The results were monitored by scanning electron microscope (SEM) images on the cross section of diced samples and confirming the thickness of the thin films from the bottom, middle section and upper part of the high aspect-ratio pores. The research question no. 2 was studied by fabrication planar integrated circuit (IC) capacitors with varying the ALD process parameters and performing tests on the electrical properties of the capacitor.

The precursors and reaction mechanisms introduced in this work are focused on Al_2O_3, TiO_2 and ZnO, which were the precursors used in the research reported in conference publications (Annex I-III). ALD is based on sequential use of self-terminating gas–solid half reactions where two precursors contribute to the film growth in cyclic manner. The two precursors A and B (sometimes separated by calling them the precursor and the reactant) are cycled ABAB.. and adsorb to the surface until the desired film thickness has been achieved. The half reactions are separated by a purge step where the unreacted precursor and reaction byproducts are removed.

This thesis presents an overview of thin film technologies, describes applications of these technologies, focusing on atomic layer deposition (ALD), and reports the results of experimental studies on the conformality of ALD films and on ALD-Al_2O_3 and Al_2O_3-TiO_2 laminates used as dielectric layers in capacitors. Chapter 2 introduces the general background of thin film technology describing the definition of thin films and applications, the major thin film deposition methods and the important material characteristics and mechanical properties. Chapter 3 examines the chosen materials (Al_2O_3, TiO_2 and ZnO) and their reaction mechanisms and processes taking

place on the substrate surface during ALD process, and describes the precursor requirements. Also plasma-enhanced ALD (PEALD) is discussed. Chapter 4 introduces the thin film capacitors in order to prepare for Chapter 6. Chapter 5 focuses on the materials and methods. Chapter 6 summarizes the results and discussion of research on film conformality and on ALD thin film capacitors. In chapter 7 the conclusions are presented and future studies are proposed.

2. THIN FILM TECHNOLOGY

This chapter collects information on the background of thin films and what kind of applications the films are used in. This thesis is focused on two aspects, namely thin film capacitors and the theory behind them and secondly on to studying conformality of ALD thin films. Thin film deposition techniques are presented to give an idea how unique ALD technology is. Thin film properties and material characteristics are summarized in order to present the inner structure of the thin films and how by modification the properties the applicability of the film can be altered.

2.1. What are thin films

Thin films are layers of materials that have a thickness range of a couple of nanometers to micrometers [1].

Thin films can be made of in principle from any solid material, such as metals and metal oxides. Examples of these materials are aluminium, aluminium oxide, respectively.

The choice of the materials allows tailoring the thin film properties and result in a specific functionality in the application through surface modification.

The thin films and bulk material differ mainly on the material properties. The thin film properties of the same material are in many cases considerably different than the bulk properties. Thin films can take more mechanical stress before breaking that bulk material (silicon is brittle in bulk materials, but thin film silicon deposited on flexible substrate may be rolled). Opaque bulk materials may become transparent in thin films. The better electrical breakdown property allows thin film integrated circuits to be used at higher voltages before breakdown than integrated circuits made of bulk material. The advantage of thin film materials is in the savings through reduced material costs.

Thin films can be deposited by chemical or physical deposition methods from liquid, gaseous or solid precursors. Examples of the chemical deposition methods are atomic layer deposition (ALD), chemical vapor deposition (CVD) and sol-gel process. Examples of the physical deposition methods are sputter deposition, vacuum evaporation and ion plating. These are introduced later in the chapter 2.3.

Thin films can be deposited as single material layers or laminates. Nanolaminates are thin films that consist of alternating layers of different materials. For example Al_2O_3 and TiO_2 can be deposited sequentially to form an Al_2O_3-TiO_2 nanolaminate to employ the beneficial properties of both films.

The ability of a thin film layer to cover a surface smoothly is described as conformality and the ability to coat the surface behind corners is described as step coverage. Different deposition methods result in different conformalities and step coverages.

2.2. Applications of thin films

Due to their unique properties, thin films are applied in myriad ways. The functional characteristics of thin films differ from those of bulk materials. Thin film deposition technologies are essential for innovation of new devices. Many microelectronic structures are based on material structures that are built using thin films [2]. Thin film microelectronics industry has an important role in communications, information processing, storage and display applications. Fruits of this technology have successfully fertilized thin film uses in diverse areas, such as coatings (optical, optically reactive, decorative, environmental, corrosion resistant, anti-tarnish, wettable or anti-wettable and wear-resistant), biotechnology and the generation of energy and conservation of energy [3].

In considering the different applications of deposited thin films, the following generic categories can be identified.

Electronic components. The most of the thin film applications are found in fabrication of electronic components (e.g. microelectronic integrated circuits) consisting of: semiconductor materials, dielectric and insulating materials and of metal conductors [2].

Optical coatings. Optical coatings are applied in: 1. Antireflection coatings are applied in dielectric thin films with known refractive indices and absorption coefficients, e.g. in solar panels, 2. Plate glass infrared solar reflectors are used to increase the luminous flux intensity, 4. Laser optics are used in metal reflective coatings that can take high radiation intensities and will not degrade [2].

Magnetic films for data storage. Thin films of magnetic materials have found wide commercial applications for data storage in computers and control systems. The substrates can be metal, glass or plastic polymeric materials [2].

Electronic displays. Electronic displays are used for interfacing electronic equipment with human operators. Different components and device structures are required, such as: Liquid-crystal displays, light-emitting diodes (LEDs), electroluminescent displays, plasma and fluorescent displays, and electro chromic displays. The fabrication of these displays requires conductive films, transparent and conductive films, luminescent or fluorescent films as well as dielectric and insulating layers [2].

Protective layers. Hard surface coatings, such as carbides, silicides, nitrides and borides are used for improved metal surface wear characteristics and hardness e.g. for tools, bearings and machine parts. Diamond-like-carbon is used for material´s heat dissipation properties, resistance to high-temperature, high-energy radiation and electrical insulation. [2]. Silver is tarnished in atmosphere by corroding and formation of a black layer that contains sulfides. Although tarnishing does not affect the electrical or contact resistance properties of the silver surface, it is a problem for appearance. Thin films are used to protect the surface, because they are invisible and they protect the surface [4].

2.3. Thin film deposition technologies

In thin film manufacturing the techniques that are used have a large impact on e.g: the electrical properties, film conformality and impurities in the film depend on the fabrication technique. The semiconductor device industry is totally dependent on the formation of thin films.

A variety of materials can be deposited from gas, vapor, liquid or solid phase [2]. The deposition technologies fall into two main categories: gas phase processes and liquid phase processes. The gas phase processes are (*i*) Physical Vapor Deposition (PVD) (e.g. evaporation, sputtering) and (*ii*) Chemical Vapor Deposition (CVD) (e.g. low-pressure CVD (LPCVD), plasma enhanced CVD (PECVD), atomic layer deposition (ALD)) and the liquid phase processes are (*iii*) Liquid Phase Deposition (LPD) (e.g. Spin-on-methods, smelting) and (*iv*) Chemical Solution Deposition (CSD) (e.g. Sol-Gel Procedure) [2][5]. Thin film deposition technologies are illustrated in Figure 1.

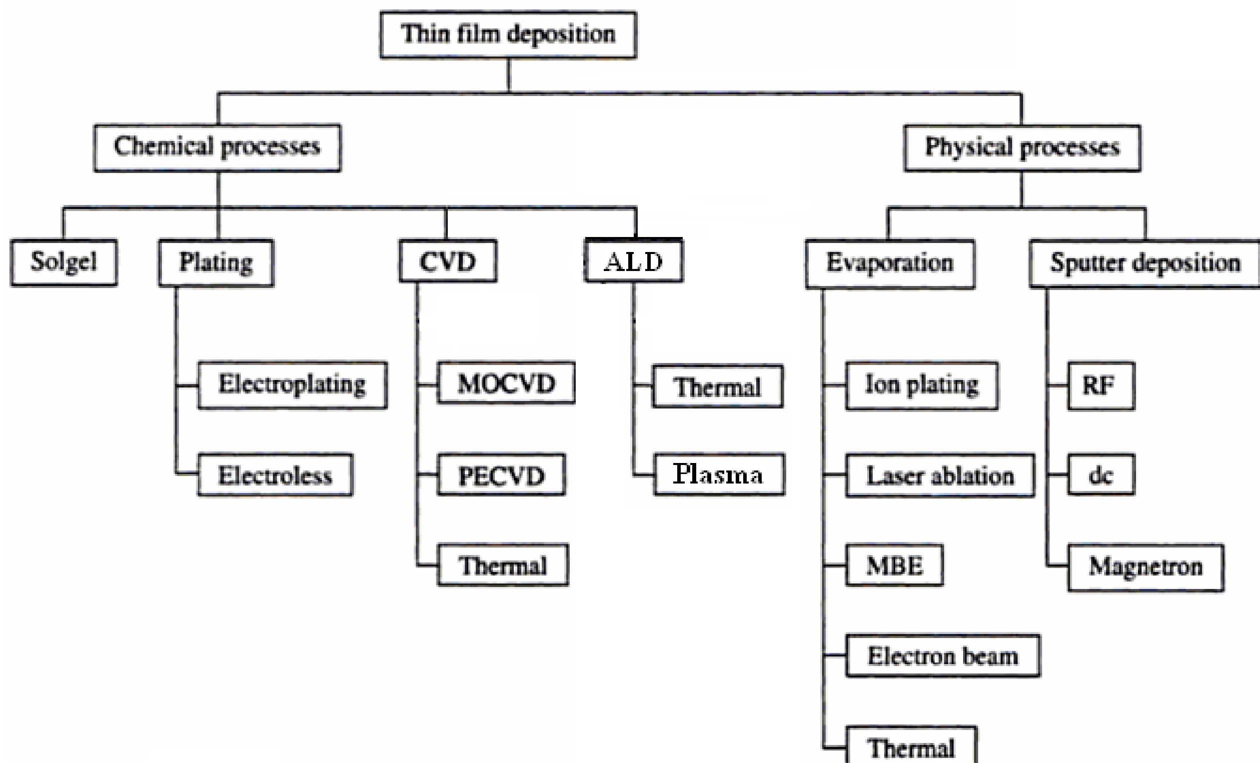

Figure 1. Illustration of the common thin film deposition processes. (Modified from [6], ALD was added to the image later).

Out of the chemical and physical thin film processes, ALD, CVD and PVD will be introduced and compared in chapters 2.3.1 and 2.3.2. ALD will be introduced in more detail in chapter 3.

2.3.1. Chemical gas phase deposition processes

Atomic layer deposition (ALD) is a chemical gas phase thin film deposition method and the technique is suitable for manufacturing inorganic material layers with thickness down to a fraction of a monolayer [7]. The technique is based on sequential self-terminating gas–solid reactions [8]. Only one precursor A or B is pulsed to the reactor at a time and between the next pulse, there is a purge step to clean the reactor before the next precursor arrives. The precursors are pulsed in ..ABAB.. manner. The amount of pulses times the thickness of one layer gives the film thickness. The reaction occurs only between the gas molecule and the surface [9-10]. The deposition temperature in thermal ALD is selected so (often ~100 °C – 300 °C is used, depending on precursors) that thermal decomposition of precursor does not occur and only one monolayer (or a fraction of a monolayer, because of steric hindrance reason) is absorbed onto the substrate surface [9].

ALD films are pin-hole free films and a non-line-of-sight technique that coats conformally the extremely complex shape samples with a uniform film thickness all over, even in high aspect ratio pores or on sharp points on the sample.

ALD process is possible to operate at atmospheric pressure and at low temperatures to reduce the cost caused by the vacuum pumps [11-12] and to enable more versatile objects to be coated such as biological templates, e.g. tobacco mosaic virus and ferritin [13].

ALD-grown materials have a wide range of applications, from catalysts and protective coatings to electroluminescent displays, devices based on magnetic, superconductive and thermal phenomena, microelectronics and beyond [2].

Chemical vapor deposition (CVD) is a synthesis process in which the chemical constituents react in the vapor phase near or on a heated substrate to form a solid deposit. Therefore, if the material deposited is a product of chemical reaction, the process is classified as CVD [20].

The number of chemical reactions used in CVD is considerable and include: thermal decomposition (pyrolysis), reduction, hydrolysis, disproportionation, oxidation, carburization, and nitridation. These reactions can be activated by several methods [14]:

- Thermal activation which typically takes place at high temperatures, i.e., > 900 °C,
- Plasma activation which typically takes place at much lower temperatures, i.e., 300–500 °C,
- Photon activation, usually with shortwave ultraviolet radiation, which can occur by the direct activation of a reactant or by the activation of an intermediate.

In the chemical vapor deposition reactor the precursors react first together in the vapor phase near or on a heated surface to form a solid film.

2.3.2. Physical gas phase deposition processes

Physical vapor deposition (PVD). PVD technology facilitates the transfer of atoms from a solid or molten source onto substrate. Evaporation and sputtering are two most widely used PVD methods for depositing thin films [15].

The main categories of PVD processing are vacuum evaporation and sputter deposition. Typically, PVD processes are used to deposit films with thicknesses in the range of a few nanometers to thousands of nanometers; however they can be used to form multilayer coatings, graded composition deposits, very thick coatings and freestanding structures [16].

Sputtering is a vacuum process, which is based on eroding the target material by ion bombardment with ion gun or accelerating the charged particles assisted by plasma. The incident particle hits the surface of the target and the kinetic energy enables breaking bonds or dislodging the surface atoms of the target. The removed surface atoms fly to the nearby substrate and form the sputter deposited film [2]. The benefit of sputtering compared to evaporation is that materials, which have a high melting point and would be challenging for evaporation method, can be easily sputtered.

Oxides and compounds can be deposited using reactive sputtering, of which an example is using an aluminium target in the presence of oxygen as the reactive gas. The aluminium is sputtered as a metal, but it reacts on the surface with oxygen to form an oxide [2].

The vacuum in sputtering processes varies from 0.13 Pa to 133 Pa. Deposition rate scales with power [2].

Evaporation process is based on heating the target metal in a crucible and transporting the evaporated atoms to the substrate. Evaporation is a low temperature vacuum process that employs either high vacuum ($0.13\text{-}0.13^{-6}$ Pa) or ultrahigh vacuum ($0.13^{-6}\text{-}0.13^{-9}$ Pa). The vacuum allows the atoms to travel to the surface without or very little collisions making it a line-of-sight process [10].

Only evaporated metal atoms hit the substrate at thermal speed bringing only a little energy to the substrate correlating to room temperature deposition. The heating of the metal can be done with electron beam. Metals with low melting point can be easily evaporated, such as gold and aluminium. Electron beam creates a high localized temperature which can melt also high melting point metals, such as tungsten. The growth rate for evaporation is typically low, 0.1-1 nm/s [10].

2.3.3. Comparison of ALD, CVD and PVD technologies

The growth mechanism in ALD is unique and different to growth mechanisms of CVD and PVD. In ALD process, the film forms on the substrate by half reactions, the film growth is sequential, saturated and self- terminating. The precursors react only with the surface species of the substrate. In CVD the precursors react in the reaction chamber and the product is deposited on the substrate. In PVD the target is bombarded with energetic particles. During the bombardment the atoms from the target are ejected and then fly to the substrate.

The temperature required for reaction to take place is higher in CVD than in ALD. In thermal activation CVD, the temperature need is <900 °C [17], whereas in thermal ALD the temperature ranges commonly between 100-300 °C depending on the process, sometimes the temperature can

be elevated to 500 °C. PVD process does not demand elevated temperatures for the deposition to take place, although elevated temperatures might improve film quality [16].

Film properties are different in ALD, CVD and PVD deposited films. Comparing these three methods, there are least pin holes in the ALD deposited films. Regarding thin film conformality the conformality is poorer in CVD than in ALD. The film thickness is usually thinner on other side of the sample than where the precursor source is and the step coverage is often uneven. CVD does not apply to film deposition in high aspect ratio morphologies. The step coverage in different methods is presented in Figure 2. Because in the PVD process target atoms fly to the substrate, the process is a line-of-sight process. In ALD and CVD processes the precursors are in gaseous form in the reaction chamber and they are not line-of-sight methods.

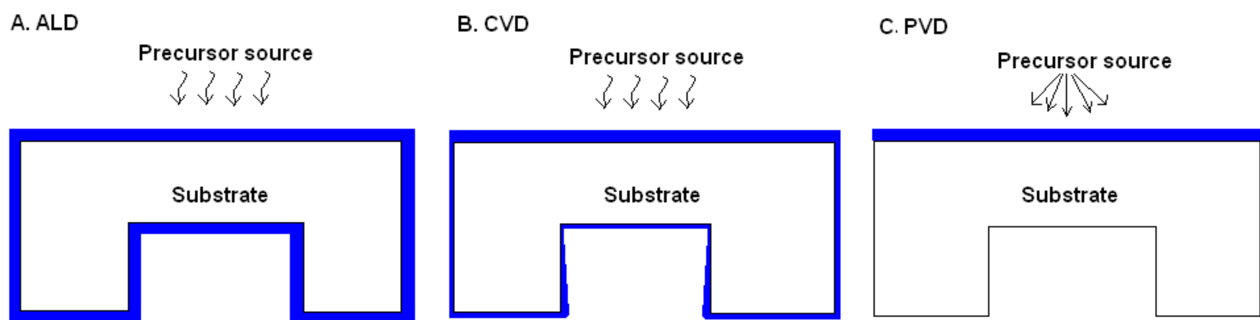

Figure 2. Step coverage. A. ALD method has excellent conformal step coverage. B. CVD has non-confromal step coverage and the uniformal film growth is poor where there is no line if sight from the precursor source. C. PVD is a line-of-sight deposition method and the film will not grow where there is no straight line from the precursor source.

The conformal step coverage occurs when the reactants migrate rapidly after adsorption on the step surfaces. Non-conformal step coverage occurs when the reactants adsorb and react without the surface migration and the deposition rate is proportional to the arrival angle of the gas molecules. [18-19].

Each of these thin film deposition technologies are good at different applications. ALD is suitable for e.g. use as an electrically insulating layer in capacitors due to the dense film and low pinhole density. Also, the conformal coating possibility allows coating of possible 3D substrates in a capacitor. CVD is suitable for e.g. wear resistant coatings and powder production. PVD is suitable for e.g. use in sensors where metallic lines are needed to electrically connect different parts of the sensor.

2.4. Properties, Characterization and Material features of Thin Films

Thin films can be evaluated in terms of their properties. Here the following properties are discussed: crystallinity, mechanical properties, electrical properties, and the surface and interface properties. These properties may be adjusted according to the thin film application.

By combining different materials into a nanolaminate film, it is possible to tailor the material properties of the layers. For example optical, electrical and morphological properties may be adjusted [20]. E.g. combining the insulating properties of aluminium oxide (Al_2O_3) with higher dielectric value of titanium oxide (TiO_2) it is possible to make a more attractive dielectric layer to be applied in capacitors.

2.4.1. Crystallinity

Amorphous, crystalline and polycrystalline films. Amorphous solids have no ordered structures like the crystals in crystalline film. There is only a short range order remaining due to the covalent chemical bonds [21]. Examples of the amorphous, single crystalline and polycrystalline materials are presented in Figure 3.

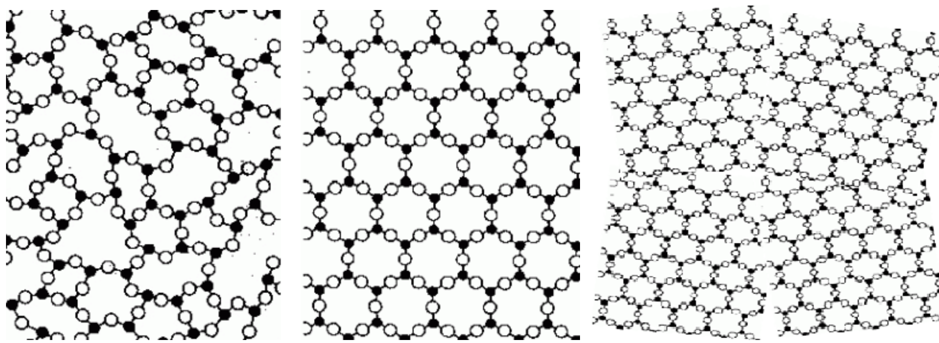

Figure 3. Material structure. Amorphous material (left), single crystalline lattice (middle) [22], polycrystalline (right) [10].

Amorphous solids do not have the long-range order of crystalline films, but they do have the short-range order due to the chemical bonds holding the material together (34). Amorphous solids have different material properties to crystalline films. The etch resistivity, electric insulating properties are different. Amorphous materials can in many cases resist etchants better than crystalline films and resist electric current better than crystalline film due to the fact that the charge carriers, such as electrons, cannot move easily in amorphous material. Nevertheless, the *k*-value is often smaller in amorphous films than in crystalline films [22].

Crystalline solids have an ordered and repeating three dimensional structures in the crystal lattice called the long-range order as presented in**Error! Reference source not found.Error! Reference source not found.**. In deposition process, the crystals may take one of the seven structures in crystallography: cubic, tetragonal, orthorhombic, hexagonal, trigonal, monoclinic and triclinic. The thin film structures can be divided into three categories according to their crystallographic perfection: epitaxial films, non-epitaxial films and amorphous films [22].

Polycrystalline solids have a large number of grains oriented in different directions and they are separated by grain boundaries [10]. The grain size can be influenced by the deposition conditions. The grain boundaries have secondary effects influencing the mean free path of electrons [21].

Amorphous films can remain amorphous or transform to polycrystalline form in high temperature process step. Single crystalline solids tend to stay single crystalline during processing. It is possible to change the crystalline lattice to amorphous by ion bombarding. Polycrystalline films stay polycrystalline, however during heating, the crystals can grow [10].

The thin films materials deposited by ALD can be either: amorphous, polycrystalline, epitaxial and in rare cases single crystalline depending on the material and on the deposition temperature. The crystallinity may be affected by post annealing.

Growthmechanism. There are three possibilities on how the initial crystalline growth takes place in the first cycles of ALD film growth. In the *first mechanism* the film starts as amorphous and the nuclei for crystallization form randomly and the crystals grow bigger as the film grows thicker when the material in the new layers adopts the crystalline structure and the next to the crystal the material continues to grow as amorphous. The film ends up as crystalline; because the neighbouring crystals eventually touch and the new layer of materials adopt the crystal structure of the whole surface. In the *second mechanism* the growth starts as in the first scheme, but the amorphous film next to the crystal becomes crystalline. In the *third mechanism* the film growth begins as crystalline only on certain sites on the surface. During the film growth only the crystals grow and eventually they touch forming a uniform crystalline surface [19].

External factors. Several external factors affect crystallinity. An overview of these factors are: *temperature, impurities, reactants, plasma enhancement, substrate, and film thickness.*

Temperature influences in inorganic materials the phase transition from amorphous material to crystalline material and temperature influences the phase transition in crystalline material e.g. whether the crystals grow on 100 orientation or 001 orientation [19] of the crystal. At low temperatures 100 orientation [19] is most often found, whereas the 001 orientation [19] is most often found at high temperatures. Increase in deposition temperature affects other ALD growth parameters that in turn affect crystallinity. The reactions get faster and so does the mass transport kinetics. With increasing deposition temperature the concentration of the impurities often decrease [19]. Al_2O_3 films deposited at 110 °C contain residual hydrogen 11.3 at.% whereas Al_2O_3 films deposited at 300 °C contain residual hydrogen 1 at.% [23]. The impurities may have a notable effect on hindering the crystallization [19].

Impurities have a notable effect on crystallinity and it is affected by other ALD parameters mentioned above (temperature, reactants, use of plasma and sometimes even the substrate affects impurities). Carbon as an impurity effectively inhibits crystallization leading to amorphous films. Chloride and hydrogen impurities affect film crystallization at higher concentrations. Some trace impurities remain in the film that come from the ligands of the reactants [19-20].

Certain *processes* produce different crystalline phases. The main reason is the reactants ability to remove ligands of the metal reactant. Water in most cases is not sufficiently reactive, but oxygen plasma is reactive enough to effectively remove the ligands by combustion. Oxygen plasma produces films of higher purity that affects the crystallization. Films of reactions that use alkoxides, alkylamides, silylamides and aminoalkoxides are generally amorphous [19]. With metalorganic reactants one factor is the carbon impurities on crystallinity and generally films using alkylamides are deposited at lower temperatures than halides [19].

Plasma enhancement effects crystallization mainly on the decreased impurity content of the PEALD processed films that allow crystallization. Temperature is another factor; the additional energy may lead to increased local temperature which induces crystallization. Plasma enhancement can either lead to amorphous or crystalline films [19].

The effect of *substrate* on crystallinity is caused by the substrate surface. The adsorption sites on the surface dictate how the film growth starts. In crystalline films the substrate can guide the size of the grains. [19].

Film thickness affects the growth of crystallinity films and it is cross fertilized with other growth parameters such as temperature and substrate. In a certain material a thin film may be amorphous and when the film grows thicker the film growth changes to crystalline growth. Increasing film thickness may turn the crystalline phase from one phase to another phase due to a competition of surface and bulk energy contribution. [19]. The film thickness limits the size of the grains. Smaller grains produce thinner films. [24].

When using CVD methods for producing titania, one can easily select which type of crystalline structure is wanted for different types of applications simply by varying the deposition temperature. Amorphous titania forms at low temperatures. Using ALD method, the temperature is 80 °C [25] and it may be the best choice if the whole wafer processing must be done at low temperature or the target is an optical coating, where amorphous titania has better optical properties than crystalline forms [26]. Anatase and rutile in turn, are composed at elevated temperatures (anatase 300-400 °C; rutile 400 °C [26]). Both of these crystalline forms have their uses. Anatase is better for photochemically active layers and rutile is used for micro-electrical coatings.

Influencing the properties. The film structure strongly influences the mechanical, thermal, optical and electronic properties of thin films. The film being amorphous or crystalline (mono- or polycrystalline) has effect on its properties in etching or electrical conductivity. In the case of crystalline films, the epitaxial growth of the next film is affected. As an etching mask the crystalline film performs a bit poorer than amorphous films. The grain borders in the crystalline films may allow the etchants to go through the film. The grain lines may stop the electrical current from passing through the film and decrease the conductivity. In addition, gases and impurities may diffuse through the film using the grain borders [21].

Effect of process parameters on structure. ALD Al_2O_3 films that are grown below 600 °C are amorphous. The common process temperature to grow amorphous alumina ranges with trimethyl aluminium (TMA)-water process from 30 °C to 300 °C. ZnO thin films are commonly crystalline, but when deposited as a thin layer on certain substrates, the ZnO film is amorphous. TiO_2 is in most cases crystalline. However, in certain conditions, it is possible to coat amorphous titanium oxide film, especially when the substrate is amorphous alumina and the deposition temperature is low [19]. Post deposition annealing can be used to transform amorphous film to crystalline film. TiN films may be deposited both amorphous or crystalline, depending on the process parameters: crystalline films can be deposited by using halide reactants and amorphous films can be deposited by using alkylamide reactants. The reason to this behaviour is in the impurities. In halide precursors the oxygen content is large and the deposition temperature is above 300 °C, whereas in alkylamide precursors the carbon content is large and the deposition temperature is 150-250 °C [19].

Epitaxial and non-epitaxial films. Epitaxial films are grown on a substrate with all atoms arranged predictably in their correct place mimicking the substrate. There may be small defects, such as vacancies, interstitial atoms or impurities. Non-epitaxial films are usually polycrystalline [21].

Dielectric constant of crystalline material is often higher than that of an amorphous material [19]. It has been well known that post annealing step of ALD thin films can have both beneficial and inhibitory effects on the electrical and physical properties of the film [19]. The dielectric constant

increases by annealing due to the formation crystalline phases, but with HfO_2 thin films the leakage current increases up to 2 orders, because of formation of the grain boundaries in crystalline film [27].

2.4.2. Mechanical properties

Four materials properties are essential for mechanical device stability. They are: 1. Elastic modulus (Young´s modulus) that is a measure of stiffness of an elastic material; 2. Yield strength (stress at which materials begins to deform plastically); 3. Interfacial adhesion and 4. Film fracture toughness [10].

Measurement of stresses. These stresses can be measured directly or indirectly. Direct measurements are: MEMS-based mechanical system and indentation tests. Indirect measurements are: elasticity (Young´s modulus, plasticity (yield stress), fracture (toughness), viscoelasticity, viscoplasticity and fatigue strength. An example of a stress measurement method is nanoindentation, which is a versatile tool for a fast measurement of many mechanical properties. A small needle is pushed into the film and the force and depth of the needle are monitored. Elastic modulus, hardness, interfacial adhesion and film fracture toughness can be measured by nanoindentation [28].

Compressive and tensile stress. Thin films are under either compressive or tensile stress when deposited on subsrates [10]. The mechanical properties of thin films are different from those of bulk materials, because of their unique microstructure, large surface-to-volume ratio, reduced dimensions and the constraints caused by the substrate [29]. See Figure 4 [10]. This elastic strain causes the substrate to deform elastically in biaxial bending (consisting of stress in the x- and y-axis) [29].

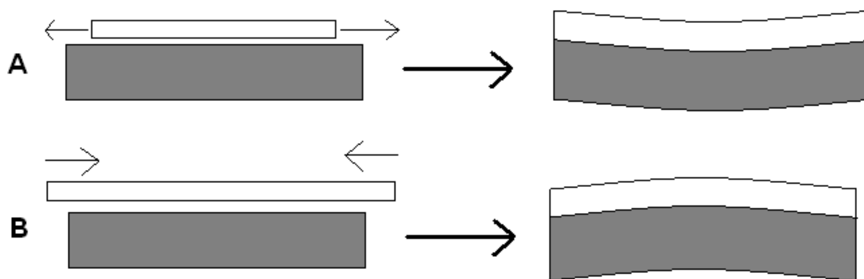

Figure 4. Thin-film stresses. A) Tensile stress (positive stress) is the stress of the film that has to be elongated to fit a wafer. B) Compressive stress (negative stress): is the stress of the film that has to be compressed to fit the wafer [10, p.58].

Substrates are significantly thicker than thin films and because of all solids have similar elastic constants, for example silicon wafer which thickness is about 1000 times higher than film have stresses and strains are about 1000 times less than those of films [10].

Extrinsic and intrinsic stresses. Stresses consist of *extrinsic stress* that is caused by mismatch in the thermal coefficient between the film and the substrate [10]. *Intrinsic stress* depends on the film microstructure and on the deposition process, which has an effect of the whole stress of the thin film [10]. Evaporated metal films are usually under tensile stress. Sputtered films can be under tensile or compressive stress and their stress can be tailored by process parameters and by post annealing [30].

Extrinsic stress is produced by the mismatch in thermal expansion coefficient between the film and the substrate. The extrinsic stress can be estimated from thermal expansion coefficient differences. The parameters affecting this phenomenon are: Young's modulus, Poisson's ratio, coefficient of thermal expansion between film and substrate, and the temperature difference between the film and the substrate. Young's modulus defines the stiffness of an elastic material. Poisson's effect is the phenomenon when material is stretched in one direction; it tends to expand in the direction perpendicular to the stretching direction. Poisson's ratio is the ratio of percentage of the expansion divided by the percentage of the compression. Extrinsic stresses are in most cases tensile at room temperature [29].

Intrinsic stress is also called growth stress [28] and it is induced by the growth process. It is the component of stress that is not induced by differential thermal expansion effects between a film and its substrate [31]. Deposited polycrystalline films are not at their energy minimum. A low deposition temperature means that the arriving atoms don´t have enough energy to reach the energetically favourable positions. This is forcing the film to grow in an unrelaxed way. Voids and incorporated foreign atoms affect the stress. Processes that lead to volume changes (e.g. crystallization, phase transitions, out-gassing) lead to stress changes. Intrinsic stresses are in most cases compressive at room temperature [29].

When calculating the stress values, Stoney´s law can be used. Stoney´s law for calculating stress values is presented in Equation 1.

$$\sigma = \left(\frac{E_s}{1-\nu_s}\right)\frac{t_s^2}{6t_f}\left(\frac{1}{R_f}-\frac{1}{R_0}\right)$$

Equation 1. [30]

E= Youns modulus
v_s = Poissons ratio
t_f = substrate thickness
R_0 = Wafer curvature radii before deposition
R_f = Wafer curvature radii after deposition

Influence of temperature on stress of thin and thick films. According to a study in [30] it was indicated that when measuring the mechanical stress of ALD deposited Al_2O_3 thin (<20 nm) and thick films (25-60 nm) at room temperature and during thermal cycling up to 870 °C the films were generally under tensile stress. For thin films (5-20 nm) the stress values increase slightly and for the thick films (60 nm) the stress values are nearly constant. Tensile stress was shown to decrease with increasing temperature; 500 MPa at 200 °C deposition temperature to 50 MPa at 500 °C. With 60 nm film (Figure 5, left) the sharp increase of stress to ~1000 MPa at about 780 °C is caused by an irreversible phase change from amorphous to crystalline Al_2O_3 and the volume reduction due to the phase change is the main reason for increase in tensile stress. With 25 nm film (Figure 5, right) the tensile stress increases to < 2500 MPa with temperature increase to 800 °C and the stress values decrease reversibly during cooling almost the same way as during heating. Possibly, the film crystallization is inhibited by small film volume and therefore the stress behavior during heating and cooling was different with thin films (< 25 nm) to thick films (60 nm)[30].

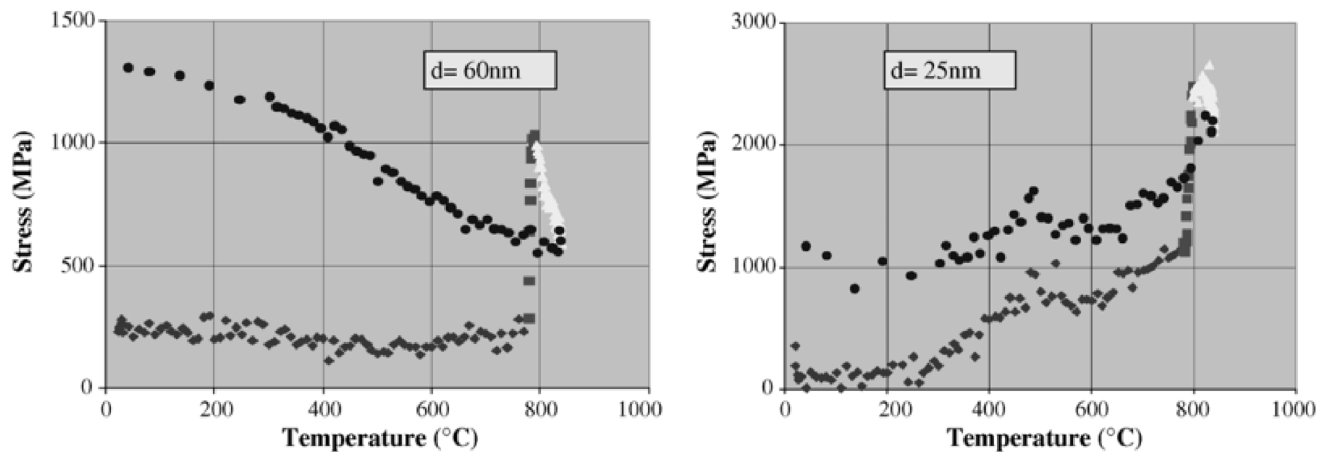

((◆) heating; (■) phase transition; (▲) phase transition; (●) cooling).

Figure 5. Effect of film thickness to stress evolution of Al_2O_3 using two thickness 60 nm (left) and 25 nm (right). For 60 nm thickness, the stress remains constant during temperature increase. An irreversible phase change from amorphous to crystalline occurs at 780 °C and this decreases the volume of the film and increases the tensile stress (60 nm, left). For 25 nm thickness the small volume of the film inhibits crystallization of the film and the stress behavior is different compared to thicker 60 nm film. [30].

2.4.3. Electrical Properties

Thin films can be electrical conductors, semiconductors or insulators. The definition of conductors, semiconductors and insulators can be described by their electrical conductivities. Conductors have high conductivities from 10^4 - 10^6 S/cm (Siemens per centimetre). Insulators have very low electrical conductivities in the order of 10^{-18}- 10^{-8} S/cm and semiconductors have electrical conductivity between insulator and conductor. The differences in the electrical conductivities can be explained by the energy bands (valence and conduction bands). The electrical properties of thin films are one of their most important physical features and they differ from bulk materials due to the dimensions of the thin films. The biggest factor affecting the electrical properties of the thin film is whether the material is a conductor, a semiconductor or an insulator (also called a dielectric) [18, 21].

Conductors have electrons in the valence band and the conduction band is partly filled. With some materials the bands may even overlap. Electrons are free to move with only a small applied field in the conductor, because there are many unoccupied states close to the occupied energy states. [18, 21].

Semiconductors have a small energy gap between the valence band and conduction band. All electrons are in the lower valence band at T= 0 K making semiconductors poor conductors at low temperatures. At room temperature and normal atmosphere the electrons can be thermally excited from the lower energy state, the valence band to the higher conduction band where there are many empty states. A small applied potential can move these electrons and cause the semiconductor material to conduct moderate electrical current. [18, 21].

In an *insulator* material the valence electrons form strong bonds between the neighbouring atoms and they are difficult to brake. This results to absence of free electrons to participate in current

conduction at or near room temperature. Insulators have a large band gap between the lower valence band and the higher conduction band. Thermal energy or energy from an applied field cannot raise electrons from the valence band to the conduction band. All electrons occupy the valence band and the conduction band remains empty resulting in high resistivity of the insulator material. [18, 21].

Effect of material properties on electrical properties. The material's phase has an effect on electrical properties of thin films. The phases are either an amorphous solid or a crystalline solid. In the crystalline solid, it makes a difference for the electrical properties if the material is polycrystalline or single crystalline. One material may have multiple crystalline structures. TiO_2 has three crystalline forms: anatase, rutile and brookite, which have different electrical properties. Film crystallinity can b single crystalline or polycrystalline. In crystalline lattice disturbances in the electric conduction in a conductor or semiconductor thin films are caused by a deviation to the normal periodic lattice. These deviations increase resistivity and they can be: lattice vibration, impurities or lattice defects such as dislocations, grain boundaries, vacancies, surfaces, scattering by grain boundaries or scattering at the surface [18, 21]. Carbon and hydrogen impurities affect the electrical properties of thin films by increasing electrical conductivity [32-34].

In thin films the surface to volume ratio is higher than in bulk material, so the electrons scatter more when meeting a surface [18]. Decreasing thin film thickness decreases the dielectric constant of ALD Al_2O_3 thin films. The decrease in dielectric constant is suggested to be explained by formation of interfacial oxide layer [35]. By doping silicon with arsenic (p-type) or boron (n-type) either acceptors (vacancies) (p-type) or donors (extra electron) (n-type) are formed in the lattice affecting the electrical conductivity. In amorphous semiconductors the electrical conductivity consists of band conduction and hopping conduction. In hopping conduction the electrons hop to nearest neighbour sites by emitting or absorbing phonons [18, 21].

To simplify the electrical properties of conducting or semiconducting thin films, electrical conductivity is caused by movement of electrons and electrical resistivity is caused by the scattering of these electrons by the lattice.

2.4.4. Surface and Interface Properties

The innate properties of the substrate that affect the film growth include the crystallographic orientation. For instance, some films prefer to grow on 100-surface and others on 111-surface. The orientation affects the surface roughness and hence the topography. Either the deposited thin film can neglect or adopt the topography of the substrate into its own topography. The dangling bonds are an innate property of the substrate. When the substrate e.g. a silicon wafer is formed, the atoms that used to have other atoms next to them in the lattice are suddenly the surface atoms and the extra bonds are left dangling and it is energetically unfavorable. The surface atoms will rearrange themselves in order to reach energetically more favorable state and even be more reactive.

The external properties of the substrate that affect the film growth include ligands that create steric hindrance and may reduce the reactive sites on the substrate by shielding them. Contaminations, impurities, absorbed gases and catalytic/inhibitory substances can affect the nucleation effects and thus the film growth mode that affects the type of film that will grow. Stress between the substrate and the film causes the wafer either to bend concave or convex and the film can crack or buckle.

The surface and/or interface properties of the substrate that can drastically influence the film characteristics are presented in Table 1.

Table 1. The properties that influence film growth and their effects on deposited films

Surface/ interface properties	Effect on the film characteristics/ growth
Surface contamination	Alter the work function in EL-devices, affect electrical and optical characteristics [36].
Nucleation effects	Affects the growth mode of the film (island growth, layer growth, island + layer growth) [37].
Surface mobility	Surface mobility is needed to deposit smooth and uniform films [38] but high surface mobility may lead to voids in the film [39].
Chemical surface reactions	Affect the number of active surface sites where a bond may form, number of dangling bonds and the diffusion rate of molecules on the surface [40].
Adsorbed gases	Can affect the film growth mode [37]. May change the surface topography through affecting the film growth mode [41].
Catalytic or inhibitory effects on film growth	Catalysts such as iodine can enable the CVD deposition of copper thin films [42]. Poly(methyl methacrylate) (PMMA) has been proved to inhibit film growth either by passivation the surface against growth or PMMA can be exploited as a lift-off layer [43].
Surface topography	Affects film roughness if the substrate is rough, in ALD surface topography does not change during film growth [42].
Crystallographic orientation	GaAs grows fast on atomically flat 100-surface and slowly on 111-surface. Crystal orientation affects the surface roughness and nucleation centres [44].
Stress effects due to thermal expansion mismatch	Stress between thin film and substrate causes tensile or compressive stress. They will lead to film buckling or cracking. [10].

2.4.5. Physical and chemical properties

The material characteristics of thin films include the physical and chemical properties of the films. *Physical properties,* e.g. electrical properties such as electrical conductivity or electrical insulating properties affect whether the film will be an optimal or a challenging choice when applied to an electronic device. Thermal and mechanical properties of the film will affect to the stress it will experience in regard to that of the substrate. The film's morphology such as crystalline orientation, conformality and microstructure affects the future process steps that can be done on top of the film. Optical properties of the film dictate its use e.g. as anti-reflection coatings.

The *chemical properties* of thin films are variable. Toxicity and carcinogenicity of the film is an important factor when considering the product for the occupational health of the manufacturer or the end user. Corrosion, wear resistant, anti-tarnish and anti-wetting coatings have myriad of applications. The physical and chemical parameters to be considered when choosing a deposition technology are presented in Table 2.

Table 2. Physical and chemical parameters of thin films [2].

Character	Parameters
Electrical	Conductivity for conductive films, Resistivity for resistive films, Dielectric constant Dielectric strength, Dielectric loss, Stability under bias, Polarization, Permittivity, Electromigration, Radiation hardness
Thermal	Coefficient of expansion, Thermal conductivity, Temperature variation of all properties, Stability or drift of characteristics, Volatility and vapor pressure
Mechanical	Intrinsic and residual stress, Anisotropy, Adhesion, Density, Fracture, Ductility, Hardness, Elasticity
Morphology	Crystalline or amorphous, Structural defect density, Conformality/ step coverage, Planarity, Microstructure, Surface topography, Crystalline orientation
Optical	Refractive index, Absorption, Birefringence, Spectral characteristics, Dispersion
Magnetic	Saturation flux density, Coercive force, Permeability
Chemical	Composition, Impurities, Reactivity with substrate and ambient, Thermodynamic stability, Etch rate, Corrosion and erosion resistance, Toxicity, Hygroscopicity, Impurity barrier or gettering effectiveness, Carcinogenicity, Stability

2.5. Conformality

Conformal coating produces films that are of same thickness everywhere on the sample. The benefit of the ALD process is that the film is deposited conformally even on demanding 3D-structures e.g. high aspect ratio pores and sharp features on the substrate. The PVD deposition method does not coat the substrate conformally since it is a line-of-sight deposition method and the film is dependent on source distance to substrate. An example of conformal coating of a very challenging morphology is presented in Figure 6.

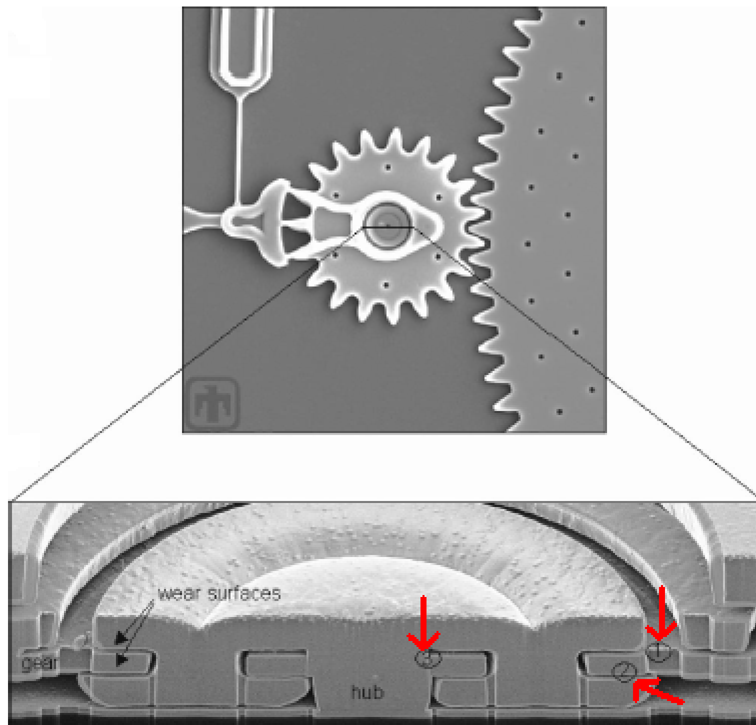

Figure 6. Example of a conformal film growth using a cross section of a micro engine. 10 nm ALD film was deposited as a wear resistant coating. At the two measurement points on the far right depicted with red arrows, the measured film thickness was 10 nm and at the furthest measurement point on the far left, the film thickness was 10,5 nm, which is a result no other film deposition method can achieve [45].

2.5.1. Conformality of low aspect ratio and high aspect ratio structures

The process recipe that is optimal for conformal coating planar or shallow structures will not necessarily produce conformal coating in 3D structures where the surface area is much higher. The exposure time increases as a function of the second power of the aspect ratio. Conformality in 3D pores is enabled by sufficient precursor dose to fill the higher surface area, surface residence time and long enough purge time.

When changing from low aspect ratio structures to high aspect ratio pores, the flow model changes from viscous flow to molecular flow, which causes challenges in conformal coating of the pores.

In a viscous flow, reactions are limited by the surface reaction times and in molecular flow; the rate limiting step is the Knudsen diffusion of the larger precursor molecules. In the viscous flow model the time it takes to completely saturate a surface is relatively short and decreases with higher pressures. However, when in the molecular flow regime, the mean free path between two molecules is so large that the flow is dominated by gas-wall collisions, taking a longer time for a reactant to find an active surface site.

To add to the complexity of the process is that conformal coating in to high-aspect-ratio pores is influenced by precursor reactivity, adsorption-desorption equilibrium process of precursor and reaction by-products [46- 47].

Another way to achieve conformal coating on through wafer high-aspect-ratio pores has been achieved with a modified reactor design. In many cases in the ALD reactor configuration the precursors travel with the carrier gas from the nozzle flow freely on the substrate and flow to the pumps. In the modified ALD reactor configuration the precursors travel with the carrier gas that is forced to travel though the substrate and after that to flow to the pumps. The schematics of these reactor configurations are presented in Figure 7. In this way the cycle times can be nearly as short as with planar substrates and the amount of wasted precursors is reduced [47].

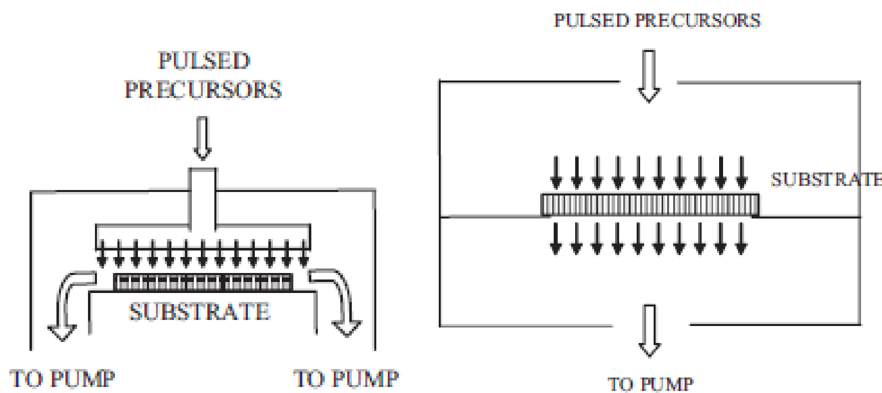

Figure 7. Reactor design schematics of a common ALD reactor configuration (left) and a reactor where the precursors are forced to flow though the substrate (right) [47].

In chapter 6 the results are presented on successfully coating through wafer pores by lifting the substrate from the sides on chips of silicon wafer allowing the gas flow under the sample.

Pores. The hazard with a non-optimized recipe for ultra-high aspect ratio pores is that the ALD mode may change to CVD mode, if the purge time is not sufficient and the reactants and by-products do not have enough time to exit the pore before the next precursor pulse enters [48]. The precursor requirements for high-aspect-ratio pores is that they should be much more volatile than for planar substrates and the precursor by-products should have sufficient volatility in order to be effectively removed from the pores. They should be stable against thermal decomposition [46].

Sharp points. ALD is able to conformally coat rough underlying topographies in which sharp asperities or nano-roughness could potentially limit device performance. ALD nucleation is rather insensitive to the topography induced nucleation. Coating of a surface with sharp points is presented in Figure 8. Conformal ALD films cause the surface topography to change with each deposited layer, ultimately leading to a rounded cap on where the sharp point was and thus decreasing surface area [48].

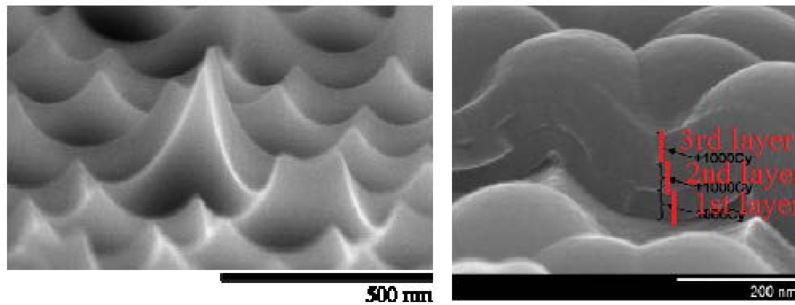

Figure 8. SEM image of a rough surface with valleys and peaks coated with separate three 1000 cycle TiO_2 films, the sample was introduced to atmosphere after each cycle. Uncoated sample (left), coated sample (right) [48].

2.5.2. Conformality Using Templates

ALD nanotubes can be achieved when nanorods are used as a template and coated with ALD thin film and then removing the core. ALD deposited thin films produce conformal coating additionally "outside the pores", on top of rods. If the core material is not removed after ALD, flexible composite material is achieved and if one still anneals this material in oxygen, oxide nanotubes are achieved.

Aerogels can be applied as templates to ALD thin films. Aerogels have been called "solid smoke". They are made cross linking wet gel and then removing the solvent. There are no rivals when it comes to surface area, which is typically >50 m^2/ g [2]. ALD thin films can be used to modify the properties of the silica, aluminum or carbon aerogel for applications such as catalysts or sensors.

ALD can be deposited at low temperatures, which allows the use of polymer fibers as templates. This is presented in Figure 9 [49].

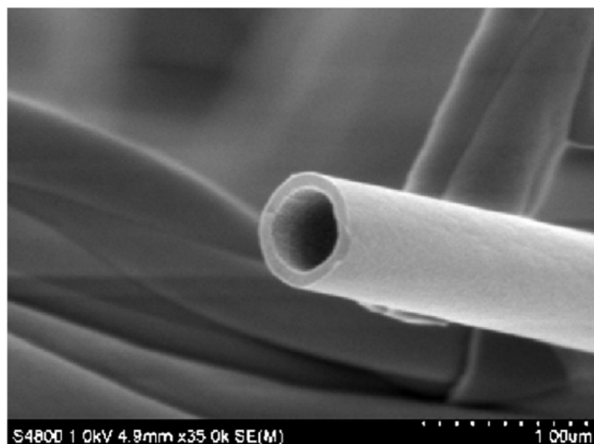

Figure 9. SEM image of Al_2O_3 nanotubes prepared using electrospun poly(vinyl)pyrroline nanofibres as templates. The template core was removed after coating with Al_2O_3, and this left only the hollow nanotube [49].

3. ATOMIC LAYER DEPOSITION (ALD)

This part of the thesis focuses on atomic layer deposition. The chapter begins with a brief insight to history of ALD and explains the growth method. The surface chemistry of ALD is introduced and the precursors requirements. The focus of materials in the experimental work was limited to Al_2O_3, TiO_2 and ZnO so the precursors and reaction mechanisms to deposit them is summarized. To help understanding the complexity of ALD process, the concept of ALD process windows and growth per cycle are introduced. Plasma enhanced ALD (PEALD) is summarized as a method to modify the material properties even at the room temperature.

3.1. History of ALD

ALD was originally known as atomic layer epitaxy (ALE), where the term "epitaxy" stands for "on-arrangement" in the Greek language [8]. The word "epitaxy" was used to emphasize the sequentially controlled surface reactions upon the previously deposited layer. The word was not intended to describe the growth of single crystalline film on a single crystalline substrate with a well-defined structural relationship between the two. Over the years many names were suggested for the process, but atomic layer deposition is now the widely accepted name [8, 19].

The inventor of ALD is not fully clear since different groups have taken credit of inventing the ALD-technology. The most commonly acknowledged origin of ALD is from Finland. T. Suntola and co-workers developed "atomic layer epitaxy" (ALE) according to patent published in the 1970s [9, 44], for which the experiments were made in 1974. In the patent ALD-process was used to deposit element reactants, such as precursors Zn/S, Sn/O_2 and Ga/P to deposit ZnS, SnO_2 and GaP thin films, respectively. Suntola and co-workers demonstrated the ALD-process based on compound precursors using $TaCl_5/H_2O$, $Zn(Mn)Cl_2/H_2S$, $AlCl_3/H_2O$ to deposit Ta_2O_5, Zn(Mn)S, Al_2O_3 thin films, respectively. This research has led to commercial applications of ALD e.g. large-area thin-film electroluminescent displays based on ZnS:Mn introduced already in the 1980s [19].

The less commonly acknowledged origin of ALD comes from the Soviet Union. The group of professor Aleskovskii worked with the technology in the 1960s. The proceedings of a conference organized in 1965 and published in 1967, Shevjakov *et al.* [50] describe using the precursors $TiCl_4/H_2O$ and $GeCl_4/H_2O$ to deposit TiO_2 and GeO_2 thin films, respectively. The first experiments in the group of Aleskovskii were made on high-surface-area silica substrates, but soon dielectric layers were grown on single-crystal substrates. Already in the 1960s, a publication series on the "molecular layering reactions" was started by Kol'tsov and co-workers [9].

3.2. Film growth and Surface Chemistry of ALD

3.2.1. Film growth

What happens in film growth is the phase transition of the material from vapor to solid phase where atoms condense and adsorb on the deposition surface. However, the adsorbed atoms (adatoms) may desorb or experience surface diffusion. If the adatoms become bigger clusters by

aggregation, they reduce the probability of desorption. When the atoms contact the surface they are still mobile and the film growth is based on these atoms merging with others or incorporating more atoms from the vapor phase and forming bigger islands and a continuous film. This is presented in Figure 10. This coalescence occurs due to the minimization of surface energy and surface area [10].

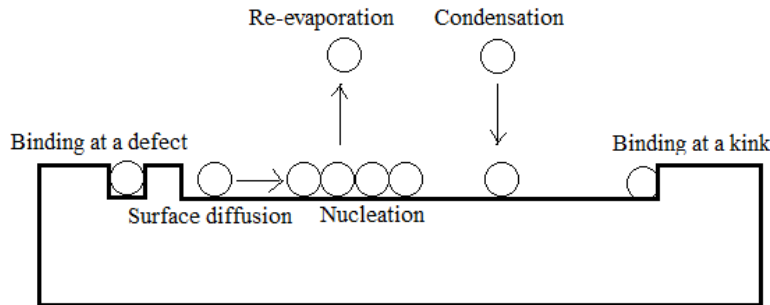

Figure 10. Thin film growth surface processes [10, p.78].

Sticking coefficient. Film growth may take place because atoms attach to the surface either through chemisorption with strong bonds resulting that the probability that the atoms leave the surface through desorption or diffusion is low. This is called the sticking coefficient. In addition, the atoms can bond trough physisorption with weak bonds and those atoms are loosely bound. The process parameters (e.g. temperature) can be designed in a way that only chemisorbed atoms stay on the surface and physisorbed atoms desorb. If the sticking coefficient is high, the atoms will come to rest on the surface, if the sticking coefficient is low, only the energetically favorable attached atoms will stick and others will desorb [10].

Adhesion is a challenge in thin film technology where poor adhesion is more common than good adhesion. Poor adhesion can arise from material properties and reduced surface cleanliness and deposition method. Some materials, e.g. noble metals do not react and no bond formation across interfaces occurs. This, however, may be overcome by using an adhesion layer between the two materials. Titanium and chromium are commonly used adhesion layer materials due to their bond forming abilities in addition to other oxide forming metals, e.g. aluminium. The strength of the adhesion may be tested by tape test where a common office tape is attached to the film surface and pulled off. If the film does not peel off with the tape, it has passed the tape test. Surface cleanliness is an important factor. Impurities and residues from previous process steps will lead to poor adhesion. The deposition method used in film growth affects adhesion if, for instance, in sputtering the energetic atoms kick off loosely bound atoms or contaminants [10].

Surfaces and interfaces. The deposition process and substrate affect the surface roughness. High temperature processes generally make smoother films. Doping of the film can make otherwise a smooth film rough, e.g. doped polysilicon has a rough surface, but undoped polysilicon has a smooth surface. The growing film may take the form of the substrate (epitaxy). A smooth substrate may result into smooth film. Interfaces between two material layers can vary from: 1. abrupt interface, 2. interface with interfacial film, 3. diffused interface, 4. reacted interface and 5. pitted interface [10]. These are presented in Figure 11.

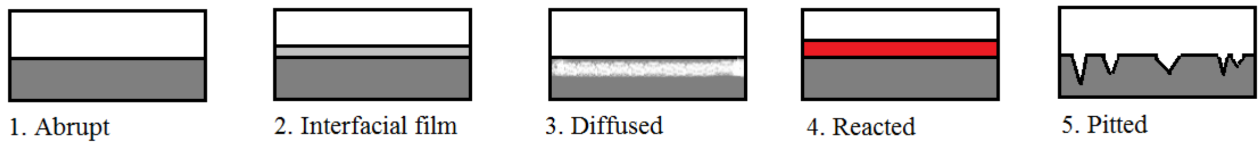

Figure 11. Different interface structures [10, p.83].

Thermodynamics can be used to estimate whether a reaction between two interfaces is possible or not. Every system seeks to achieve a minimum of free energy. The difference of Gibbs free energy for products and reactants tells if a reaction can happen. If the result is negative, the reaction can take place. If the reaction is positive the reaction cannot happen. An adhesive layer can be used to deposit a film on a substrate that otherwise would not be possible [10].

3.2.2. The surface chemistry of ALD

The surface chemistry of ALD can be described in terms of the following features: self-terminating reactions, adsorption and adsorption kinetics to form monolayers, chemisorption of precursors on the surface, and saturation of the surface. Additionally, growth modes are presented.

Self-terminating reactions. ALD is based on the sequential use of self-terminating gas–solid reactions [9]. The two gaseous precursor that contribute to the film growth can be named A and B. In the process, the precursors are cycled ..ABABAB.. as many time as needed to achieve the desired film thickness. The reactants that contribute to the film growth chemisorb on the surface. Between the precursor pulses there is a purge step that removes the un-reacted precursor and reaction byproducts before the next precursor pulse. The reactions are irreversible and they will saturate the surface. [9, 19].

Adsorption

Adsorption is an interaction between the precursor molecule and the substrate surface. If the interaction is strong the type of absorption is *chemisorption* and if the interaction is weak, the type of absorption is *physisorption* [51]. In chemisorption, a chemical bond is formed between the precursor molecule (adsorptive) and the substrate surface (adsorbent). Chemical bonds may be broken in the process. In chemisorption, the substrate surface accepts only one monolayer of the adsorbate [51]. In physisorption there are no or minimal structural changes between the molecule and the surface, but the interaction is based on Van Der Waals force in which the attraction arises from interaction of dipoles in the molecules, which in turn, allows the absorption to take place in multilayers [9, 51].

A way to describe the ALD-process is that the process utilizes the difference between chemical and physical adsorption. By the time the first reactant atoms of molecules reach a solid surface, there is a strong interaction by chemisorption. Subsequent layers tend to interact with the surface less strongly by physisorption. If the substrate surface is heated sufficiently one can achieve a condition that only the chemisorbed layer remains attached [9, 44].

Adsroption kinetics. Precursor molecules attach to the surface and they might also desorb, depending on their sticking coefficient. Parameters as temperature, partial pressure of the reactant and reactant concentration affect the rate in which the molecules attached and detach per unit time.

Adsorption can be considered reversible, which is presented in reactions (Equation 2) and (Equation 3). *A* represents the gaseous compound and ||* is the surface site [9]

$||^* + A(g) \rightarrow {}^{ra}||^* A,$ **Equation 2. [9]**

$||^*A \rightarrow {}^{rd}||^* + A(g)$ **Equation 3. [9]**

ra= adsorption rate of attaching molecules per a time unit
rd= desorption rate of detaching molecules per a time unit

Reversible and irreversible reactions. Irreversible reactions are needed for the self-terminating ALD reactions to avoid desorption of material from the substrate during the process. Physisorption is always reversible and chemisorption can be either irreversible or reversible [9]. The amount of material that adsorbs during gas–solid reactions can depend on various ways that are presented in Figure 12. In *irreversible* and saturating reaction the amount of adsorbed molecules does not change after the precursor pulse is over and the purge step has begun (panel a). In *reversible* and saturating reaction the amount of the adsorbed molecules diminish after the precursor step is over (panel b). Irreversible and reversible reactions can occur in the same process step, but the reversible reaction does not contribute to the film growth (panel c). An irreversible reaction may not be saturating, if the amount of adsorbed molecules is continuing and does not reach saturation before the process step is over, which is the same for CVD process (the amount of adsorbed material increases with increasing amount of precursors) (panel d). In order for the reaction to function in optimal way, the irreversible reaction should not be interrupted (panel e) [9].

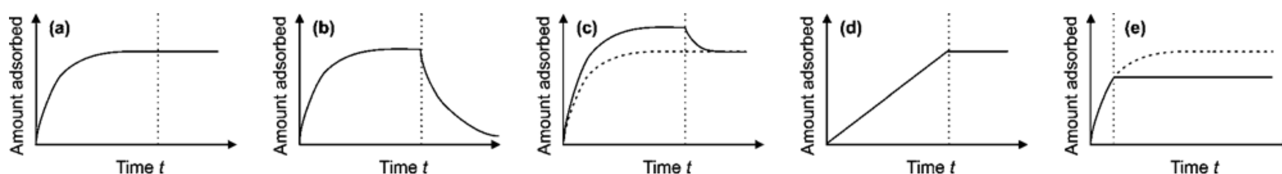

Figure 12. Amount of adsorbed material can change with time in different scenarios: (a) saturating adsorption that is irreversible (self-terminating reaction), (b) saturating adsorption that is reversible, (c) combination of irreversible and reversible saturating adsorption, (d) adsorption that is irreversible and non-saturating, and (e) saturating adsorption that is irreversible and it is not allowed to saturate. The vertical dashed line marks the end of the reactant supply and the beginning of a purge or evacuation [9].

Monolayers. The type of monolayer differs according to the interaction between the adsorptive and absorbent. The type of monolayer depends on three factors: *chemisorption, physisorption and ALD* deposited films [9, 51]. In *chemisorption,* the monolayer is described by the amount of adsorbed molecules which is needed to occupy all adsorption sites. In *physisorption* the monolayer is described by the amount of adsorbed molecules needed to form a close-packed array. In *ALD* deposited films the monolayer is described as the plane where the material is grown on top of the substrate in the preferred orientation of growth. The three different types of monolayer are presented in Figure 13 [9, 51]. However, only in rare cases one monolayer of material is deposited on a surface during one cycle. Commonly only 5-50 % of a monolayer is deposited [20].

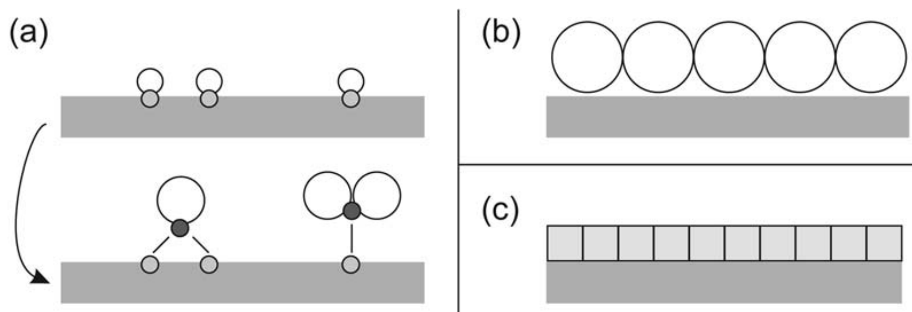

Figure 13. Three types of ALD monolayers: (a) a chemisorbed monolayer (above: the reactive sites of the substrate before chemisorption, (b) a physisorbed monolayer, (c) a monolayer of the ALD-grown material [9].

Chemisorption mechanisms. There are three main classes of chemisorption mechanisms for the self-terminating reactions. They are 1) *ligand exchange* [9, 51], 2) *dissociation* [9, 52] and 3) *association* [9, 52].

In *ligand exchange*, the gaseous reactant molecule (ML_n) arrives to the surface and the ligand (L) of the molecule forms a bond with the surface group ($||-a$) and forms a reaction by-product (aL), which will be removed in the purge step. The molecule (ML_{n-1}) chemisorbs to the surface. This is presented in (Equation 4). The ligand exchange reaction may continue on the surface provided that there is a free reactive site nearby and the molecule still has a bond to spare with a ligand [9, 51].

$||- a + ML_n\ (g) \rightarrow ||- ML_{n-1} + aL\ (g).$ **Equation 4. [9]**

In *dissociation*, the gaseous reactant molecule is broken onto the reactive sites on the surface ($M'-Z$) and the reactant molecule forms surface species with more than one reactive sites on the surface. This is presented in (Equation 5) [9, 52].

$||M' - Z|| + ML_n\ (g) \rightarrow ||M' - L + ||Z - ML_{n-1}.$ **Equation 5. [9]**

In *association*, the gaseous reactant molecule forms a coordinative bond with a reactive site on the surface and is chemisorbed without a release of ligands (Equation 6). The coordinative bond is similar to a covalent bond, but instead of the two atoms giving the electrons to the bond as is the case in the covalent bond, in the coordinative bond the electrons come only from the other atoms [9, 52].

$||+ ML_n(g) \rightarrow ||ML_n.$ **Equation 6. [9]**

Different chemisorption mechanics are presented in Figure 14.

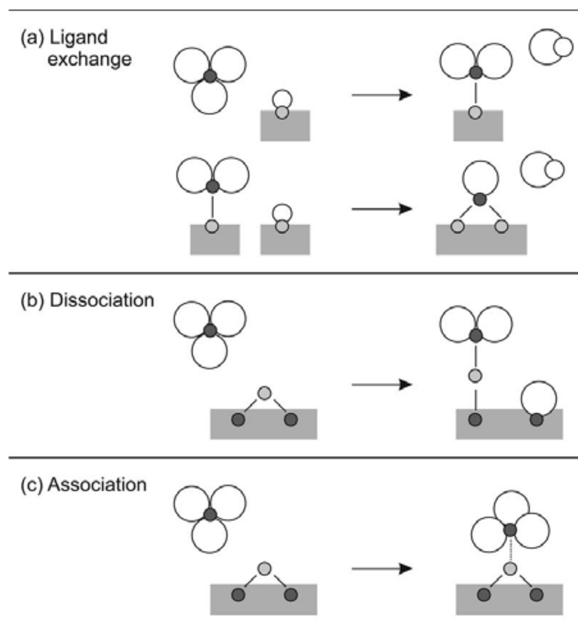

Figure 14. ALD chemisorption mechanisms: (a) *ligand exchange* reaction of the *MLn* reactant with surface "−*a*" groups, the byproduct *aL* is released, (b) *dissociation* of the *MLn* in surface *M–Z* sites, and (c) association of the *MLn* species onto the surface [9].

Factors causing saturation. There are two factors that cause the saturation of the surface with adsorbed species in a self-terminating gas–solid reaction, as shown in Figure 15: 1. *steric hindrance of the ligands [9, 53]* and 2. *the number of reactive surface sites [9, 54]*. Steric hindrance of the ligands can cause the ligands of the chemisorbed species to shield like an umbrella part of the surface from being accessible to the reactant and the reactant finds the surface being full. There may not be enough of *bonding sites* on the surface that would require for getting a full surface of ligands, because there is a not free reactive site for the abundance of ligands. Irrespective of the factor causing saturation, the chemisorption coverage equals one after the self-termination of the reactions [9].

The temperature dependency of saturation was studied in [23]. Thickness per cycle was tested by repeating the same pulse for multiple times and the film thicknesses were calculated at different stages of repeated pulses. Al_2O_3 films deposited at 300 °C were closer to saturation than films deposited at 110 °C.

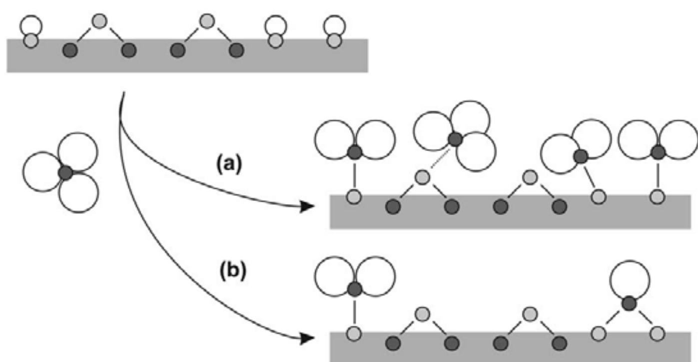

Figure 15. Saturation of irreversible chemisorption of the substrate and factors leading to it: (a) steric hindrance of the ligands and (b) number of reactive surface sites [9].

The amount of material that is adsorbed in irreversible and saturating chemisorption is defined by the reaction mechanisms and the factor causing saturation. The surface chemistry allows the maximum number of reactive sites on the substrate surface for the ligand exchange reaction. Then the most ligands are released in the gas phase in the reaction chamber, the reaction will continue until there are either no more reactive sites left or the steric hindrance declares that the surface is saturated, a monolayer is finished and the highest growth per cycle (GPC) is achieved [9]. Growth per cycle can be described as the film growth during an ALD AB cycle, which is may be less than a monolayer, e.g. due to possible hindrances.

Model I represents the maximum GPC from the size of the ML_n reactant shown in Figure 16(a). The size of the ML_n reactant is calculated from the density of the liquid reactant and the area covered by the reactant, assuming a close-packed monolayer of ML_n [14]. Model I corresponds to a physisorbed monolayer of the ML_n molecules. Because the chemisorbed ML_z species differs from the ML_n reactant, Model I gives at best a rough estimate of the achievable GPC. [55-56].

Model II represents the maximum GPC from the size and geometry of the adsorbed ML_z species [Figure 16 (b)]. The sizes of the ligand *L* and the metal *M* must be known. The bond lengths and angles must be known or assumed for the adsorbed species. In Model II, the GPC increases in steps with decreasing size of the adsorbate ML_z. [9, 53].

Model III represents the maximum GPC from the size and number of the adsorbed ligands *L* [Figure 16 (c)]. A theoretical maximum amount of ligands adsorbed is calculated assuming a close-packed monolayer of the ligands. [3, 58].

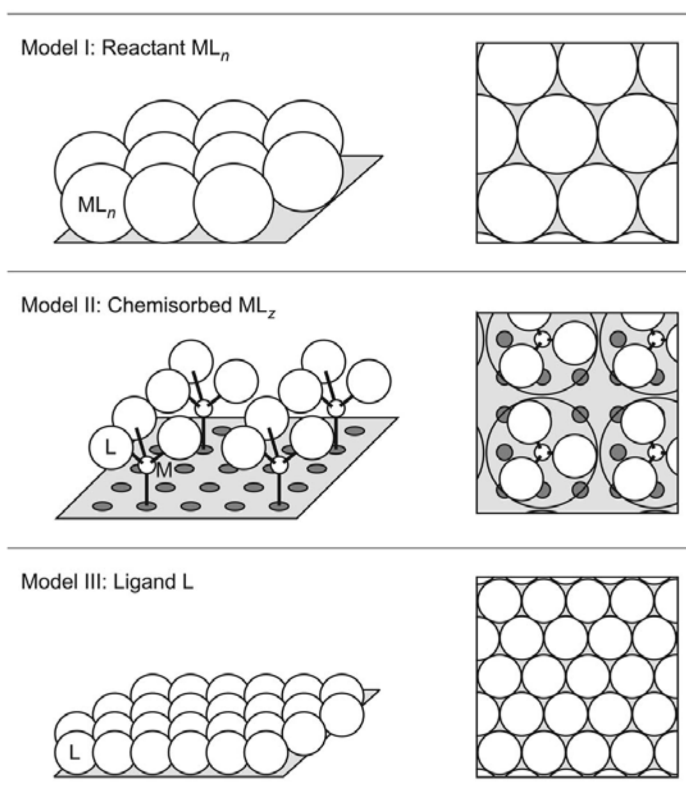

Figure 16. Above: Illustration of maximum GPC from size of the *MLn* reactant (Model I) [55-56]. Middle: maximum GPC from from size and ligands (Model II) [53]. Bottom:

maximum GPC from the size and number of ligands *L* (Model III) [58]. Left: side view, right: top view [9].

The growth per cycle (GPC) means the absorbed layer of material per one reaction cycle [9] and it may vary with temperature, as illustrated in Figure 17. The decrease of GPC with temperature is presented in panel (a). In this case the number of reactive surface sites affects the amount and/or the type of chemisorbed species. The case where the GPC stays constant with temperature is presented in panel (b). An example of this case is, if steric hindrance causes saturation and the number of reactive sites does not affect the amount of adsorbed species. Also presented in panel (b) is the case when the GPC settles to different constant values at different temperatures. The increase GPC with increasing temperature is presented in panel (c). At higher temperatures, energy barriers may be overcome and reactions occur, which would not occur at lower temperatures. The case where the GPC increases first and then decrease with temperature is presented in panel (d). First, some reactions are activated with increasing temperature, after which the decreasing number of reactive sites starts decreasing the GPC [9]. For example, when depositing Al_2O_3 using TMA and water, increasing the deposition temperature by 100 °C will decrease the GPC by 20 % using the temperature range of 180 °C to 300 °C. This is caused by the reduction of -OH groups with increasing temperature [9, 19]**.**

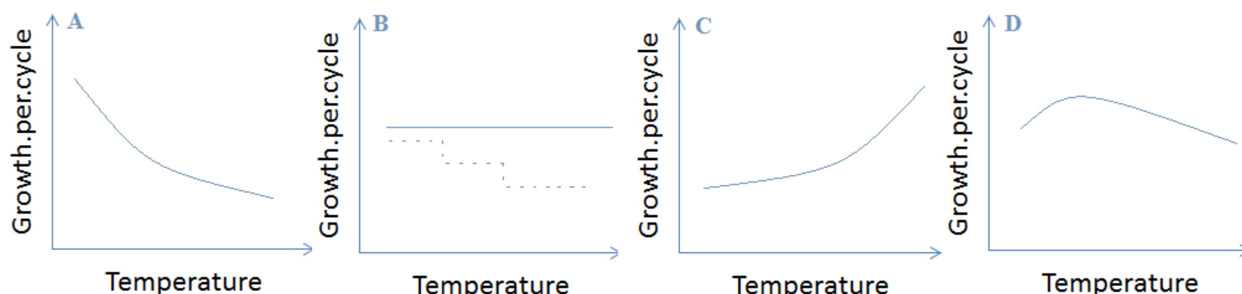

Figure 17. The GPC can vary according the ALD processing temperature in the *ALD window*: (a) decreasing GPC with increasing temperature, (b) constant GPC with increasing temperature (it is possible for GPC to vary at different temperature ranges, presented by the dashed line), (c) increasing GPC with increasing temperature, and (d) first increasing and then decreasing GPC with increasing temperature [9].

Growth per cycle can be calculated by the concentration of surface groups that take part in the reaction cycle, e.g. in the case of TMA and water process, the -OH groups [49]. The thickness of GPC is commonly 0.01-0.1 nm (depending on material, reactants, temperature). In reality, GPC is typically in ALD in the range of 5-50 % of a monolayer of the material with the full monolayer growth being exceptional [49]. During the reaction cycle several reactions can take place at the same time and cause steric hindrance. This means that one -OH group does not always bind one aluminum atom to the surface. Depending on the -OH concentration on the surface, binding one aluminum atom may take three -OH groups. Or by dissociation or association of -OH groups binding the aluminium atom may take only one oxygen. The different reaction possibilities of binding one aluminium atom to the oxide surface are presented in Figure 18 [49, 20].

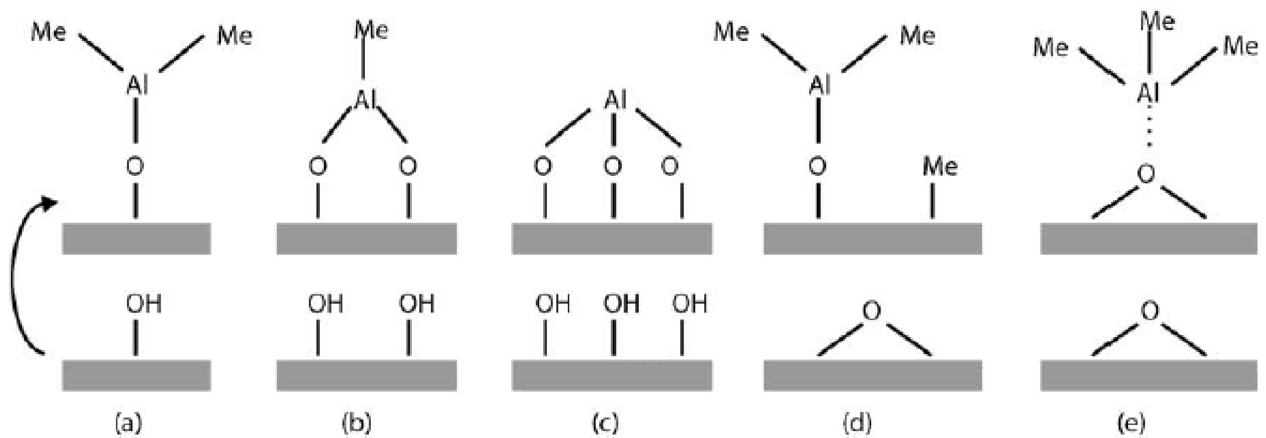

Figure 18. Possible reactions of trimethylaluminum (TMA) and water on oxide surface. a.) ligand exchange with one OH group, b) ligand exchange with two OH groups, c.) ligand exchange with three OH groups, d.) dissociation of OH groups, e.) association of OH groups [49].

During each ALD process cycle in the first half reaction the absorbed mass of the surface increases. This mass includes the reacted species and the ligands. During the purge step the absorbed mass stabilizes and the ligands leave causing a slight reduction in the mass. Fitting a line in the growth curve gives the average growth rate, which is presented in Figure 19 [20].

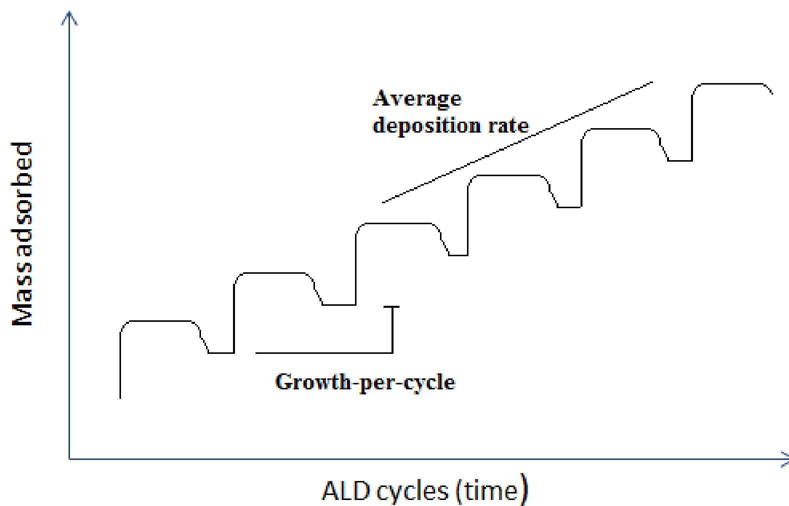

Figure 19. Mass deposition during increasing ALD cycles [20].

Growth modes in ALD. Growth mode decides the way the ALD deposited material and all other deposited thin films are arranged on the surface [9]. The growths modes are: two dimensional growth [59], island growth [60] and random deposition [61]. The *two-dimensional growth* is presented in Figure 20a. The deposited material settles in the lowest unfilled material layer and one monolayer of the ALD-grown material covers the substrate completely. However, this growth mode is not universally valid. The *island growth* is presented in Figure 20b. The new material units are attracted to deposit on the previously grown ALD material and this is the growth mode case in several ALD processes. The *Random deposition* is presented in Figure 20c. It is a statistical growth mode, where the new material units are deposited with an equal probability on all surface sites. Because of the self-terminating reactions, random deposition results in smoother layers in ALD than in continuous deposition processes ("shower model" versus "rain model" of

random deposition). Random deposition has been concluded at least for two ALD processes [9, 10].

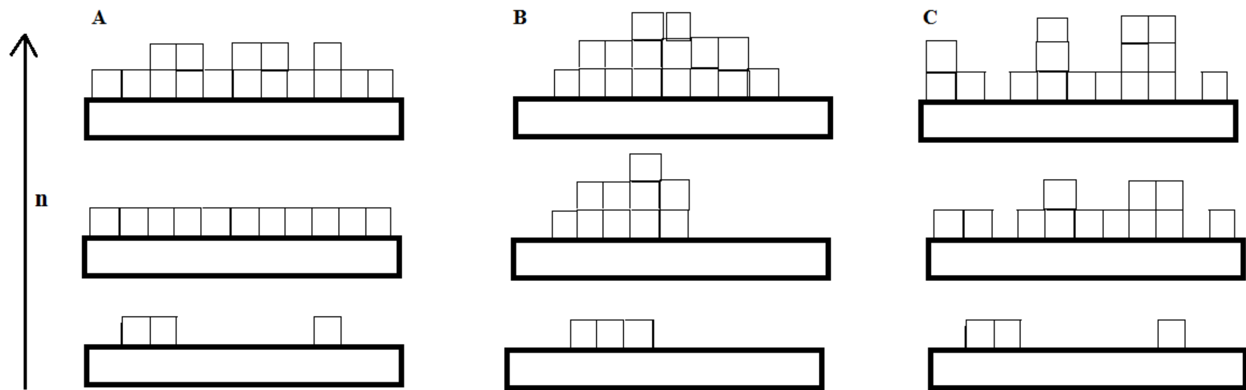

Figure 20. Schematic illustration with increasing number of reaction cycles *n* of selected growth modes possible in ALD: (a) two-dimensional growth, (b) island growth and, (c) random deposition [9].

3.3. *Precursor requirements and process windows*

The most essential issue in ALD thin film technology is the precursor chemistry. The precursors must be reactive, volatile and thermally stable [62]. They may be gases, liquids or solids. Volatility of the liquid substances is dictated by their vapor pressure. The precursors have to be gaseous or vaporizable under the process reaction temperature [63]. Solid substances have a low vapor pressure; nevertheless it is not a hindrance, but a challenge that needs a special equipment to characterize the vapor pressure. Precursors must chemisorb on the surface or react rapidly with the surface groups and react aggressively with each other [62, 63].

Solid precursors are not regarded as optimal in CVD because in that method a continuous and homogenous reactant feed is needed [64]. With the sublimation of the solid precursors the rate is varying, because sintering occurs. ALD is more permissive, because the only requirement is that during the reactant pulse the surface must be saturated but due to the self-limiting growth mechanism constant precursor feed is not required and therefore solid precursors are more easily adapted [62-63].

The metal precursors used for CVD are generally suitable for ALD provided that certain requirements are fulfilled [62]. Since ALD deposition technique allows much more reactive precursors than CVD technique so many precursors have been synthesized for ALD [62-63]. To avoid uncontrolled reactions, sufficient thermal stability of the precursors is needed in the gas phase and as well on the substrate within the deposition temperature range which is typically 80-500 °C [62-63]. In the CVD method, a constant flux of precursor vapor is needed to obtain a controlled process. ALD, in turn relies on self-limiting reactions and only a sufficient amount of precursor vapor is required during one pulse to cover the adsorption sites on the surface, the excess will be removed by the inert gas purge. Reaction byproducts should be inert and not interfere with the film growth [64].

Many properties are required of a good precursor in order to develop successful ALD processes [65]:

- Sufficient vapor pressure at a temperature at which thermal decomposition is negligible
- Volatility
- Self-limiting deposition reactions
- Non-corrosive, non-toxic
- Stable during transport and no ageing during storage

Temperature is an important factor. The reactant must decompose in the gas phase at the selected temperature. No self-decomposition is allowed below the deposition temperature, because decomposition destroys self-controlled nature of the reaction. The reaction temperature should be high enough for chemisorption. Thermal stability of the precursor is enhanced by chelating ligands, which attach to the metal by more than one bond. Low melting points are shown by precursors that have low symmetry, which can be provided by decreasing the symmetry of the ligand and by lengthening alkyl groups on ligands (8).

Most *volatile* precursors are monomeric and the structure is achieved by having sufficiently bulky ligands surrounding the metal center [65]. The ligands need to be removed by another reactant (H_2O, O_2, O_3) to make pure films. Volatility is affected by several factors. Smaller molecules are more volatile than large. Monomers are more volatile than dimers. Polymers are usually not volatile. Non-polar molecules are more volatile than polar molecules, because polarity binds molecules together making them bigger. Surface reactions are more likely to be fast and complete when the metal-ligand bonds are weaker than the bonds to be formed in the deposited film. Thus pure metal oxide films are formed more quickly from weaker metal-nitrogen bonds or metal-carbon bonds, than from precursors with stronger metal-oxygen bonds [65].

Reactions are *self-limiting* when they are fast enough to be completed before any thermal decomposition occurs. There should be no self-decomposition below the deposition temperature. Decomposition destroys self-controlled nature of the reaction.

Corrosive effects are often seen with precursors containing halogens, which should not etch the substrate or the growing film during the process. *Toxicity* cannot be predicted from the structure of a precursor, but precursors containing toxic elements, such as arsenic, can be expected to be toxic no matter what ligands are used with them [65-66].

The precursors must be *stable during transport* and usually they travel by sea freight. No *ageing* is allowed for during storage [65].

Challenges of the precursors. All reactants have their positive and negative features in respect to the reactivity, stability, gaseous by-products and impurities left in the film. Organometallic *alkyls* have a carbon-metal bond and they are very reactive in general. However, many alkyls are not stable and this limits the choice of deposition temperature in order to avoid decomposition of the reactants. In the class of halides, *chlorides* are reactive, stable in many temperatures and available for many metals. The resulting film may suffer from chlorine residues and of corrosive hydrochloric acid (HCl) that is a byproduct of a secondary reaction. *Hydrides* of the non-metal elements are: water (H_2O), ammonia (NH_3) and hydrogen sulfide (H_2S) and their benefit is that they have high stability and reactivity in broad temperature range even at high temperatures.

Ozone is used for deposition of oxides from compounds that do not react with water. The negative side to ozone is that it is unstable and the deposited film may catalyze the decomposition of ozone. This limits conformality in high aspect ratio pores. *Plasma enhanced ALD* (PEALD) enables the use of molecular elements (O_2, H_2, N_2) that would not be reactive enough otherwise. The drawback of PEALD is that the conformality of PEALD film is limited due to the finite lifetime of radicals and charged species. [25].

Process windows. The ALD process is sensitive to control and the settings for each part of the process cycle require carefully considered adjustments in order to achieve a self-limiting and saturating process and high quality film. The deposition temperature and purge cycle times need to be optimized to achieve the self-limiting growth. The adjustment of temperature and purge parameters within the optimal ALD windows have an effect on the growth per cycle (GPC).

ALD temperature window. Tuomo Suntola introduced the concept of an ALD window, which indicates the temperature range where the thin-film growth proceeds in a self-limiting manner. Outside the optimal ALD window, the growth is limited:

At low temperatures by [11, 67]

- Reactant condensation/ physisorption. If the reactants or by-products from the previous stay behind when the next process pulse and reactant arrive, they can condensate or physisorb to the surface. This can lead to parasitic CVD mode.
- Insufficient precursor reactivity. The reactant is unable to overcome the activation energy necessary to chemisorb on the surface.

At high temperatures by [11,67]

- Precursor decomposition. The precursors decompose at high temperature before they can react with the second reactant of the cycle (reactant A or B in AB cycle)
- Precursor desorption. The precursors desorb at high temperature before they can react with the second reactant of the cycle (reactant A or B in AB cycle)

The above mentioned issues destroy the self-limiting growth mechanism and the constant growth rate. ALD temperature window is presented in Figure 21.

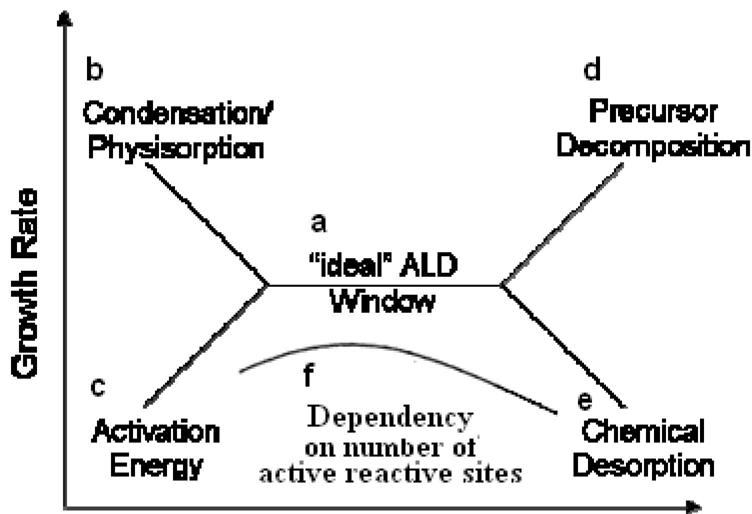

Figure 21. (a) The ideal ALD window, (b) growth rate limited by precursor condensation or physisorption, (c) insufficient reactivity, (d) precursor decomposition, (e) precursor desorption (11). Sometimes if the deposition rate is dependent on the number of available reactive sites as in (f), no actual ALD window is observed [67].

ALD purge window. Besides the ALD temperature window, a similar window of process parameters can be applied to the purge time. The purge time is a key factor that enables the self-limiting growth during an ALD cycle. An insufficient purge step in the process cycle can result in poor removal of the unreacted precursors or the reaction by-products can lead to overlap of two precursors in the process chamber. This in turn allows the ALD process to transition to a CVD process. The ALD purge window applies to ALD temperature window that is presented in Figure 21 [42].

When the purge time is optimal, the ideal ALD processing window is achieved. If the purge time is too short and the growth rate is low, then there process is in CVD mode and the reactants are more likely to react in the gas phase than on the surface. If the purge time is too short and the growth rate is high, the excess reactants will remain in the reaction chamber and react with the next precursor pulse increasing the growth rate. This can occur inside of a high aspect ratio pore. If the purge time is too long and the growth rate is low, desorption takes place. If the purge time is too long and the growth rate is high, thermal decomposition of the adsorbed species may take place and lead to film contamination and contributes to the growth rate [42].

3.4. Materials and reaction mechanisms

The focus of materials in this thesis is limited to aluminium oxide (Al_2O_3), titanium dioxide (TiO_2) and (ZnO) using the trimethyl aluminium and water (TMA + H_2O), titanium tetrachloride and water ($TiCl_4$ + H_2O) and diethyl zing and water (DEZ + H_2O) processes. The reaction mechanisms and processes are introduced.

3.4.1. Al_2O_3: TMA + H_2O process

In order to deposit alumina (Al_2O_3) films, the TMA + H_2O process is needed (68-71). The process is presented in Table 3

Table 3. TMA + H_2O process [22, 68].

$Al(CH_3)_3 + H_2O$	
1st step (A)	$(-OH)^* (s) + Al(CH_3)_3 (g) \rightarrow OAl(CH_3)_2^* (s) + CH_4 (g)$
2nd step (B)	$OAl(CH_3)_2^* (s) + H_2O (g) \rightarrow AlOH^* (s) + CH_4 (g)$

The TMA - water process temperature region is 30-300 °C with 300 °C being the maximum limit to all organometallic aluminium precursors [9]. However, temperature up to 500 °C has been reported for the process [23].

3.4.2. Al_2O_3: TMA + Ozone (O_3) process

In energy-enhanced processes, typically utilizing energetic but unstable reactants such as ozone or plasma, problems with conformality may arise through reactant decomposition, at least on 3D substrates [6]. The TMA + ozone process is presented in Equation 7.

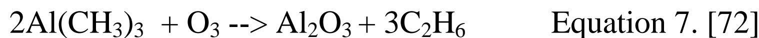

$2Al(CH_3)_3 + O_3 \rightarrow Al_2O_3 + 3C_2H_6$ Equation 7. [72]

There is no significant difference on growth rate or film uniformity when using H_2O and O_3 as oxygen source. The difference between is that at low temperatures the growth rate in H_2O process is higher than in O_3 process. At high temperatures, above 350 °C in H_2O process the growth rate becomes slower while in O_3 process the growth rate slightly increases. The decrease of growth rate in H_2O process is caused by the enhanced dehydroxylation of the Al_2O_3 surface. The O_3 process is controlled by the amount of decomposition of O_3. The difference between growth rates of using O_3 and H_2O processes as a function of growth temperature is presented in Figure 22 [72].

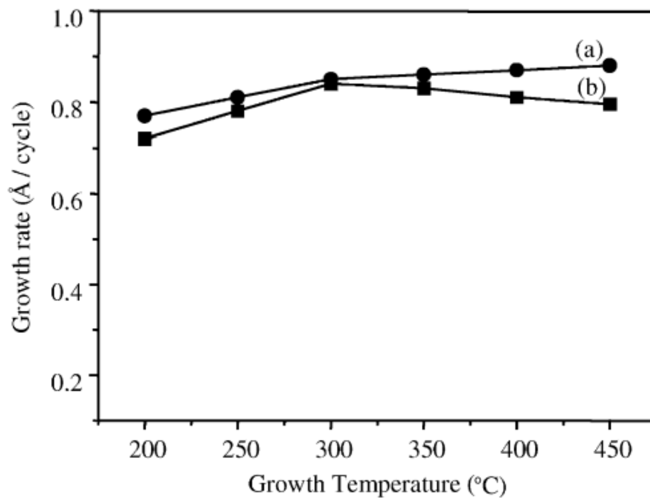

Figure 22. Comparison of growth rates as a function of growth temperature between (a) O_3 and (b) H_2O [72]

3.4.3. TiO_2: $TiCl_4$ + H_2O process

In order to deposit titania (TiO_2) films the $TiCl_4$ + H_2O process is needed. An ALD deposition cycle is shown in Figure 23. Normally one growth cycle consists of four steps: 1) Exposure of the first precursor, 2) purge of the reaction chamber, 3) exposure of the second precursor, and 4) a further purge of the reaction chamber. The growth cycles are repeated as many times as required for the desired film thickness [8, 73].

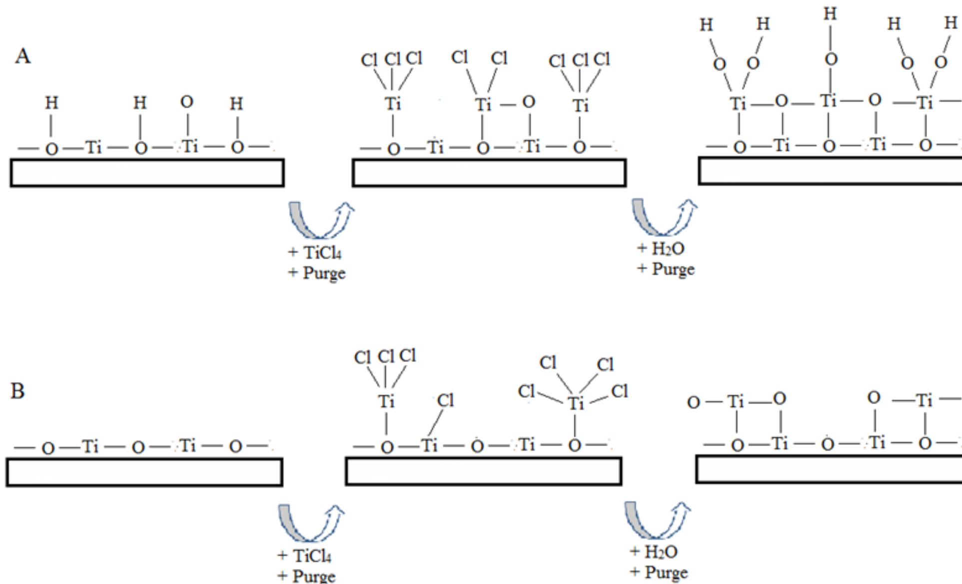

Figure 23. An example of ALD film deposition cycle using the $TiCl_4$ - H_2O processes: (a) reaction with hydroxyl group terminated surface and (b) dehydroxylated surface after the water pulse [8].

Assuming that $TiCl_4$ reacts with one surface hydroxyl group the two step reaction is presented in Table 4. When the surface temperature exceeds 400 °C and $TiCl_4$ adsorbs on such surface, exchange reactions are possible. For instance, in the exchange reaction with two hydroxyl groups two chlorine ligands can be released from adsorbing $TiCl_4$ [74]. The reaction process is presented in Table 5.

Table 4. $TiCl_4 + H_2O$ process. Reaction with one surface hydroxyl group [74]. (* indicates the surface species.)

$TiCl_4 + H_2O$ process (reaction with one surface hydroxyl group)	
1st step (A)	(-OH)* (s) + $TiCl_4$ (g) → (-O-)$TiCl_3$ (s)* + HCl (g)
2nd step (B)	(-O-)$TiCl_3$ (s)* + 2 H_2O (g) → (-O-)TiO(OH)* (s) + 3 HCl (g)

Table 5. $TiCl_4 + H_2O$ process. Exchange reaction with two hydroxyl groups [74]. (* indicates the surface species.)

$TiCl_4 + H_2O$ process (exchange reaction with two hydroxyl groups)	
1st step (A)	2(-OH)* (s) + $TiCl_4$ (g) → $(\text{-O-})_2TiCl_2$* (s) + 2HCl (g)
2nd step (B)	$(\text{-O-})_2TiCl_2$* (s) + 2 H_2O (g) → $(\text{-O-})_2Ti(OH)_2$* (s) + 2 HCl (g)

3.4.4. ZnO: DEZ + H_2O process

In order to deposit zinc oxide (ZnO) films the diethyl zinc (DEZ) + H_2O process is needed. The two step process is presented in Table 6.

Table 6. DEZ + H_2O process [75- 76] (* indicates the surface species)

DEZ + H_2O process	
1st step (A)	(-OH)* (s) + $Zn(C_2H_5)_2$ (g) → $OZn(CH_2CH_3)$* **(s)** +C_2H_6 (g)
2nd step (B)	$OZn(CH_2CH_3)$* (s) + H_2O (g) → OZn(OH)* (s) + C_2H_6 (g)

According to mass spectrometry measurements much more ethane is released during the DEZ half-reaction than during the oxidizing step at all temperatures, but the ethane is shown as balanced between these two half-reactions for simplicity [75].

ZnO is an *n*-type metal oxide semiconductor and undoped ZnO films can have a low resistivity resulting from oxygen vacancies that produce electron charge carriers. [76].

3.5. Limitations of ALD

The major limitation of ALD is its slowness. Usually only a fraction of a monolayer is deposited in one cycle. Typical deposition rates are 0.1-1 nm/h on flat substrates and on substrates with high-aspect-ratio 3D structures, the deposition rate is even slower. Therefore it is not very practical to grow micrometer-thick films by ALD. The slow growth rate can be compensated by processing large batches of substrates in one process. In microelectronics single-wafer processing is preferred, but fortunately the films needed for most cases are very thin and thus the slowness of

ALD is not such an important issue. However, the spatial ALD reactor has been stated to be able to achieve deposition rate up to 1nm/s [77] and an industrial throughput of 3000 wafers/hour, so the advancing reactor design may help to overcome the slowness.

The selection of ALD-deposited film materials is wide, but many technologically important materials (Si, Ge, Si_3N_4, several multicomponent oxides, certain metals) cannot be deposited by ALD in a cost-effective way.

The impurity content of the films depends on the completeness of the reactions. ALD technology uses chemistry and thus there is a risk of having precursor residues as impurities on the sample. In typical oxide processes where metal halides or alkyl compounds are used together with water as precursors, impurities found in the films are at the 0.1–1 atom% level [73].

Because of their unique impurity background, ALD-grown materials may have different properties than those made by PVD [8]. In PVD methods the environment is much cleaner due to the high vacuum used and the lack of precursor compounds with unwanted elements. The different properties have been seen in transition metal nitride films, where small variations in composition markedly affect the electrical properties. Microstructure and morphology of ALD films may differ from PVD films. Therefore the ALD materials have to be characterized thoroughly before use. Post-deposition treatments, particularly high-temperature annealing under varied atmospheres may have both beneficial and adverse effects on ALD thin film purity and microstructure [73].

Ideally all reactors using the same precursors and the same recipe should produce the same amount of material on the substrate, but this is seldom the case. Most processes have some non-ideal factors e.g. the reactants may behave unexpectedly and the reaction is not irreversible or the reactants start to decompose. The reaction byproducts may not be inert and interact with the just deposited surface and may block further growth [25].

4. THIN FILM CAPACITORS

The motivation of this chapter is to introduce the background of thin film capacitors, before the results of the experimental work on capacitors is presented in chapter 6.

4.1. Capacitors

A capacitor is an electronic component designed to store energy that is built of a pair of conductors, the top and bottom electrodes, separated by an insulator, a dielectric. This is illustrated in Figure 24A. One way to enhance the capacitance is to increase the surface area of the electrodes by applying 3D structures such as trenches, seen in Figure 24B and Figure 25b. The dielectric can be a vacuum or a material. When there is a voltage potential difference between the conductors, an electric field is present in the dielectric and the energy of the capacitor is stored in that electric field, and the field produces a mechanical force between the plates [6, 78].

A capacitor consists of an insulating layer (insulation to the substrate) bottom electrode e.g. silicon oxide, a dielectric layer and an upper electrode and a passivation layer e.g. PECVD-oxide. The dielectric layer can be a thin film or and ALD-thin film (alumina, laminate of alumina-titania). An example of a planar capacitor is presented in Figure 24A. An example of a supercapacitor with increased surface area is presented in Figure 24B.

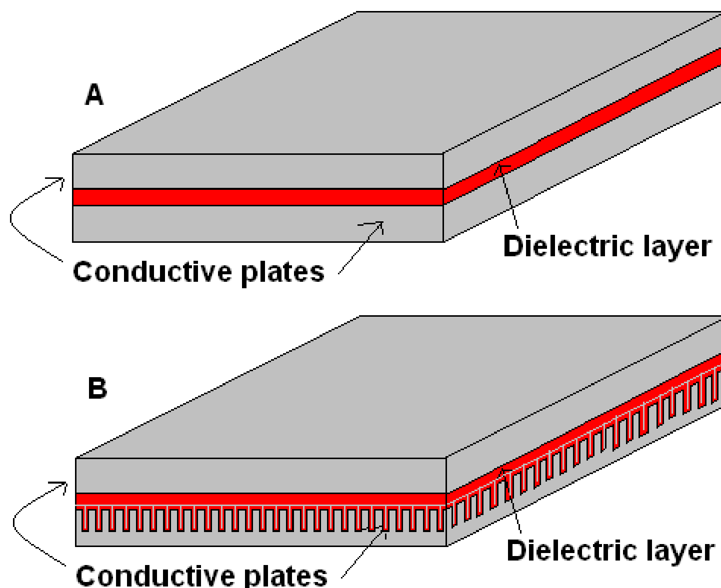

Figure 24. An illustration of a planar capacitor (A) and a supercapacitor (B). In the supercapacitor the surface area is increased formation on 3D structures by etching high aspect ratio pores

The SI unit of capacitance is the Farad (F) [78]. Capacitance depends on the geometry of the capacitor and it is directly proportional to the area A of each plate and inversely proportional to

their separation d. Capacitance is proportional to the dielectric constant. The definition of capacitance is presented in Equation 8.

$$C = \varepsilon_r \varepsilon_0 \frac{A}{d}$$

Equation 8. [78]

C = capacitance
A = surface area of overlap of the two plates
ε_r= relative static permittivity
ε_0 = electric constant
d = separation between the plates

4.2. Characteristics of Capacitors

High-quality thin film capacitors have low pinhole density, little leakage of current, low dissipation factor and low temperature coefficient in addition to reasonably high capacitance per unit area.

Characteristics of capacitor elements include [6]:

- capacitance per unit area
- dielectric constant
- breakdown voltage
- maximum working stress, the dielectric strength
- leakage current
- temperature coefficient of capacitance
- dissipation factor

The temperature coefficient means the change in capacitance with temperature. Cold temperature reduces the capacitor's performance. The dissipation factor describes the loss of energy. The characteristics are described below.

Dielectric constant. The dielectric constant (k) is a measure of the material's ability to store charge. The higher the value the better the ability to store a charge. The dielectric constant is defined by the ratio of the capacitance with the dielectric material in between the plates (C) to the capacitance without any dielectric material between the plates (C_0). The definition of dielectric constant is presented in Equation 9 [6, 78].

$$k = C/C_0$$

Equation 9. [78]

k= dielectric constant
C= capacitance
C_0= original capacitance

A large focus in microelectronics is high-*k* oxides for Dynamic Random Access Memory (DRAM) capacitors and Complementary Metal Oxide Semiconductor (CMOS) technology. The aim is to increase the dielectric value and to make the films more stable by doping the oxide film

when making thin films that consist of layers of two different materials (nanolaminates) and films containing three elements (ternary compounds) [19-20].

The dielectric constants of different materials are presented in Table 8. Estimation has been made on the correlation between the dielectric constant and the surface area to be hundred-fold. If the dielectric constant value can be increased by hundred-fold, the surface area can be reduced by hundred-fold. This helps to improve the packing density of integrated circuits [27, 79].

Table 7. Properties of thin film dielectric materials

Film material	Dielectric constant	Deposition technique	Reference
Al_2O_3	6-9	Sputter	[80]
	9.6	Spray pyrolysis	[81]
	8.3	Evaporation	[81]
	9	ALD	[82]
TiO_2 using Ti-tetra-isopropoxide + O_3 (250 °C) + post anneal at 400 °C	103	ALD	[83]
TiO_2 using Ti-tetra-isopropoxide + O_3 (295 °C)	32	ALD	[84]
TiO_2	44	Sputter	[85]
TiO_2 anatase	36	Sputter	[85]
TiO_2 rutile	89-170	Sputter	[85]
TiO_2 50% oxygen	44	Sputter	[85]
TiO_2 100% oxygen	21	Sputter	[85]
Al-doped TiO_2	67	ALD	[83]
$TiO_2(TiCl_4)$	136	ALD	[83]
Ta_2O_5	20-25	ALD	[86]
$((TiO_2)_x(Ta_2O_5)_{x-1})$	120	ALD	[86]
La_2O_3	23	ALD	[82]
HfO	25-40	ALD	[27]
$SrTiO_3$	265	Sputter	[87]

There are ways to affect the dielectric constant such as:

- annealing (crystallization)
- doping
- oxidation or nitridation

Effect of temperature on the dielectric constant. Structural changes via annealing of HfO_2 have been studied in three temperatures 300 °C, 500 °C and 700 °C. HfO_2 films are known to poly-crystallize in high temperatures. The film stays amorphous at 300 °C. When the temperature increases to 500 °C, the crystallization starts from top of the film. By varying the temperature, the dielectric constant of HfO_2 can be changed from k=25 to k=40. However, at the crystalline form,

the other properties of the film are not beneficial to dielectric layers in capacitors due to the increase of leakage current [79, 86].

Effect of crystallinity on dielectric constant. It is known that the crystallinity of the film has a big effect on the dielectric constant in an increasing way. When studying the electrical properties of amorphous $Bi_5Nb_3O_{15}$ thin films deposited by rf sputtering, it was found out that the crystalline B_5N_3 phase in the amorphous film had an increasing effect on the dielectric constant value. The ceramic B_5N_3 has *k* value of 200. The film deposited at 550 °C showed a crystalline phase and had a *k* value of 160. The film deposited at 200-300 °C showed a crystalline phase inside the amorphous film and had a *k* value of 70. It was thus hypothesized that the crystalline phase inside the amorphous phase contributed to the high dielectric value. In the case of using HfO_2 in MIM capacitors the post annealing step below 500 °C showed an increase in the dielectric value with the film remaining partly amorphous. However, the post annealing step in 700 °C increased the dielectric value even more, but the leakage current increased by 2 orders and thus the annealing temperature was not acceptable [27, 88].

Oxidation. In-situ oxidation by O_2 plasma causes micro-structural changes in the film that reduces the film thickness and thus increases the film density during a short-time process. This has shown to have an increasing effect on the dielectric constant [27, 88].

Breakdown and dielectric strength. When a dielectric material that normally is an insulator, is placed under strong enough electric field, the electrons in the dielectric material are kicked loose from their molecules and in their turn kick other electrons loose from other molecules, creating an avalanche of moving charge. The insulator suddenly becomes a conductor and causes irreversible damage to the electronic device. This is called a dielectric breakdown. A side product of this occurrence can be a spark or arc discharge [6]. The dielectric strength defines the maximum electric-field that the material can withstand without the dielectric breakdown happening. The reason for a breakdown is usually stress, thin spots, cracks and impurities within the dielectric rather than an inherent property of the dielectric material [78]. Breakdown reflects more on the processing and the quality of the material, and this causes the larger-area capacitors being more prone to breakdown than smaller ones [79].

Leakage current. Although a material would have a high dielectric constant, it still could have a high leakage current. All dielectric materials are not optimal insulators. However in our work in Annex III, it was found out that titania conducts electricity better and the leakage current most likely in the alumina-titania laminates travelled on the surface of the wafer. Leakage current slowly discharges a capacitor with time [79].

4.3. ALD capacitors

It is possible by employing the ALD process to make planar stacked capacitors (see Figure 25a) and supercapacitors with high-aspect ratio topography using non-line-of-sight, conformal film deposition into the pores with fast pulse times. ALD thin films have low number of pin-holes in the films that provide better etching qualities than the CVD films. Using PEALD the quality of the film can reach even higher with higher density of the film and thus etch resistance.

The surface area in the supercapacitors with 3D topography exceeds greatly the surface area of a parallel-plate capacitor leading to higher capacitance values (89). Cross section of a multilayer stack capacitor (supercapacitor) is presented in Figure 25b. The ALD technology provides ability to conformally coat the high aspect ratio pores, nevertheless the pulse parameters must be well modified in order to allow sufficient purging and obtaining uniform film throughout the pore.

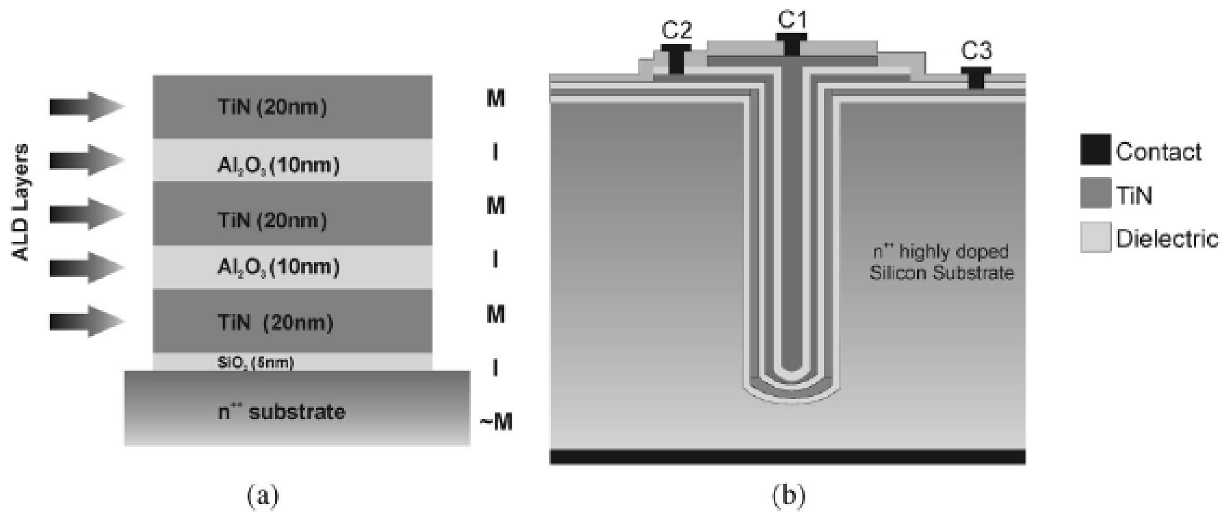

Figure 25. (a) Illustration of the cross section of a stack capacitor with a triple layers (MIMIMIM). The capacitors consists of three metallic TiN layers and three insulating Al_2O_3 layers. (b) Illustration of the 3D multilayer stack capacitor that is deposited in a high aspect-ratio pore [89]

5. MATERIALS AND METHODS

The experimental work for this thesis focused on three materials, Al_2O_3, TiO_2 and ZnO. The precursors used to process these materials are trimethylaluminum [$Al(CH_3)_3$] (TMA), titanium tetrachloride [$TiCl_4$] and diethyl zinc [$Zn(C_2H_5)_2$] (DEZ). Their reaction mechanisms are summarized in chapter 3.4. The ALD thin film depositions were performed using the ALD thin film deposition tools: Beneq TFS500 reactor and Picosun R-series reactor.

5.1. Materials and Reaction Mechanisms

To grow ALD-alumina (Al_2O_3) film, the TMA + H_2O process is used. To grow ALD-titania (TiO_2) film, the $TiCl_4$ + H_2O process is used. To grow ALD –zinc oxide (ZnO) film, the DEZ + H_2O process is used

5.2. Methods

The ALD thin film depositions were performed using the following ALD deposition tools: Beneq TFS500 reactor and Picosun SUNALE^{TM} R-150 reactor. The stability ALD thin films were studied in the most common microfabrication chemicals to explore sample cleaning and post production options.

Process parameters. Alumina (Al_2O_3), titania (TiO_2) and zinc oxide (ZnO) were deposited using the Beneq TFS500 reactor. For Al_2O_3 deposition, TMA was used as the metal precursor and H_2O or ozone was used as the oxygen precursor. The growth temperature was 220 °C for work presented in Appendix I. The deposition temperature was 60 °C, 80 °C, 220 °C for work presented in Appendix II. The cycle length for depositing Al_2O_3 was 7 seconds including 3 s purge after each precursor cycle. In the case of studying conformality in high-aspect-ratio pores, the precursor pulse was 1 second and the purge was 30 s. The growth rate was 0.9 Å/cycle for H_2O and 0.84 Å/cycle for ozone as oxidant precursor. In order to deposit ~100 nm Al_2O_3 film, 1000 cycles were used using H_2O as the oxidant precursor and using the ozone as oxidant precursor 1200 cycles were used to deposit ~100 nm.

For *TiO_2* deposition, the $TiCl_4$ + H_2O process was used. The growth temperature was 350 °C. The total cycle length was 7.85 s including 3 s purge after each precursor cycle. The growth rate was 0.45 Å/cycle. In order to deposit 100 nm TiO_2 film, 2000 cycles were used.

For *ZnO* deposition, the DEZ + H_2O process was used. The growth temperature was 220 °C; the cycle length was 7 seconds, including 3 s precursor purge after each precursor cycle. The growth rate was 1.8 Å/cycle. In order to deposit ~100 nm ZnO film, 500 cycles were used.

Using the Picosun SUNALE^{TM} *R-150* reactor Al_2O_3 and TiO_2 were deposited. For *Al_2O_3* deposition, TMA was used as the metal precursor and H_2O was used as the oxygen precursor. For the work presented in Appendix III: for depositing Al_2O_3 the TMA + H_2O process was used. The growth temperature was 110 °C, 200 °C and 300 °C; the cycle length was 2.2 seconds including 0.1 second precursor cycle and 1 second purge after each precursor cycle. The growth rate was 0.9 Å/cycle. For depositing Al_2O_3 film ~20 nm, ~40 nm and ~60 nm, cycles used were 200, 400 and 600, respectively.

For *TiO_2* deposition, the $TiCl_4$ + H_2O process was used. The growth temperature was 200 °C; the cycle length was 8.2 s including 0.1 s precursor cycle and 4 seconds purge cycle after each precursor cycle. The growth rate was 0.45 Å/cycle. For depositing Al_2O_3-TiO_2 nanolaminate thin films, the TiO_2 volume fraction in the film was varied from 0.46 % to 0.73 % by including 6-10 TiO_2 layers in the nanolaminate film that had overall film thickness 40 nm.

For **stability study** of the ALD films in microfabrication chemicals, Al_2O_3 and ZnO films were chosen. The thickness of the deposited samples was measured with ellipsometry (Plasmos SD2300). The film thickness was measured prior and after to dipping in etchants and rinsing in water. The etch rate was calculated from the results as nm/ min. The etchants used were:

- Phosphoric acid 85 % (20 °C)
- Al-etch (50 °C) (85 % o-H_3PO_4 + HNO_3)
- Al-etch (20 °C)
- BHF (20 °C) (Sioetch NH_4F:HF 9:1; ammoniumfluoride: hydrofluoric acid)
- BHF (32 °C)
- HF 1% (Hydrofluoric acid)
- TMAH 25 % (20 °C) (Tetramethylammonium hydroxide)
- THAM 25 % (80 °C)
- KOH 20 % (20 °C) (Potassium hydroxide)
- KOH 20 % (80 °C)
- Developer AZ451 (photoresist developer)

6. RESULTS AND DISCUSSION

The results present and analyze the experimental work on studies on the conformality of thin films in high aspect ratio pores and the studies on ALD thin film capacitors.

6.1. ALD Thin Film Conformality in High Aspect Ratio Pores

This chapter presents the results of experiments on conformal coating of ALD thin films in high aspect pores. In the experimental work reported in the Appendices I and II, a study was made of the conformal growth of thin films around a spherical object and in high aspect ratio pores in two cases: through-wafer-pores and closed pores. The focus of the parameters in this study was the purge pulse.

The manufacturing process for through-wafer pores is presented in Figure 26. The process flow included four stages. 1. First, lithography was used to obtain even spacing between the initial pits and then the initial pits were etched in TMAH exploiting the directional etching on 111-oriented silicon. 2. Etching continues with electrochemical etching in HF: water: ethanol electrolyte. 3. The wafer is turned around. 4. The backside of the wafer is etched away carefully with ICP etching.

Additionally, commercially available 60 µm thick Anopore membranes (Whatman) with 200 nm pores (aspect ratio 300:1) were used for the conformality tests.

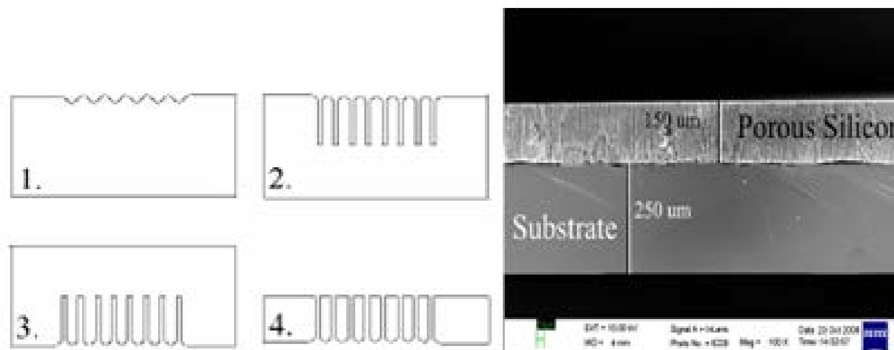

Figure 26. Left: cross section images on the manufacturing process of through wafer pores. Right: SEM image of stage 2. Electrochemical etching was performed using HF:water:ethanol electrolyte.

Coating of closed pores. Closed pores were manufactured using the steps 1 and 2 in Figure 26 and commercial nanopore membranes were used (Figure 27). Deep macropores etched on N-type 100-oriented silicon with HF: water: ethanol electrolyte. Pores with aspect ratio 100:1 were achieved. The depth of the pores was 200 µm and the width was 2 µm.

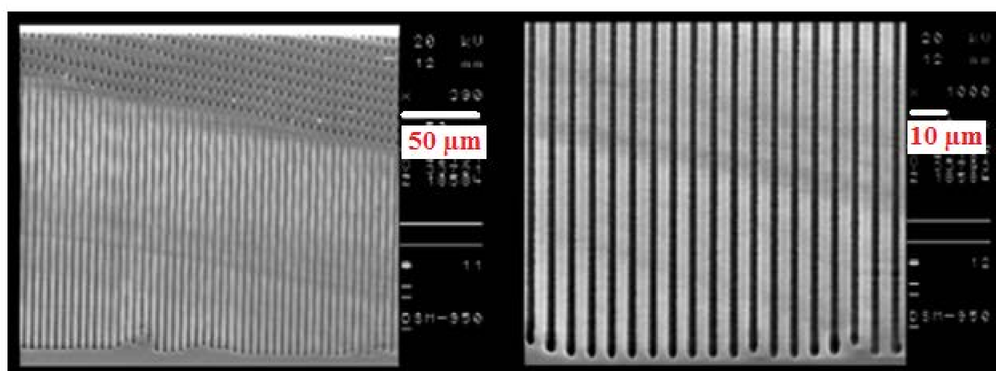

Figure 27. Cross section of deep uncoated macropores presented in SEM-image

Process parameters. The coating of the closed pores with ALD thin films was done using the Beneq TFS500 reactor. The TMA + H_2O process was used for depositing Al_2O_3 films and growth temperature 220 °C. The $TiCl_4$ + H_2O process was used to deposit TiO_2 thin films and the growth temperature was 350 °C. The DEZ + H_2O process was used to deposit ZnO thin films and the growth temperature was 220 °C.

Conformality of the closed pores. Coating of the deep macropores was successful with double layers of Al_2O_3/ZnO and Al_2O_3 / TiO_2. The film thicknesses were ~215 nm ZnO on bottom and ~158 nm Al_2O_3 on top in the Al_2O_3/ZnO bilaminate film. The film thicknesses were ~100 nm Al_2O_3 on bottom and ~50 nm TiO_2 on top in the in the Al_2O_3 / TiO_2 bilaminate thin film. Good film conformality can be seen in Figure 28.

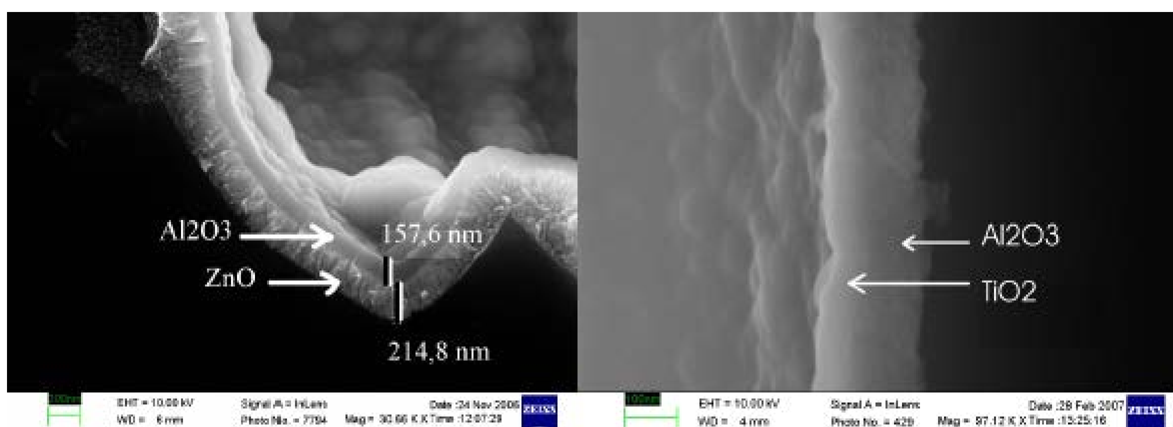

Figure 28. Cross-section SEM-image of the bottom of a closed pore (left and right). Dual layers were done with Al_2O_3/ZnO (left) and Al_2O_3/ TiO_2 (right). The SEM-images show good conformality

Coating of ~20 nm ZnO into 60 nm pores with aspect ratio 8:1 was performed using the DEZ + H_2O process at 220 °C. Good film conformality can be seen in Figure 29.

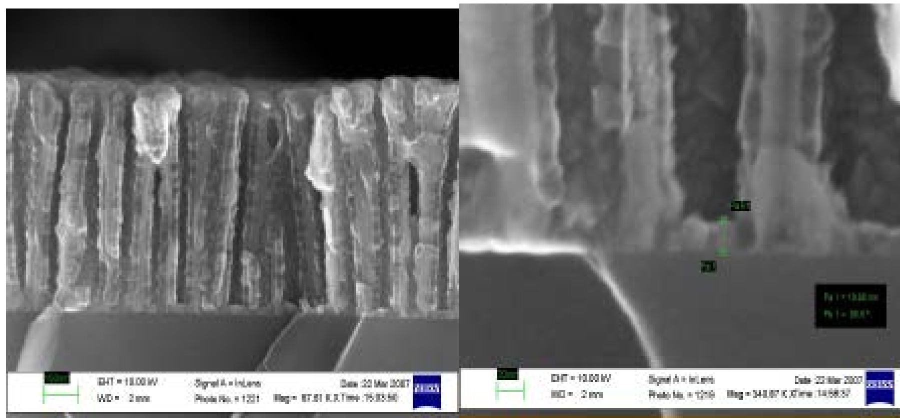

Figure 29. Crystalline ZnO film deposited inside pores of porous silicon. The 20 nm thick ZnO layer is conformal on top, middle and bottom of the pores.

Through wafer pores. High aspect ratios of 300:1 through wafer pores of Anopore membrane before and after deposition are shown in Figure 30. Because of the polypropylene ring supporting the Anopore membrane, the deposition temperature had to be low, 80 °C. 1 s precursor pulse was used and the purge was 30 s. Achieving uniform film growth requires long reactant exposure times and long purging times. Otherwise, if the purging is incomplete, the unreacted precursor molecules stay in the pore and react with the next step causing excess growth of film. In the ALD reaction chamber the through wafer pores were carefully elevated 400 µm by supporting the edges of the sample on wafer pieces. This was done to allow the process gas stream to flow through and under the sample.

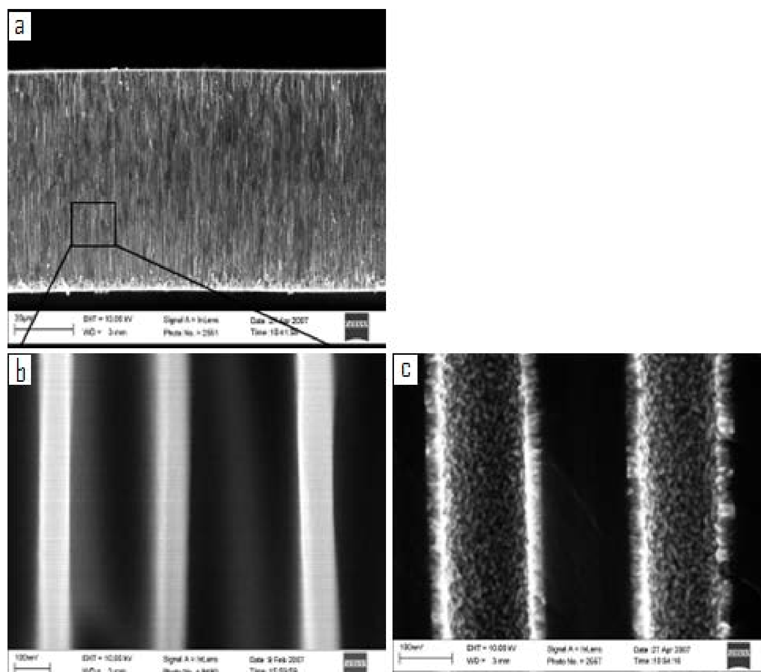

Figure 30. a.) Cross section of a commercial Anodisc alumina pores (aspect ratio 300:1). b.) Pores before deposition. Pore width is approximately 200 nm. c.) Pores after 30 nm ZnO deposition. Long reactant exposure times and purging times were needed

Coating the through wafer high aspect ratio pores of 300:1 with 30 nm of ZnO showed that it is possible to achieve continuous layer of film throughout the pore. This is presented in Figure 31. The films thickness decreases 24 % from top to center (34.43 nm to 26.08 nm) and 7 % from top to bottom (34.43 nm to 32.05 nm). The SEM-image shows that the precursor pulse was not sufficient, but it is evident that better uniformity can be obtained with thorough optimization of the process cycle parameters.

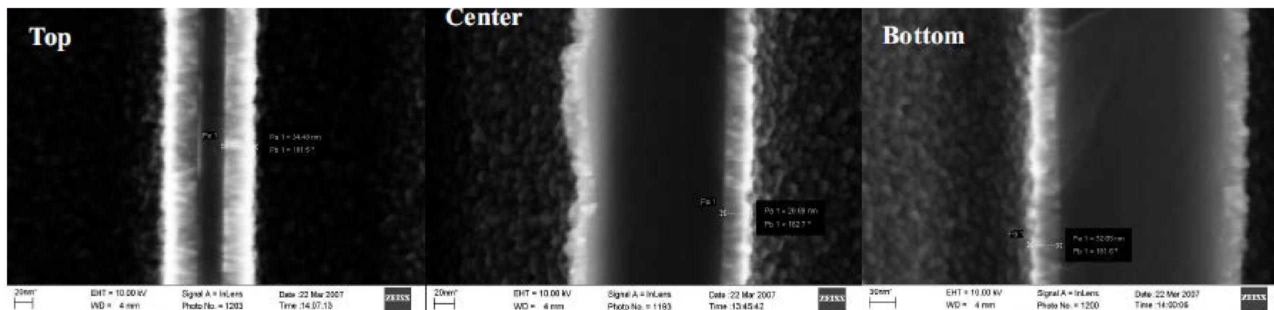

Figure 31. ZnO coating to high aspect ratio of 300:1 pores. 30 nm film was obtained on top, center and bottom of the pores using longer cycles of 1s precursor pulse + 30s purge pulse. The SEM-image shows continuous coating throughout the pore, but the layer thickness was not uniform. The thicknesses were 34.43 nm (top), 26.08 nm (center) and 32.05 nm (bottom).

Coating of spherical objects. The film conformality was studied by coating spherical polystyrene microbeads with alumina. This is presented in Figure 32. Later the polystyrene was dissolved and the hollow alumina shells remained confirming good thin film conformality. The deposition temperature was low, 60 °C, because of the polystyrene spheres. The polystyrene beads were coated with 40 nm Al_2O_3 and then the polystyrene was dissolved in acetone to leave only hollow Al_2O_3 coating.

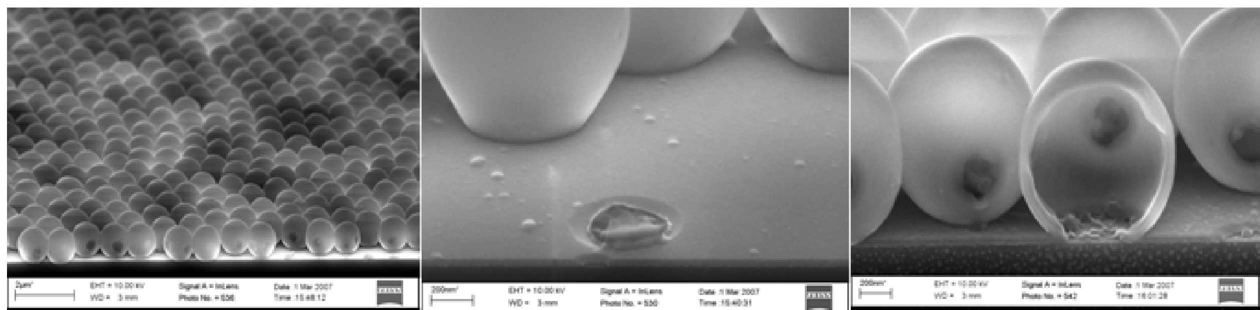

Figure 32. Conformal ALD Al_2O_3 coating on polystyrene microbeads (left), the only place left uncoated was the contact point of the microbead to the substrate (middle). Hollow alumina micro-spheres (after dissolving the polystyrene). The cross section of a micro-sphere reveals the conformal deposition of the film everywhere, except on the contact points of the microbeads (right).

Factors affecting conformality. The excellent conformality of ALD thin films can be attributed, in part to the non-line-of-sight feature of ALD technology and the self-limiting nature of reactions occurring on the surface of the substrate. However, with severe topographies, such as high aspect ratio pores, the process parameters have to be adjusted to enable a long purge step. If this is not done, the unreacted precursor molecules may not have time to leave the pore and remain there when the next precursor step is pulsed causing parasitic CVD growth.

The 3D pores drastically increase the surface area of the sample relative to a 2D planar wafer, resulting to higher need of precursor dose than for a planar wafer.

The time the reactant molecules need to react on the surface is longer when film is deposited in the pores. The gas flow model changes from the viscous flow mode on the planar wafer to molecular flow mode in the pores. In the viscous flow model the reactant molecules contribute to the film growth by finding an active surface site fast. In the molecular flow model the reactant molecules need more time to move, by gas-wall collisions, to find an active surface site.

Careful adjustment of process parameters is required when conformal ALD thin films are deposited in high aspect ratio pores. The aspect ratio of the pore changes constantly in increasing manner as film is deposited in the pore and the cross section of the pore diminishes with increasing film thickness. This study focused on the purge pulse. More research is needed to study the effect of the precursor dose.

6.2. ALD Thin Film Capacitors

This chapter presents the results experiments on alumina and alumina-titania laminate thin film capacitors investigating the effects of variations in temperature of deposition, film thickness, and reactor configuration on capacitance and the effects of film precursors on leakage.

Capacitors prepared with thin films deposited by ALD methods are described and the benefits of the different methods are compared.

6.2.1. ALD Capacitor Characteristics

The results of experimental studies on the electrical properties of capacitors prepared with ALD-grown Al_2O_3 and Al_2O_3-TiO_2 nanolaminate thin film dielectric layers were reported in the publication of Appendix III and are summarized below. Deposition temperature and its influence on film thickness and capacitance, reactor configuration and leakage characteristics of the capacitors were studied.

Process parameters. The Picosun^{TM} SUNALE R-150 reactor was used to deposit the Al_2O_3 thin films. In the test the depositions, the temperature was varied 110 °C, 200 °C and 300 °C while keeping the film thickness as constant at 40 nm. Then, the film thickness was varied 20 nm, 40 nm and 60 nm, while keeping the temperature as constant at 200 °C.

The wafer containing 226 capacitors was diced and the capacitance value of the individual capacitors was measured.

The IC capacitors were manufactured on a silicon wafer (150 mm diameter) and a thermal oxidation for ~ 1 µm was performed for insulation. The bottom electrode was deposited by 200 nm molybdenum (Mo) by sputtering at room temperature and the bottom electrode was patterned by dry etching. ~500 nm SiO_2 was deposited by PECVD at 300 °C and it was patterned using buffered oxide etch. The dielectric layer was deposited by ALD films was deposited as described above and patterned using photoresist AZ451 developer and dry etch. The bilayer upper electrode was deposited by sputtering 200 nm molybdenum at room temperature and Al:Si 1% sputtering at

room temperature. Patterning of the bilayer upper electrode was done by wet Al etch. Finally ~500 nm SiO_2 was deposited by PECVD at 300 °C and it was patterned using buffered oxide etch. The cross section of the IC capacitor is presented in Figure 33.

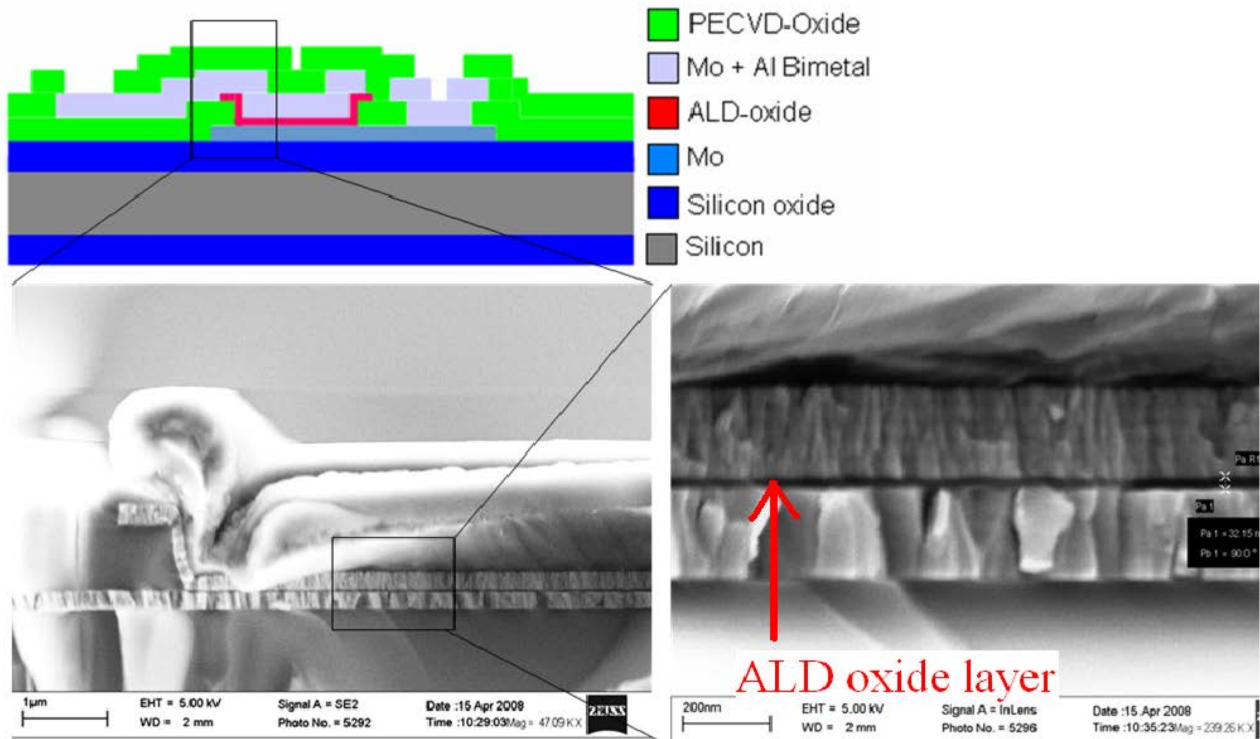

Figure 33. Cross section of an IC capacitor. The top image shows the material layers that the capacitor is constructed of. The image on bottom left shows a SEM-image of the same structure and the image on the bottom right presents the thin, ~40 nm thick Al_2O_3 dielectric layer seen as black line in the middle of the image.

Table 9 presents the results of studies on the effects of deposition temperature and the calculated film thickness on capacitance. Because accurate measurement of the dielectric layer in completed capacitor is challenging, the final thickness of Al_2O_3 was calculated using Equation 8 assuming the relative permittivity ε_r for Al_2O_3 to be ~8.

Table 8. Effects of growth temperature (top) and film thickness (bottom) on capacitance using capacitors with Al_2O_3 dielectric layer.

Growth temperature	Capacitance density	Target thickness	Calculated thickness	Difference of calculated and target thicknesses
110 °C	2.42 nF	40 nm	29.3 nm	26.8 %
200 °C	2.15 nF	40 nm	32.9 nm	17.8 %
300 °C	2 nF	40 nm	35.4 nm	11.5 %

Growth temperature	Capacitance density	Target thickness	Calculated thickness	Difference of calculated and target thicknesses
200 °C	4.92 nF	20 nm	14.4 nm	28 %
200 °C	2.15 nF	40 nm	32.9 nm	17.8 %
200 °C	1.39 nF	60 nm	51.0 nm	15 %

Interpretation of results. As can be seen, higher deposition temperatures (Table 9, top) produce slightly thicker film and the capacitance, while acceptable, is lower. The capacitance obtained with thicker films (Table 9 bottom) is lower than that obtained with thin film. Thus, when the deposition temperature was increased from 110 °C to 300 °C, the capacitance density decreased from 2.42 nF/mm^2 to 2.00 nF/mm^2 when a nominally 40 nm thick Al_2O_3 insulator was used. When the film thickness was increased the capacitance density decreased from 4.92 nF to 1.39 nF when deposition temperature of 200 °C was used.

It was noted that the calculated film thickness was lower than the target film thickness. When, the deposition temperature was varied (Table 9, top), the difference of calculated and target film thicknesses was reduced from 26.8 % (110 °C) to 11.5% (300 °C). When the film thickness was varied (Table 9, bottom), the difference of calculated and target film thicknesses was reduced from 28 % (20 nm) to 15% (60 nm). The reason was assumed to be erosion of the insulator during photoresist development. Erosion is faster for films deposited at low temperature. Likewise because of erosion, the capacitance density did not appear to depend fully linearly on the target film thickness.

During the stability study of the ALD films in the Annex I, using the most common microfabrication chemicals, it was noted that the etch rate for Al_2O_3 in AZ451 photoresist developer is 13nm/min for Al_2O_3 as is presented in Table 10.

Table 9. Etch rates of ALD Al_2O_3 and ZnO. Fast = film is completely etched in one second.

	Etch rate (nm/min)	
Etchant	**Al_2O_3**	**ZnO**
Phosphoric acid 85 % (T= 20 ^{0}C)	0,4	fast
Al-etch (50 ^{0}C)	11	fast
Al-etch (20 ^{0}C)	0,7	fast
BHF (20 ^{0}C)	53	260
BHF (32 ^{0}C)	1184	fast
HF 1 %	22	fast
TMAH 25% (20^{0}C)	1,6	12
TMAH 25% (80^{0}C)	185	498
KOH 20% (20^{0}C)	4	85
KOH 20%(80^{0}C)	331	914
Developer AZ451	13	0,2

According to the finding of erosion of the insulator film during photoresist development, it is recommended to plan the deposition process using thicker films. It is noteworthy to take into consideration of the vulnerability of the alumina film being soluble in several other microfabrication chemicals that were presented in Table 10.

Effect of reactor configuration on capacitance was studied. The reactor configuration has an effect on the capacitance values of capacitors. Multiple capacitors were fabricated on a single wafer and, after processing, the wafer was diced to obtain separate capacitors. Figure 34 presents two wafer maps of capacitance measurement before the capacitors were diced out of the wafer. Figure 35 presents the statistical data of the capacitance measurement. The wafer maps present capacitance values over wafers in a shower-head-type reactor. The map on left refers to alumina dielectric capacitors and the map on right to alumina-titania laminate dielectric capacitors. The reactor configuration causes the difference in the maps. With respect to the wafer, the inlet nozzles for $TiCl_4$, TMA, and water are situated in the top, right and bottom, respectively.

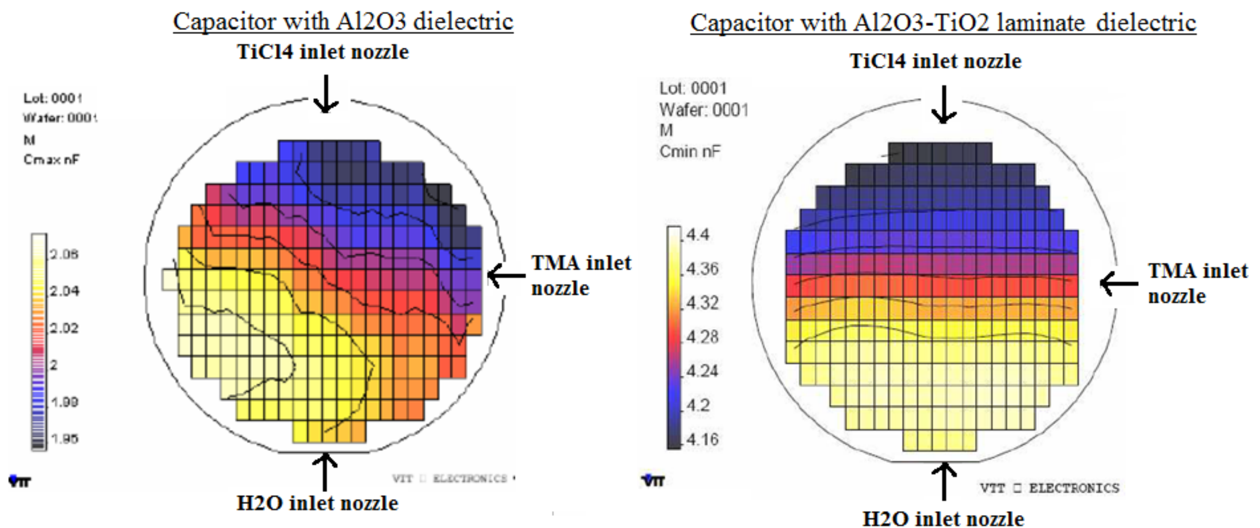

Figure 34. Wafer maps of capacitance value of test capacitors. The dielectric films were deposited in a showerhead reactor configuration. Map of alumina-titania dielectric capacitors (left). Map of alumina- dielectric capacitors (right).

In the wafer map of Al_2O_3 dielectric (left), the precursors are pulsed from right and bottom, creating a gradient from lower left side to upper right side. The deposited film is thickest in the blue section of the map, resulting in lowest capacitance value, and thinnest in the yellow section, resulting in the highest capacitance value on the wafer. The thinner the film, the higher the capacitance value.

In the wafer map of Al_2O_3-TiO_2 laminate dielectric (right), the precursors are pulsed from top and bottom creating a gradient from bottom to top. It is apparent that the TMA precursor nozzle on the right side did not affect this gradient

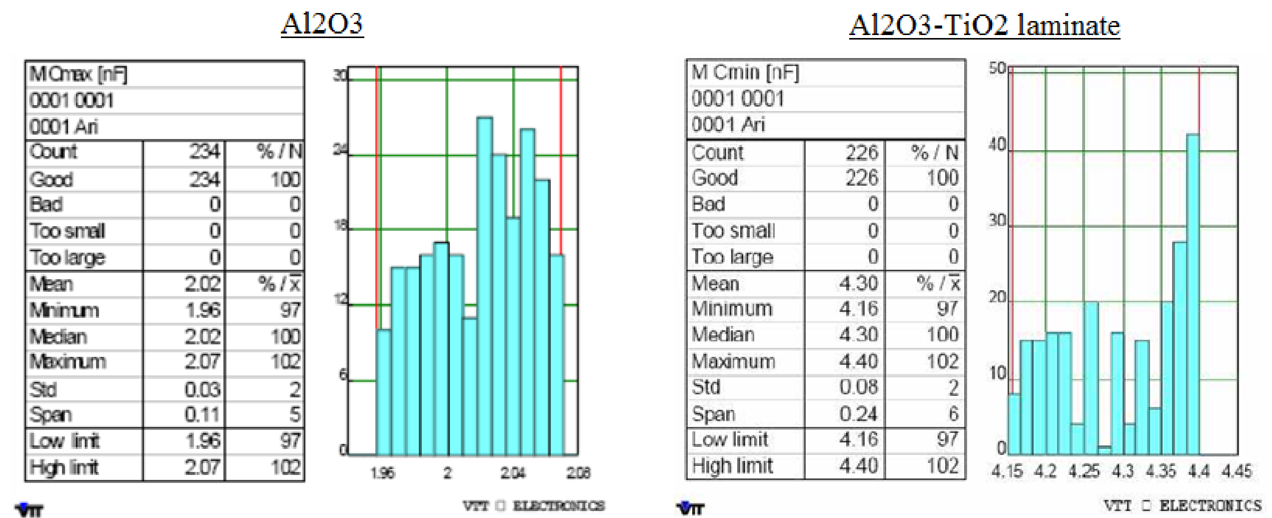

Figure 35. Statistical data of the capacitance wafer maps. Capacitors with Al_2O_3 dielectric (left) and Al_2O_3-TiO_2 dielectric (right).

For capacitors with Al_2O_3, the statistical information is presented in Figure 35 (left). The table indicates that for that all of the 234 diced capacitors were good. The capacitance values ranged from minimum of 1.96 nF to maximum of 2.07 nF, the difference of which is 0.11 nF (Span). The median value is 2.02 nF and the standard deviation (σ) is 0.03 nF. In this case the Standard deviation (Sigma) is meaningless, because the shape of the measured output is not normal and is restricted in x direction. Better understanding of the variation can be seen looking at the histogram. The histogram presents the number of capacitors per each capacitance value. It is visible in the histogram that there are two peaks on both sides of the median value (2.02 nF). This is explained by the flow of the precursor gas in the reactor and leading in difference in film thickness, presented by the color gradient of the wafer map that was presented in Figure 34 (left).

For capacitors Al_2O_3-TiO_2 laminates, the statistical information is presented in Figure 35 (right). The table indicates that all of the 226 capacitors were good. The capacitance values ranged from minimum of 4.16 nF to maximum of 4.40 nF, the difference of which is 0.24 nF (Span). The median was 4.30 nF and the standard deviation (σ) is 0.08 nF. The histogram reveals also two peaks on the edges. A large number of the capacitors have a high capacitance value. Multiple capacitors have a low capacitance value. This trend is visible in the color gradient in the wafermap in Figure 34 (right) and it is caused by changes in the film thickness

The difference of capacitance values across the map for capacitors using Al_2O_3 dielectric is 0.11 nF (span), that is 5.3 %. The difference of capacitance values across the wafer map for capacitors using Al_2O_3-TiO_2 laminate dielectric is 0.24 nF (span), that is 5.4 %. It is estimated that this will not compromise the successful performance of the end device, but it is good to acknowledge.

6.2.2. Leakage Characteristics of Capacitors

The results of studies on the leakage characteristics of capacitors prepared with alumina-titania nanolaminate and alumina thin films were reported in the publications attached as Appendix III and are summarized below.

Nanolaminate thin film capacitors were studied. Capacitors with Al_2O_3-TiO_2 nanolaminate dielectric films were manufactured with two variables. The Picosun^{TM} SUNALE R-150 reactor was used to deposit the Al_2O_3 and TiO_2 thin films. The growth temperature for the Al_2O_3-TiO_2 nanolaminate thin films was held constant at 200 °C.

In the first case, the surface area of the capacitor was held constant at 1 mm^2 and the TiO_2 content of the film was varied by pulsing ratio of the precursors between 0.46 % -0.73 %. The values were calculated from ratio of TiO_2 pulses in the laminate film. The results are presented in Figure 36.

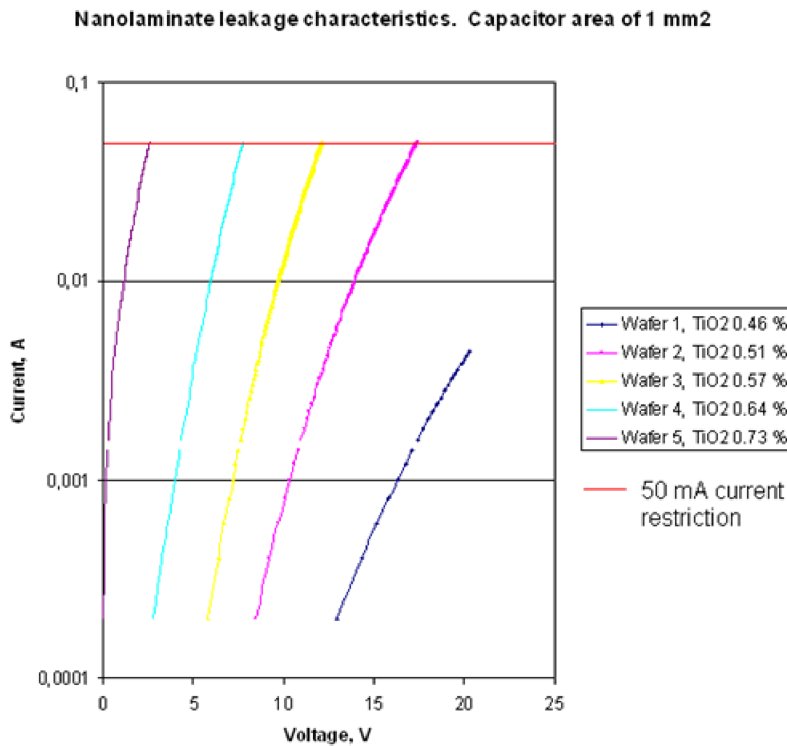

Figure 36. The leakage characteristics of alumina-titania nanolaminate. The capacitor surface area is held as constant and the titania content of the film was varied. The best result was achieved with the lowest titania content of 0.46 mass%.

The capacitors were tested with a 50 mA current restriction. The results for the leakage characteristics of capacitors prepared with Al_2O_3-TiO_2 nanolaminate dielectric films indicated that the leakage current density increased significantly when the TiO_2 content of the film was increased. The best result was achieved with the lowest titania content of 0.46 % that resulted in the lowest leakage current density value. The highest titania content of 0.73 % resulted in the

highest leakage current density value. With the laminate thin films a non-reversible breakdown was not observed.

In the second case the TiO_2 content of the film was held constant and the surface area of the capacitor varied from 0.25 mm^2 to 4 mm^2. This is presented in Figure 37.

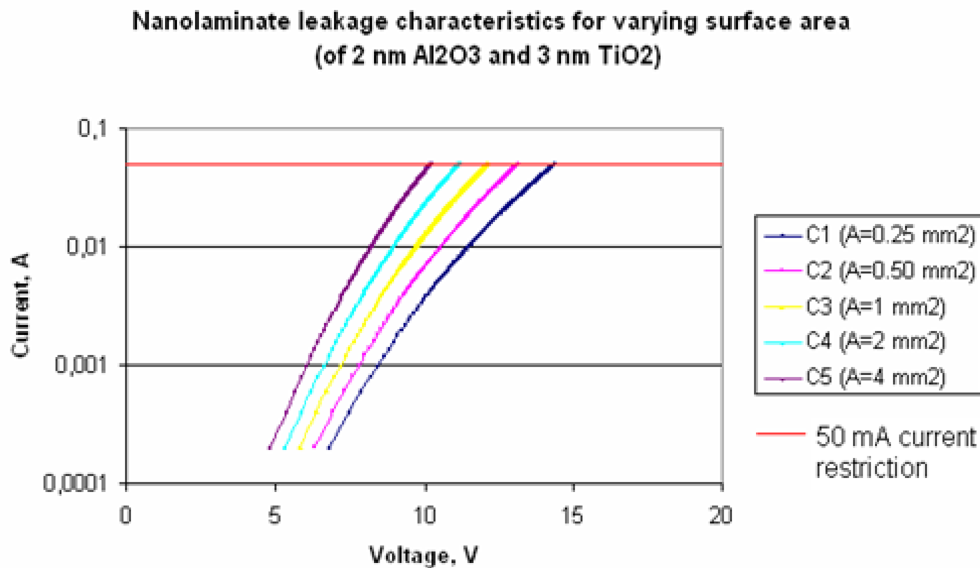

Figure 37. The leakage characteristics of alumina-titania nanolaminate. The surface area of the film was held as constant and the surface area of the capacitor was varied. When the surface area was increased, the leakage current increased. The best result was achieved with the smallest surface area of 0.25 mm^2

The capacitors were tested with a 50 mA current restriction. The results for leakage characteristics of capacitors prepared with Al_2O_3-TiO_2 nanolaminate dielectric films indicated that for the Al_2O_3-TiO_2 nanolaminates, the leakage current density increased when the surface area of the capacitor was increased. The best result for capacitance value was achieved with smallest 0.25 mm^2 surface area that resulted in the lowest leakage current. The highest leakage current density value resulted from the largest surface area value of 4 mm^2.

The merit of the nanolaminate thin film capacitors was that they tolerated heavy electrical stressing (power) prior to non-reversible breakdown.

Alumina thin film capacitors were studied. The capacitor manufactured for testing ALD alumina as a dielectric layer was presented in Figure 33. The film thickness was held constant of 40 nm. The film thickness was estimated to be 40 nm due to the difficulty of accurate measurement of the film thickness in the fabricated capacitor and the deposition temperature was varied 110 °C, 200 °C and 300 °C. Capacitors with alumina insulators deposited at low temperatures showed very good electrical characteristics. The results are presented in Figure 38. The permittivity was assumed to be 8 for Al_2O_3.

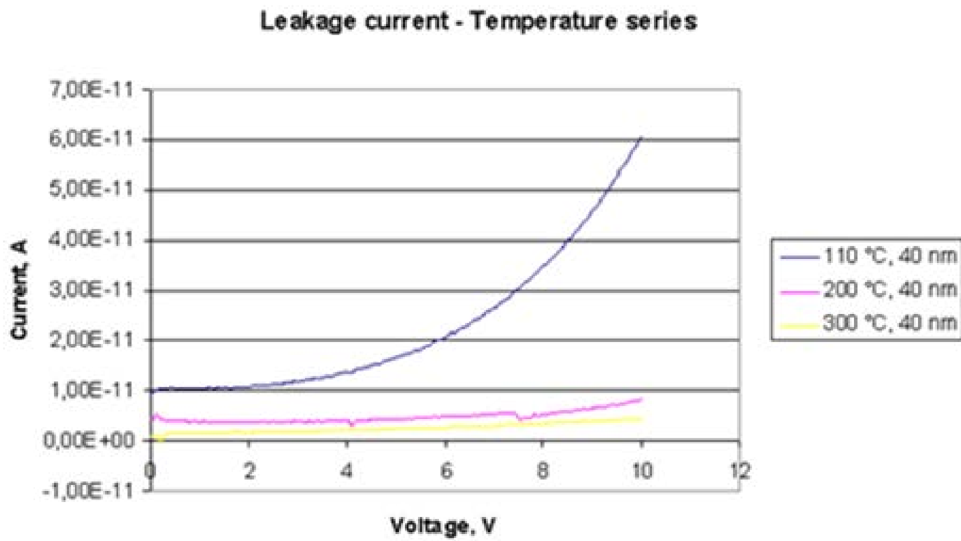

Figure 38. DC leakage characteristics of alumina dielectric films with varying deposition temperatures

The results show that the films deposited at 200 °C and 300 °C behaved similarly. In both cases, the leakage current remained under 1.00E^{-11} A/mm^2 at voltage of 10 V. The film deposited at 110 °C exhibited somewhat inferior electrical characteristics. The leakage current increased to 6.00E^{-11} A/mm^2 at voltage of 10 V.

The leakage current density test was continued to study the breakdown strength. Aluminium oxide films was used and the deposition temperature was 200 °C and film thickness was increased to 50 nm. This is presented in Figure 39.

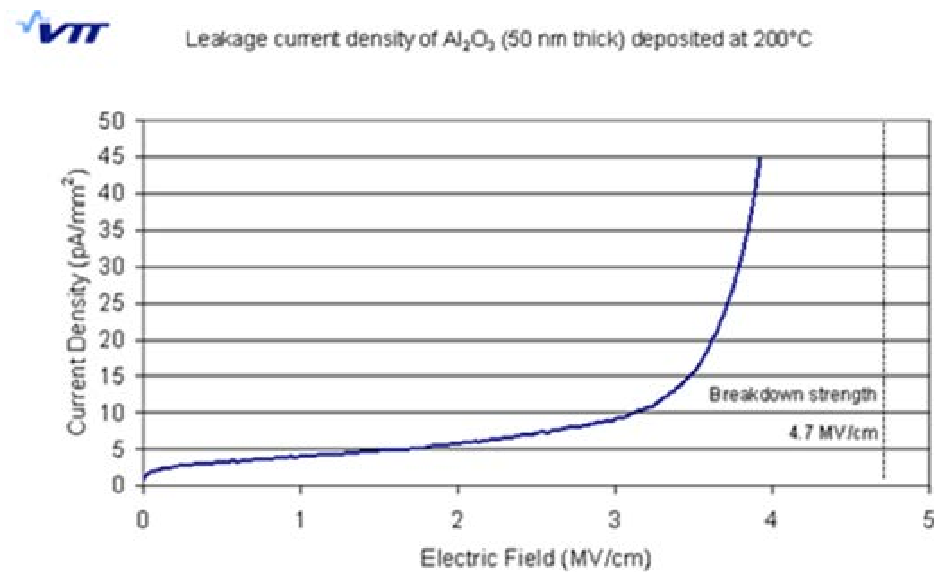

Figure 39. DC leakage for alumina dielectric deposited at 200 °C. The breakdown strength was 4.7 mV/cm

The results show that the leakage current densities were below 10 pA/mm^2 for alumina films deposited at 200°C at field strengths up to 3 MV/cm. Such aluminium oxide films, however, suffered from non-reversible dielectric breakdown in the field of 4.7 MV/cm.

The results of the work reported in the publications of Appendix I show that fabricating capacitors using ALD thin films as the insulator is an excellent way to achieve high quality devices at low temperature. The low leakage current aluminium oxide promotes its use in high performance capacitors over large effective area while nanolaminates endure short energetic peaks without failure.

6.3. Discussion

In the first part of the experimental work, the focus was on the conformality of ALD films. In the tests, both planar and high aspect-ratio topographies were deposited with ALD films with different parameters. The dependence of conformality to process cycle times and temperature was studied.

The following cycle times were used: TMA: 220 °C 7s cycle including 3s purge, 0.9 Å/cycle; DEZ: 220 °C 7s cycle including 3s purge, 1.8 Å/cycle; TiO_2: 350 °C, 7.85s cycle including 3 s purge, 0.45 Å/cycle.

It was noted that cycle times did not differ significantly between the two processes. Conformal coatings were achieved in close-end pores, but in through wafer pores, the film deposition was not conformal. The total cycle time of 5-10 s is short and similar to the cycle times reported by M. Ritala et al. [90] where a specially designed through-wafer ALD reactor is used. Longer reaction cycles for deposition of high aspect-ratio pores of 300:1 are tested using reaction cycles 1 s precursor pulse + 30 s purge pulse. This cycle time is similar to cycle times reported by G. Pardon et al [91]. Pt-Al_2O_3 dual layer was deposited in 16:1 aspect ratio pores using 0.95 s precursor pulses and 25 s purge pulses. These cycle times are considerably less than e.g. total cycle time of 500 s (300 s reactant pulse and 200 s purge pulse) used for coating silica aerogel (S.O. Kucheyev et al. [92]). The benefit of the short cycle time of 5-10 s in this experimental work was that it was possible to achieve similar results that were achieved with significantly longer cycle times. The long cycle times may be caused due to the process difference and difference in aspect ratios of coating silica aerogel and porous silicon. The short cycle time saves resources and improves throughput of the process.

The film conformality in top- middle and bottom of the pore was studied. In SEM analysis of through wafer pores it was noted that the long reaction cycle did not result in enhanced conformal film growth throughout the pore. The film was conformal on top and bottom part of the pore, but in the middle part the deposited film conformality was non-ideal. This is supported by J.W. Elam et al. [93] who reports coating ultra-high aspect-ratio of 1:5000 pores. The top and bottom of the open-end pores are coated before the middle part of the pore. Elam et al. also reported that deposition of a film into pore is either diffusion controlled or reaction controlled, depending on the sticking co-efficient and aspect ratio.

The work of G. Pardon et al. [92] and F.W. Elam et al. [93] indicates that due to the larger surface area of high aspect-ratio pores, longer time is needed for the precursor molecules to find a reactive site and higher precursor doses are needed. The results achieved in this work partially support the work of G. Pardon et al. and F.W. Elam et al. It was found out that longer cycle times did not produce conformal coating throughout the pores. Also, the conformality of the ALD deposited film was similar on planar surface, closed-end pores and through wafer pores. It was found out

that the inside the pores the conformality was non-ideal. This indicates that a careful adjustment of the process parameters is needed and the theory in this case is supported.

In the second part of the experimental work, the focus was on electric properties of the ALD dielectric films in capacitors. Thin films of Al_2O_3 and Al_2O_3-TiO_2 laminates were studied. Leakage current dependence on deposition temperature was tested. The film thickness was kept constant at 40 nm and the deposition temperature was varied from 110 °C to 300 °C. Al_2O_3 films deposited at 200 °C and 300 °C showed similar behaviour to each other and good electrical characteristics. In both cases, the leakage current remained under $1.00E^{-11}$ A/mm^2 at voltage of 10 V. Films deposited at 110 °C showed poor electrical characteristics. The leakage current increased to $6.00E^{-11}$ A/mm^2 at voltage of 10 V. The cause for this behaviour is estimated to be that films deposited at 110 °C have higher impurity content (than films deposited at 300 °C) of hydrogen [23, 33-34] and carbon, which increase the electrical properties [32-33]. The leakage current test was continued with Al_2O_3 deposited at 200 °C. The results show that the leakage current densities were below 10 pA/mm^2 for Al_2O_3 films deposited at 200 °C at field strengths up to 3 MV/cm. Such aluminium oxide films, however, suffered from non-reversible dielectric breakdown in the field of 4.7 MV/cm. Similar results were reported by K. Kukli et al. [94]. Al_2O_3 films and Al_2O_3-TiO_2 laminates are used to deposit dielectric layer to planar capacitors. The results show that a thin film of Al_2O_3 was insulating and a better dielectric layer that the laminate layer including TiO_2, which increases the leakage current. The leakage current density of the capacitor with Al_2O_3 dielectric layer is 5 nA/mm^2. The leakage current density of the capacitor with laminate film including TiO_2 was 900-1400 nA/mm^2.

7. CONCLUSIONS AND FUTURE STUDIES

In the first part of the thesis the focus of the study was on how good the conformality of ALD thin films is on 3D structures and what are the affecting factors.

The dependence of conformality to process cycle times was studied. It was shown that cycle times in ALD high aspect ratio of 300:1, 100:1, 50:1 and planar surface deposition processes did not differ significantly. The conformality on closed and through wafer pores was different. Conformal coatings were achieved in close-end pores, but in through wafer pores, the film deposition was not conformal. This was observed when the film conformality in top- middle and bottom of the pore was studied in SEM analysis of open pores. It was noted that the long reaction cycle did not result in enhanced conformal film growth throughout the open pore. The film was conformal on top and bottom part of the pore, but in the middle part the deposited film conformality was non-ideal. The possibilities of these results cover that long pulses are not needed to coat high aspect-ratio pores. This results in savings of resources and enhances the throughput of the process. The limitation of the non-ideal conformality of the film should be carefully evaluated.

The factors that affect the film conformality in this study were deposition temperature and cycle (pulse/purge) times. In addition, the constantly changing aspect ratio as the thickness of the film increases causing pore diameter to decrease also affects the film conformality to somewhat extent.

The ALD method is optimal for conformal coating of high aspect ratio pores and spherical objects due to the non-line-of-sight property of the method and self-limiting film growth. Uniform film thickness is observed on the walls of the high-aspect ratio pores and on the surface of the polystyrene microspheres. The experimental work in this thesis has shown that achieving the right process conditions for depositing ALD thin film conformally in high aspect ratio pores is a challenging task. Success depends on careful choice of parameters. The aspect ratio of the sample effects on the precursor dose and length of purge steps.

In the second part of this thesis the focus of the study was on the electrical properties of capacitors with ALD Al_2O_3 and Al_2O_3-TiO_2 laminate thin films as dielectric layers. The measurements included capacitance, dc leakage, and breakdown strength in planar capacitors. It was studied how the deposition temperature, film thickness, TiO_2 content of the laminate film, surface area of the capacitor and reactor configuration affect the capacitance.

The capacitor value dependence on deposition temperature was tested on Al_2O_3 dielectric film. The film thickness was kept constant and the deposition temperature was varied. Increasing deposition temperature increases growth rate and film thickness. Increasing film thickness decreases the capacitance value.

It was noted that the calculated film thickness was lower than the target film thickness. The reason was assumed to be compilation of factors: erosion, change in permittivity and different growth rate for films deposited at different temperatures. Erosion of the insulator occurs during photoresist development. Erosion is faster for films deposited at low temperature. Likewise because of erosion, the capacitance density did not appear to depend fully linearly on the theoretical film thickness. In addition, it is possible that the calculated film thickness has been affected by variation in capacitance value.

The reactor configuration was noted to cause variation in the capacitance value over the wafer in the temperature dependency tests. The precursor nozzles are situated in the used shower-head type reaction chamber in different places, which causes difference in gas flow inside the reaction

chamber and causes the film thickness to vary slightly in different parts of the wafer. The implication of this finding is not significant, but it is good to know.

The implication of these results is that when planning the process flow for the capacitors, it is important to take the erosion of the dielectric film during the process into consideration and the possibility of the reaction configuration affecting the capacitance value through variation of film thickness over the wafer.

Leakage current dependence on deposition temperature was tested. The best results for Al_2O_3 film leakage characteristics were achieved with higher deposition temperatures of 200 °C and 300 °C, which showed similar behaviour to each other and low leakage current, whereas film deposited at low temperature showed high leakage current.

The impact of the results on the leakage current dependence on deposition temperature is that the limiting factor is the low deposition temperature. At lower deposition temperature, the impurity level increases and the insulating properties are compromised by hydrogen and carbon impurities that increase electrical conductivity. Good leakage current performance can be achieved with films deposited in higher temperatures. This information makes possible using good quality ALD thin films in applications that can tolerate high deposition temperature.

Capacitors with Al_2O_3-TiO_2 laminate dielectric film were studied. The TiO_2 content of the film was varied. The results showed that the high TiO_2 content of the film resulted into high leakage current density. The best results were achieved with the lowest TiO_2 content. The result is in accordance with Al_2O_3 capacitors, where the leakage current is negligible. The lower titania portion in the film results in lower the leakage current.

The capacitor value dependence on surface area of the film was tested for Al_2O_3-TiO_2 laminates. The surface area was varied. The results showed that high surface area caused high leakage current. The best result for capacitance value was achieved with lowest surface area. The relation of surface area increase to current increase is almost linear, which probably is caused by surface area effect.

In this work, the Al_2O_3-TiO_2 laminates had a higher dielectric constant than pure Al_2O_3, and higher dc leakage. The key finding was that capacitors prepared with TiO_2 in the dielectric thin film layer exhibited ability to short energetic peaks without irreversible failure. Also, low leakage current in ALD Al_2O_3 dielectric capacitors was achieved with use of relatively low deposition temperature.

The outcome of results was as expected in relation to the theory. Both materials, Al_2O_3 and Al_2O_3-TiO_2 laminate thin films are appropriate for use in capacitor applications. Both films have their advantages and disadvantages. The advantage of Al_2O_3 dielectric film is that the leakage current of the capacitors is low. The disadvantage is that the dielectric constant is lower than Al_2O_3-TiO_2 laminate dielectric film and the capacitors are subject to non-reversible breakdown. The advantage of Al_2O_3-TiO_2 laminate dielectric film is that the leakage current of the capacitors is higher than in Al_2O_3 dielectric film. The advantages are that the dielectric constant is higher than in Al_2O_3 dielectric film and the capacitors are can tolerate high electric stressing prior to non-reversible breakdown. It depends on the end user of the capacitor application, which property is valuated more in a capacitor, lower leakage current or reliability against electrical breakdown. The benefit of ALD process in manufacturing capacitors is the excellent quality of ALD deposited films compared to other deposition methods e.g. sputtering. The ALD film is denser, there are lesser pin holes, making the films more resistant to etching, and the method is non line-of-sight process. The

limitation of the study was that only two materials were tested of the vast amount of possible ALD deposited materials.

ALD is a beneficial technology to use in IC applications due to short pulse times, meaning faster output both for the whole process and for the product. The small amount of pin-holes or the lack of them will enhance the properties of the end product making the film more resistant to etching.

Future studies**.** There is currently a great demand for research on high-k dielectric materials. It is possible to tailor the already known materials with post treatments to get higher k-values. For example post annealing, oxidation or nitridation can increase the dielectric value. However, more research is called for discovering other innovative methods to enhance the dielectric value. Discovering new materials and their composites should not be excluded from the research programme. Research is needed for achieving further knowledge on the complexity of conformal coating in high-aspect-ratio pores.

8. Bibliography

1. **L. I. Maissel, M. H. Francombe.** An Introduction to thin films. New York, Gordon and Breach Science Publishers (1973) pp. 1-2
2. Edited by: **Seshan, K.** Handbook of Thin-Film Deposition Processes and Techniques - Principles, Methods, Equipment and Applications (2nd Edition). s.l. : William Andrew Publishing/Noyes, 2002. pp. 12-29, 319-320, 338
3. **Ohring, Milton.** Materials Science of Thin Films, Deposition and Structure. s.l. : Academic Press, 2002. p. xiii.
4. **L. Paussa, L. Guzman, E. Marin, N. Isomaki, L. Fedrizzi.** Protection of silver surfaces against tarnishing by means of alumina/titania-nanolayers. Surface & Coatings Technology 206 (2011) 976-980.
5. **G. Gerlach, W. Dötzel.** Introduction to Microsystem Technology, A Guide for Students. s.l. : Series Edited by R. Pethig. The Wiley Microsystem and Nanotechnology Series, 2008. pp. 83-84.
6. **A. Elshabini-Riad, F. D. Barlow.** Thin Film Technology Handbook. McGraw-Hill 1998. ISBN 0-07-01925-9. Chapter 1,2.
7. **R.L. Puurunen, H. Kattelus, T. Suntola**. Handbook of Silicon Based MEMS Materials and Technologies, chapter 26 Atomic Layer Deposition in MEMS Technology. 2010. pp. 433-445.
8. **Ritala M, Leskelä M.** Handbook of thin film materials, Volume 1: Deposition and processing of Thin Films. s.l. : Edited by H.S. Nalwa. Academy Press, San Diego, Vol 1, 2002. pp. 103-159.
9. **Puurunen, R. L.** Surface chemistry of atomic layer deposition: A case study for the trimethylaluminum/water process. Journal of Applied Physics, 2005, Vol 97, No 12. pp 121301 1-52.
10. **S. Franssila.** Introduction to Micro Fabrication – 2nd edition. John Wiley & Sons Ltd. Copyright 2011. pp. 4, 49-50, 58-59, 77-90.
11. **S.M. George**. Atomic Layer Deposition: An Overview. Chem. Rev. 2010, 110, 111-131. DOI: 10.1021/cr900056b
12. **S. Nonobe, N. Takahashi. T. Nakamura**. Preparation of HfO_2 nano-film by atomic layer deposition using $HfCl_4$ and O_2 under atmospheric pressure. Solid State Sciences 6 (2004) 1217-1219
13. **M. Knez, A. Kadri, C. Wege, U. Gosele, H. Jeske, K. Nielsch**. Atomic Layer Deposition on Biological Macromolecules: Metal Oxide Coating of Tobacco Mosaic Virus and Ferritin. Nano Lett. 2006, 6, 1172

14. **L.B. Freund, S. Suresh.** Thin film materials, Stress, Defect formation and Surface evolution. s.l. : Cambridge University Press, 2003. pp. 6-7.

15. **Pierson, H.O.** Handbook of Chemical Vapor Deposition (CVD) - Principles, Technology and Applications (2nd Edition). s.l. : William Andrew Publishing/Noyes , 1999. pp. 36-37.

16. **Mattox, D.M.** Handbook of Physical Vapor Deposition (PVD) Processing. s.l. : William Andrew Publishing/Noyes, 1998. p.31.

17. http://www.circuitstoday.com/chemical-vapour-deposition-cvd (8.11.2012)

18. **S.M. Sze.** Semiconductor devices. Physics and technology. 2nd edition. pp.32-33, 381-382. John Wiley & Sons Inc. ISBN 0-471-33372-7.

19. **V. Miikkulainen, M. Leskelä, M. Ritala, R.L. Puurunen.** Crystallinity of Inorganic Films Grown by Atomic Layer Deposition: Overview and General Trends. Applied Physics Review, In press (2012) pp. 1-6, 26-27, 30-32, 47-54.

20. **R.L. Puurunen, H. Kattelus, T. Suntola**. Handbook of Silicon Based MEMS Materials and Technologies, chapter 26 Atomic Layer Deposition in MEMS Technology. 2010. pp. 433-445.

21. Edited by **S. Kasap, P. Capper.** Springer Handbook of Electronic and Photonic Materials. pp. 22-23, 30, 573, 682-683, 696. 2006. ISBN-10: 0-387-26059-5.

22. http://bahancourtney.edu.glogster.com/solids/ (25.10.2012)

23. **O. M.E. Ylivaara, X. Liu, L. Kilpi, J. Lyytinen, D. Schneider, M. Laitinen, J. Julin, S. Ali, S. Sintonen, M. Berdova, E. Haimi, T. Sajavaara, H. Ronkainen, H. Lipsanen, J. Koskinen, S-P. Hannula, R. L. Puurunen.** Aluminum oxide from trimethylaluminum and water by atomic layer deposition: The temperature dependence of residual stress, elastic modulus, hardness and adhesion. Thin Solid Films Vol. 552 (2014) pp. 124-135.

24. **S. Jakschik, U. Schröder, T. Hecht, M. Gutsche, H. Seidl, J. W. Bartha.** Crystallization behavior of thin ALD-Al2O3 films, *Thin Solid Films 425 (2003) 216–220*

25. **D.R.G. Mitchell, G. Triani, Z.M. Zhang,** Hydrothermal crystallization of amorphous titania films deposited using low temperature atomic layer deposition. Thin Solid Films, (2008). 516(23), 8414-8423.

26. **H. Tang, K. Prasad, R. Sanjines, P.E. Schmid, F. Levy.** Electrical and optical properties of anatase thin films, Journal of Applied physics, Vol 75, Issue 4, pp. 2042-2047.

27. **S-W. Jeong, H.J. Lee, K.S. Kim, M.T. You, Y.Roh, T. Noguchi, W. Xianyu, J. Jung.** Effects of Annealing Temperature on the Characteristics of ALD-deposited HfO_2 in MIM capacitors. Thin solid films 515 (2006) 526-530.

28. **W.D. Nix**. Mechanical Properties of Thin Films. Metallurgical Transactions A. Volume 20A, November 1989 pp. 2217, 2219, 2236, 2242, 2243.

29. **P. S. Alexopoulous, T.C. O´Sullican.** Mechanical Properties of Thin Films, Vol 20: 391-420. 1990. Doi: 10.1146/annurev.ms.20.080190.002135

30. **G. Krautheim, T. Hecht, S. Jakschik, U. Schröder, W. Zahn.** Mechanical Stress in ALD-Al_2O_3 films. Applied Surface Science 252 (2005) 200-204. DOI: 10.1016/j.apsusc.2005.01.118.

31. **Y. Yin, D. McKenzie, M. Bilek.** Intrinsic Stress Induced by Substrate Bias in Amorphous Hydrogenated Silicon Thin Films. Surface and Coating Technology 198 (2005) 156-160.

32. **Z. Lin, S. Guangjie, S. Shitao, Q. Xiujuan, H. Sihuizi.** Development on transparent conductive ZnO thin films doped with various impurity elements. Rare Metals, Vol. 30, No. 2, Apr 2011, p. 175.

33. **J.L. Lyons, A. Janotti, C. G. Van de Walle.** Effects of carbon on the electrical and optical properties of InN, GaN, and AlN. Phys. Rev. B 89, (2014) 035204

34. **Y. Hayashi, T. Ishikawa, D. Shimokawa.** Modification of electrical and optical properties of metal nitride thin films by hydrogen inclusion**.** Volumes 330–332, 17 (2002), pp. 348–351

35. **M.D. Groner, J.W. Elam, F.H. Fabrequette, S.M. George.** Electrical characterization of thin Al2O3 films grown by atomic layer deposition on silicon and various metal substrates. Thin Solid Films 413 (2002) pp. 186–197

36. **S.K. So, W.K. Choi, C.H. Cheng, L.M. Leung, C.F.Kwong.** Surface preparation and characterization of indiumtin oxide substrates for organic electroluminescent devices. s.l. : Appl. Phys. A, 1999, Vol. 68. pp.447–450.

37. **J. A. Venables, G. D. T. Spiller, M. Hanbücken.** Nucleation and growth of thin films. s.l. : Rep. Prog. Phys., 1984, Vol. 47. pp. 401-402.

38. **Z. Zhang, M. G. Lagally.** Atomistic Processes in the Early Stages of Thin-Film Growth. s.l. : SCIENCE, 1997, Vol. 276. p. 377.

39. **Y.-Y. Lin, D. J. Gundlach, S. F. Nelson, T. N. Jackson.** Stacked Pentacene Layer Organic Thin-Film Transistors with Improved Characteristics. No. 12, s.l. : IEEE ELECTRON DEVICE LETTERS, 1997, Vol. 18. p. 606.

40. **S.M. Gates, S. K. Kulkarni.** Kinetics of surface reactions in very low-pressure chemical vapor deposition of Si from SiH4. s.l. : Appl. Phys. Lett., 1991, Vol. 58. pp. 2963-2965.

41. **K.E. Johnson, D.D. Chambliss, S. Chiang.** Growth and morphology of partial and multilayer Fe thin films on Cu(100) and the effect of adsorbed gases studied by scanning tunneling microscopy. 4, u.o. : J. Vac. Sci. Technol. A, 1993, Vol. 11. pp. 1658-1659.

42. **A.W. Ott, J.W. Klaus, J.M. Johnson, S.M. George.** A1203 thin film growth on Si (100) using binary reaction sequence chemistry. s.l. : Thin Solid Films, 1996, Vol. 292. pp. 135-144.

43. **E. Färm, M. Kemell, M. Ritala, M. Leskelä.** Selective-area atomic layer deposition using poly(methyl methacrylate) films as mask layers. Poster presentation. 8th International Conference on Atomic Layer Deposition. June 29-July 2, 2008-Bruges Belgium.

44. **C. H. L. Goodman, M. V. Pessa.** Atomic Layer Epitaxy. s.l. : J. Appl. Phys., 1986, Vol. 60. R65-R68.

45. **T.M. Mayer, J.W. Elam, S.M. George, P.G. Kotula, R.S. Goeke.** Atomic-layer deposition of wear-resistant coatings for microelectromechanical devices. Applied physics letters 2003, volume 82, number 17, p. 2884.

46. **S.O. Kucheyev, J. Biener, T.F. Baumann, Y.M. Wang, A.V. Hamza**. Mechanisms of Atomic Layer Deposition on Substrates with Ultrahigh Aspect Ratios. Langmuir 2008, 24, pp. 943-948.

47. **M. Ritala, M. Kemell, M. Lautala, A. Niskanen, M. Leskelä, S. Lindfors**. Rapid Coating of Through-Porous Substrates by Atomic Layer Deposition. Chem vap. Deposition 2006, 12, 655-658. DOI: 10.1002/cvde.200604228.

48. **T. Blanquart, V. Longo, J. Niinisto, M. Heikkilä, K. Kukli, M. Ritala, M. Leskelä.** High-performance imido–amido precursor for the atomic layer deposition of Ta_2O_5. Semicond. Sci. Technol. 27 (2012) 074003 (6pp).

49. **M. Leskelä, M. Kemell, K. Kukli, V. Pore, E. Santala, M. Ritala, J. Lu.** Exploitation of Atomic Layer Deposition for Nanostructured Materias. Materials Science and Engineering C 27 (2007) pp.1504-1508.

50. **K.H. Cho, C.H. Choi, K.P. Hong, J-Y. Choi, Y.H. Jeong, S. Nahm, C-Y. Kang, S-J. Yoon, H-J. Lee.** Electrical Properties of Amorphous $Bi_5Nb_3O_{15}$ Thin film for RF MIM Capacitors. IEEE Electron Device Letters, Vol 29, No. 7, July 2008.

51. **D.H. Everett.** Pure Appl. Chem. 31, 579 (1972). Web version http://www.iupac.org/reports/2001/colloid_2001/-manual_of_s_and_t.pdf

52. **E.-L. Lakomaa, A. Root, T. Suntola.** Appl. Surf. Sci. 107, 107 (1996).

53. **R.L. Puurunen, A. Root, S. Haukka, E.I. Iiskola, M. Lindblad, A.O.I, Krause**. J. Phys. Chem. B 104, 6599 (2000).

54. **E.-L. Lakomaa, S. Haukka, T. Suntola**. Appl. Surf. Sci. 60/61, 742 (1992).

55. **S.A. Morozov, A.A. Malkov, A.A. Malgyin**, Zh. Prikl Khim. (S.-Peterburg) 76, 9 (2003) [Russ. J. Appl chem. 76, 7 (2003)].

56. **M. Ritala, M. Leskelä, E. Rauhala,** Chem. Mater. 6, 556 (1994).

57. **M. Ylilammi.** Monolayer thickness in atomic layer deposition, Thin Solid Films 279 (1996) 124-130.

58. **R.L. Puurunen.** Growth per cycle in atomic layer deposition: A theorethical model. Chemical Vapor Deposition (2003) 9, No. 6.

59. **R.L. Puurunen, W. Vandervorst, W.F.A. Besling, O. Richard, H. Bender, T. Conrad, C. Zhao, A. Delabie, M. Caymax, S. De Gendt**. J. Appl.Phys. 96, 4878 (2004).

60. **R.L. Puurunen, W. Vandervorst.** J. Appl. Phys 96, 7686 (2004).

61. **R.L. Puurunen.** Chem. Vap. Deposition 10, 159 (2004).

62. **Fischer, R.A.** Precursor chemistry of advanced materials, CVD, ALD and Nanoparticles . s.l. : Birkhäuser, 2005. p. 125.

63. **M. Leskelä, M. Ritala.** Review. Atomic layer deposition (ALD): from precursors to thin film structures. Thin Solid Films 409, s.l. : Elsevier, 2002. 138–146.

64. **A. Niskanen, T. Hatanpää, M. Ritala, M. Leskelä.** Thermogravimetric study of volatile precursors for chemical thin film deposition: estimation of vapor pressure and source temperatures. 2001, Journal of Thermal Analysis and Calorimetry Vol. 64, pp. 955-964.

65. **R. G. Gordon, J-S. Lehn, H. Li, Q.M. Qang, D. V. Shenai.** Design precursors for ALD, Oral presentation. 8th International Conference on Atomic Layer Deposition. June 29-July 2, 2008- Bruges Belgium.

66. **T. Blanquart, V. Longo, J. Niinisto, M. Heikkilä, K. Kukli, M. Ritala, M. Leskelä.** High-performance imido–amido precursor for the atomic layer deposition of Ta_2O_5. Semicond. Sci. Technol. 27 (2012) 074003 (6pp)

67. **M. Putkonen, T. Sajavaara, L. Niinistö, J. Keinonen.** Analysis of ALD-processed thin films by ion-beam techniques. pp. 1791–1799, s.l. : Anal Bioanal Chem, 2005, Vol. 382.

68. **M.K. Tripp, C. Stampfer, D.C. Miller, T. Helbling, C.F. Herrmann, C. Hierold, K. Gall, S.M. George, V.M Bright.** The mechanical properties of atomic layer deposited alumina for use in micro- and nano-electromechanical systems. s.l. : Sensors and Actuators A, 2006, Vols. 130–131. pp. 419–429.

69. **L.G. Gosset et al.** Interface and material characterization of thin Al2O3 layers deposited by ALD using TMA/H2O. Section 2. ALCVD of high-k dielectrics – deposition and characterization. s.l. : Journal of Non-Crystalline Solids, 2002, Vol. 303. pp. 17–23.

70. **S.M. Geroge, A. W. Ott, J. W Klaus.** Surface Chemistry for Atomic Layer Growth. s.l. : J. Phys. Chem., 1996, Vol. 100. pp. 13121-13131.

71. **A.W. Ott, K.C. McCarley, J.W. Klaus, J.D. Way, S.M. George.** Atomic layer controlled deposition of A1203 films using binary reaction sequence chemistry. s.l. : Applied Surface Science, 1996, Vol. 107. pp. 128-136.

72. **J. Kim, K. Chakrabarti, J. Lee, K-Y. Oh, C. Lee.** Effects of ozone as an oxygen source on the properties of the Al_2O_3 thin films prepared by atomic layer deposition. Materials Chemistry and Physics 78 (2003) 733-738.

73. **M. Leskelä, M. Ritala.** Atomic Layer Deposition Chemistry: Recent Developments and Future Challenges. Issue 45, s.l. : Angewandte Chemie International Edition, 2003, Vol. 42. pp. 5548 - 5554.

74. **J. Aarik, A. Aidla, H. Mändar, T. Uustare.** Atomic layer deposition of titanium dioxide from TiCl4 and H2O: investigation of growth mechanism. s.l. : Applied Surface Science, 2001, Vol. 172. pp. 148-158.

75. **D.M. King, X. Liang, P. Li, A. W. Weimer.** Low-temperature atomic layer deposition of ZnO films on particles in a fluidized bed reactor. s.l. : Thin Solid Films, 2008, Vol. 516. pp. 8517–8523.

76. **J. D. Ferguson, A. W. Weimer, S. M. George.** Surface chemistry and infrared absorbance changes during ZnO atomic layer deposition on ZrO2 and BaTiO3 particles. Issue 1, s.l. : J. Vac. Sci. Technol. A, 2005, Vol. 23. pp. 118-125.

77. http://www.solaytec.com/ (8.11.2012)

78. **H.D. Young, R. A. Freedman**. University Physics, 9th edition. Addison-Wesley Publishing 1996. pp.772-773, 787.

79. **J.F. Scott** High-Dielectric Constant Thin Films For Dynamic Random Access Memories (DRAM), Annu. Rev. Mater. Sci. 1998. 28:79–100, p.1

80. **S. Prasanna, R.G. Mohan, S. Jayakumar, M.D. Kannan, V. Ganesan.** Dielectric propertids of DC reactive magnetron sputtered Al_2O_3 thin films. Thin solid films 520 (2012) 2689-2694.

81. **K.S. Shamala, L.C.S. Murthy, K. Narasimha Rao.** Studies on optical and dielectric properties of Al2O3 thin films prepared by elecetron beam evaporation and spray pyrolysis method. Materials Science and Engineering B 106 (2004) 269-274.

82. **B. Lee, A. Hande, T.J. Park, K.J. Chung, J. Ahn, M. Rousseau, D. Hong, H. Li, X. Liu, D. Shenai, J. Kim.** ALD of $LaHfO_x$ nano-laminates for high-*K* dielectric applications. Microelectronic Engineering 88 (2011) 3385-3388.

83. **B. Hudec, K. Husekova, A. Tarre, J.H. Han, S, Han, A. Rosova, W. Lee, A, Kasikov, S.J. Song, J. Aarik, C. S. Hwang, K. Frölich**. Electrical properties of TiO_2 based MIM capacitors deposited by $TiCl_4$ and TTIP based atomic layerd deposition processes. Microelectronic Engineering 88 (2011) 1514-1516.

84. **E. Cianci, S. Lattanxio, G. Sequini, S. Vassanelli. M. Fanciulli.** Atomid Layer Deposition TiO_2 for implantable brain-chip interfacing devices. Thin solid films 520 (2012) 4745-4748. DOI: 10.1016/j.tsf.2011.10.197.

85. **K. Sudheendran, D. Pamu, M. Ghanshyam Krishna. K.C. James Raju**. Determination of dielectric constant and loss of high-*K* thin films in the microwave frequencies. Measurement 43 (2010) 556-562.

86. **Q. Fang, C. Hodson, M. Liu, Z.W. Fang, R. Potter, R. Gunn.** Preliminary investigation of high-*k* materials - TiO_2 doped Ta_2O_5 films by remote plasma ALD. Physics proceedings 32 (2012) 379-388. 18th International Vacuum Conference.

87. **Y-G. Liang**. Integration of high-*k* perovskite capacitor on transparent conductive Zr-doped InwO3 epitaxial thin films. Thin Solid Films 518 (2919) S22-S25.

88. **K.H. Cho, C.H. Choi, K.P. Hong, J-Y. Choi, Y.H. Jeong, S. Nahm, C-Y. Kang, S-J. Yoon, H-J. Lee.** Electrical Properties of Amorphous $Bi_5Nb_3O_{15}$ Thin film for RF MIM Capacitors. IEEE Electron Device Letters, Vol 29, No. 7, July 2008.

89. **J.H. Klootwijk, K.B. Jinesh, W. Dekkers, J.F. Verhoeven, F.C. van den Heuvel, H-D. Kim, D. Blin, M.A. Verheijen, R.G.R Weemaes, M. Kaiser, J.J.M Ruigrok, F. Roozeboom.** Ultrahigh Capacitance Density for Multiple ALD-Grown MIM Capacitor Stacks in 3-D Silicon, IEEE Electron Device Letters, Vol. 29, No. 7, July 2008, pp. 740-742.

90. **M. Ritala, M. Kemell, M. Lautala, A. Niskanen, M. Leskelä, S. Lindfors**, Rapid coating of through-porous substrates by atomic layer deposition. Chem Vap. Deposition Vol. 12, pp. 655-658, 2006.

91. **G. Pardon, H. K. Gatty, G. Stemme, W. van der Wijngaart, N. Roxhed.** Pt-Al_2O_3 dual layer atomic layer deposition coating in high aspect ratio nanopores. Nanotechnology 24 (2013) 015602 (11pp).

92. **S. O. Kucheyev, J. Biener, Y. M. Wang, T. F. Baumann, K. J. Wu, T. van Buuren, A. V. Hamza, and J. H. Satcher, Jr,** Atomic layer deposition of ZnO on ultralow-density nanoporous silica aerogel monoliths. Applied physics letters 86, 083108 (2005).

93. **J.W. Elam, D. Routkevitch, P.P. Mardilovich, S.M. George.** Conformal coating on Ultrahigh-Aspect-Ratio nanopores and anodic alumina by atomic layer deposition. Chem. Mater. (2003) 15, 3507-3517.

94. **K.Kukli, M. Ritala, M. Leskelä, J. Sundqvist, L. Oberbeck, J. Heitmann, U, Schröder, J. Aarik, A. Aidla**. Influence of TiO_2 incorporation in HfO_2 and Al_2O_3 based capacitor dielectrics. Thin Solid Films 515 (2007) pp. 6447–6451.

Appendix I

The abstract of Appendix I is presented below and the poster related to the abstract of appendix I is presented in Figure 40. The abstract and poster was presented at Transducers 2007 Conference in France,

ATOMIC LAYER DEPOSITION OF Al_2O_3, TiO_2 and ZnO FILMS INTO HIGH ASPECT RATIO PORES

S. Sirviö*, L. Sainiemi, S. Franssila, K. Grigoras
Micro and Nanosciences Laboratory, PO Box 3500, Helsinki University of Technology, Helsinki, Finland
(Tel. +358-9-451-4689; Email. *sari.sirvio@tkk.fi)

Abstract: Atomic Layer Deposition (ALD) of aluminium, zinc and titanium oxides into high aspect ratio electrochemically etched pores is described. Macroporous silicon was fabricated by electrochemical etching. Aspect ratios of 50:1 were routinely obtained. Commercial Anodisc alumina pores were used for reference. ALD thin films Al_2O_3, TiO_2 and ZnO were deposited in the pores. The results were studied with scanning electron microscope (SEM). The layer thicknesses were close to the theoretical value calculated from the cycle number, indicating excellent conformality in high aspect ratio structures.

Keywords: porous silicon, anodic alumina, nanopores, micropores, aluminium oxide, zinc oxide, titanium dioxide, ALD

1. INTRODUCTION

Micro- and nanopores are of interest in fluidic sieves and filters and in biological and chemical applications where high surface areas are required. Atomic layer deposition (ALD) is a superb technique for conformal coating of such pores. ALD utilizes a binary sequence self-limiting chemical reactions between gas-phase precursor molecules and a solid surface. Thin film material can be deposited by repeating the binary reaction sequence in an ABAB… fashion where each AB cycle deposits approximately one monolayer material [1]. ALD can be used to deposit films in to ultrahigh-aspect-ratio pores using sufficient reactant cycle times [2]. Alumina (Al_2O_3) is an interesting material in bioanalytical applications; it can, for example, be used to bind proteins during washing steps, enabling salt concentration reduction and improved mass spectrometry analysis [3]. Titania (TiO_2) is known for its (photo)catalytic properties which have potential in microchemical reactors and analyzers [4,5]. Zinc oxide is a transparent conductive oxide which is interesting as an electrode in optical and electrochemical devices. These high aspect ratio pore structures are suitable for facilitated diffusion [6] and as templates for growth of nanostructures.

2. EXPERIMENTAL

N-type 100-oriented silicon wafers 1-10 Ohmcm were used for fabrication of porous silicon. Electrochemical etching was performed in HF: H_2O: C_2H_5OH electrolyte. Silicon macropore formation was initiated by either TMAH or RIE initial pits. Electrochemical etching was carried out as described in [7]. Aspect ratios of 50:1 were routinely obtained (Fig. 1).

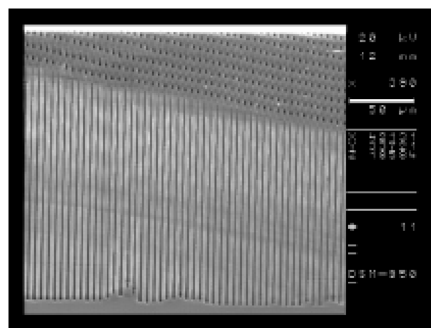

Figure 1. SEM picture of deep macropores.

Through-wafer silicon pores were fabricated by a combination of anisotropic wet etching, electrochemical etching and ICP (Inductively

coated structure was cut into two samples. In Fig. 3a both aluminium and zinc oxide layers are visible and the interface between them is sharp. In Fig. 3b Al-etch has removed the zinc oxide layer, therefore only the aluminium oxide layer is seen. The small differences observed in layer thicknesses along the length of the pore can be explained by the non-optimized precursor and purge pulse lengths in ALD. The SEM shows that film thickness even at the bottom of a 50:1 aspect ratio hole is very good.

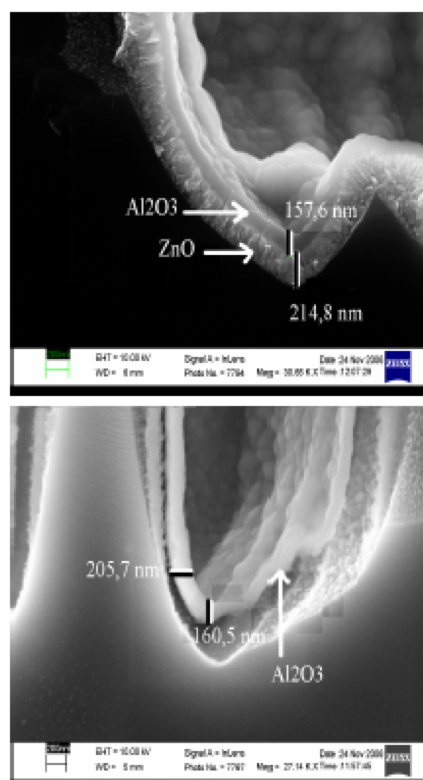

Figure 3. Coating at the bottom of the pore of (a) unetched sample (b) etched sample.

The deposition of TiO_2 film in open and closed pores proved problematic. Texture inheritance was studied by depositing TiO_2 film with and without 50 nm Al_2O_3 underlayer. The former were amorphous while the latter were crystalline. In closed pores the layer thicknesses were close to the theoretical value. In open pores the layer thicknesses were close to the theoretical value only at the top and bottom of the pores (Fig.4). In the middle of the pores, the conformality of the layer was non-ideal.

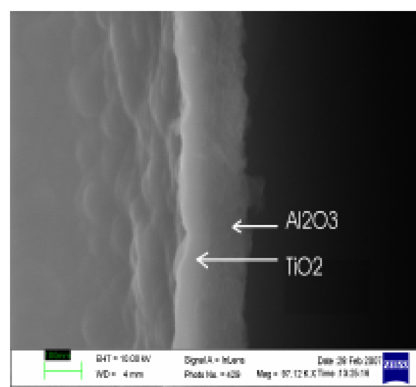

Figure 4. TiO_2 film on top of amorphous Al_2O_3 film is amorphous.

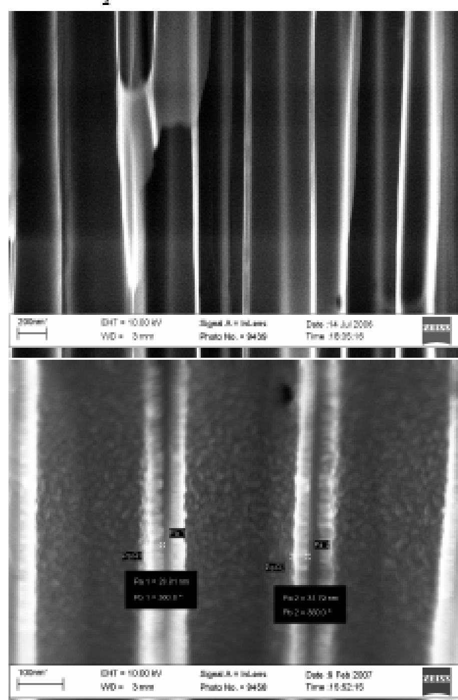

Figure 5. Cross section of anodic alumina membrane pores before (a) and after ALD (b). Pore diameter is ca. 200 nm and thickness of ZnO is ca. 30 nm.

Coupled Plasma) etching, as shown in Fig. 2. The through-wafer samples were lifted on two holders in the ALD chamber leaving 400 um space under the sample to facilitate the gas flow through the pores.

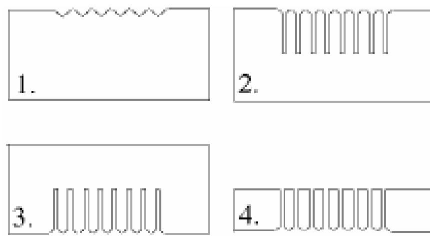

Figure 2. The fabrication of the through wafer pores. 1. Initial pits; 2. Electrochemical etching; 3. Flipping wafer upside down; 4. ICP backside thinning etch. Pore depths are 200 µm and aspect ratios up to 100:1.

Before ALD the samples were pretreated in ultrasound bath using a dilute NaOH-solution for 10 minutes to remove any nanoporous silicon dendrites. Commercially available Anopore discs were used for alumina pores. Films were grown by atomic layer deposition (ALD) technique in Thin Film Systems TFS-500 reactor (Beneq Oy, Finland). Aluminum oxide layer was grown using trimethyl aluminum (TMA) as the metal precursor, with water or ozone as the oxygen precursor. The process was carried out at 220°C. Cycle length was 7 seconds, including 3 s purge pulse after each precursor pulse. The growth rate was 0.9 Å/cycle and 0.84 Å/cycle for water and ozone as oxidant precursors, respectively. Zinc oxide was deposited using diethylzinc (DEZ) and H_2O as precursors, also at 220°C, at 1.8 Å/cycle. Other parameters were identical to Al_2O_3 deposition. Titanium dioxide layer was deposited using $TiCl_4$ and H_2O as precursors at 350°C temperature. Total cycle length was 7,85 seconds, including 3 s purge pulse after each precursor pulse. The growth rate was 0,45 Å/ cycle.

3. RESULTS AND DISCUSSION

Porous material ALD coating has been done previously for catalysts with molecular size pores (nanometers or tens of nanometers). In these applications ALD pulse times have been minutes [8]. In the present work pore diameters are in the range 100 nm to 5 um and aspect ratios 50:1 (for porous silicon) to 300:1 (for anodic alumina).

The stability of ALD films was tested in the most common microfabrication chemicals, to explore sample cleaning and post processing options. As seen in Table 1, the alumina films cannot be processed in BHF, and care must be taken in lithography as resist developer attacks the film. Zinc oxide is even more vulnerable to attack by fluoride and hydroxyl.

Table 1. The etch rates of Al_2O_3 and ZnO.

	Etch rate (nm/min)	
Etchant	**Al_2O_3**	**ZnO**
Phosphoric acid 85 % (T= 20 °C)	0,4	fast
Al-etch (50 °C)	11	fast
Al-etch (20 °C)	0,7	fast
BHF (20 °C)	53	260
BHF (32 °C)	1184	fast
HF 1 %	22	fast
TMAH 25% (20°C)	1,6	12
TMAH 25% (80°C)	185	498
KOH 20% (20°C)	4	85
KOH 20%(80°C)	331	914
Developer AZ451	13	0,2

Fast = completely etched in one second etching.
Comments:
- Al-etch (85 % o-H_3PO_4 + HNO_3)
- BHF (Sioetch NH_4F : HF 9 :1)

The conformality of the coatings was studied with scanning electron microscope (SEM). A multi-layer coating was done by deposition 200 nm zinc oxide film into the pores first and by subsequent deposition of 100 nm aluminium oxide film. The

4. CONCLUSIONS

In the case of closed pores, the deposition of Al_2O_3 and ZnO films was successful. The layer thicknesses were conformal in all parts of the high aspect ratio pores and the thicknesses were close to the theoretical value calculated from the cycle number. TiO_2 film deposition was successful in the closed pores, but the deposition was non-ideal in the open pores according to the initial tests. The layer thicknesses were close to predicted at the top and bottom of the pores, but the conformality of the film was non-ideal at the middle of the pores. This can be explained by unoptimised precursor gas flows in the process. Film microstructure changes probably also contributes to poorer thickness control.

Our results indicate that cycle times can be very close to planar deposition. More surprisingly, closed pores and through-wafer open pores are coated similarly. In through-wafer pores the conductance is in fact fairly mildly scaling as a function of pore size: according to [9] conductance is linearly proportional to pore diameter.

Our total cycles times of 5-10 seconds are similar to ones reported in [9] but in that work a specially designed through-flow ALD reactor was used. This is considerably less than the 5 minutes pulses used in [10] for coating nanoporous silica aerogel with ZnO.

5. REFERENCES

[1] M. Ritala and M. Leskelä, In Handbook of Thin Film Materials; Nalwa, H. S; Ed.; Academic Press: San Diego, CA, 2001.

[2] J. W. Elam, D. Routkevitch, P.P Mardilovich, S. M. George, "Conformal coating on Ultrahigh-Aspect-Ratio Nanopores of Anodic Alumina by Atomic Layer Deposition", Chem. Mater. pp. 3507-3517, 2003.

[3] Y. Wang, X. Xia, Y. Guo, "Porous anodic alumina membrane as a sample support for MALDI-TOF MS analysis of salt-containing proteins", J. Am. Soc. Mass. Spectrom., pp. 1488, 2005.

[4] G. Takei. T. Kitamori, H.-B. Kim, "Photocatalytic redox combined synthesis with TiO_2 film modified microchannel", Proc. MicroTAS, p. 93, 2004.

[5] B.J. Jones, L. Locascio, M.A. Hayes, "Radical activated cleavage of peptides and proteins: an alternative to proteolytic digestion", Proc. MicroTAS, p. 286, 2005.

[6] Sang Bok Lee, David T Mitchell, L. Trofin, T. Nevanen, H. Söderlund, C.R. Martin, "Antibody-based bio-nanotube membranes for enantiomeric drug separations", Science, p. 2198, 2002.

[7] K. Grigoras, A.J. Niskanen, S. Franssila, "Plasma etched initial pits for electrochemically etched macroporous silicon structures", J. Micromech. Microeng. Vol. 11, pp. 371-375, 2001.

[8] S. Mahurin, L. Bao, W. Yan, "Atomic layer deposition of TiO_2 on mesoporous silica", J. Non-crystalline solids, Vol. 352, pp. 3280-3284, 2006.

[9] M. Ritala, M. Kemell, M. Lautala, A. Niskanen, M. Leskelä, S. Lindfors, "Rapid coating of through-porous substrates by atomic layer deposition". Chem. Vap. Deposition Vol. 12, pp. 655-658, 2006.

[10] S.O. Kucheyev, J. Biener, Y.M. Wang, T.F.Baumann, K.J. Wu, T. van Buren, A.V. Hamza, J.H. Satcher Jr., "Atomic layer deposition of ZnO on ultralow-density nanoporous silica aerogel monolitos", Appl.Phys.Lett. Vol. 86, pp. 083108-1-3, 2005.

ATOMIC LAYER DEPOSITION OF Al_2O_3, TiO_2 AND ZnO FILMS INTO HIGH ASPECT RATIO PORES

S. Sirviö, L. Sainiemi, S. Franssila, K. Grigoras

Micro and Nanosciences Laboratory, Helsinki University of Technology, P.O. Box 3500, Finland

Overview

- Fabrication of high aspect ratio pores in silicon and alumina
- Closed pores and open pores
- Coating of the pores
- Conformality studies of the thin films
- High surface area applications
- Filters and fluidic sieves

Atomic layer deposition (ALD)

-ALD is a superb technique for conformal coating of high aspect ratio pores.

-Micro- and nanopores are of interest in fluidic sieves and filters and in biological and chemical applications where high surface areas are required.

-Alumina (Al_2O_3) is an interesting material in bioanalytical applications.

-Titania (TiO_2) is known for its (photo)catalytic properties which have potential in microchemical reactors and analyzers.

-Zinc oxide (ZnO) is a transparent conductive oxide which is interesting as an electrode in optical and electrochemical devices.

Figure 1a and b. The ALD reactor (Beneq Oy, Finland)

Porous Silicon was fabricated by electrochemical etching of silicon wafer. Aspect ratios of 50:1 were routinely obtained.

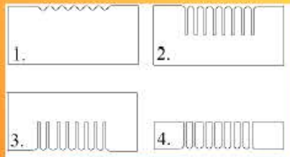

Figure 2. The fabrication of the through wafer pores in silicon.
3. The initial pits are etched.
4. Electrochemical etching follows in HF :H_2O: C_2H_5OH electrolyte.
3. The wafer is flipped upside down.
4. ICP backside thinning etch.

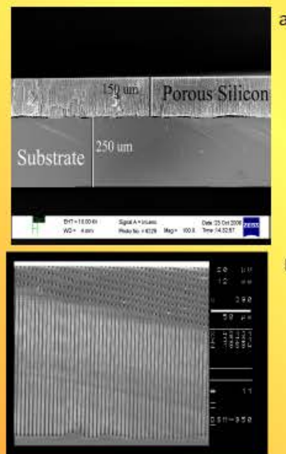

Figure 3. Cross section of 150 μ m thick (a) and 200 μ m thick (b) porous layer.

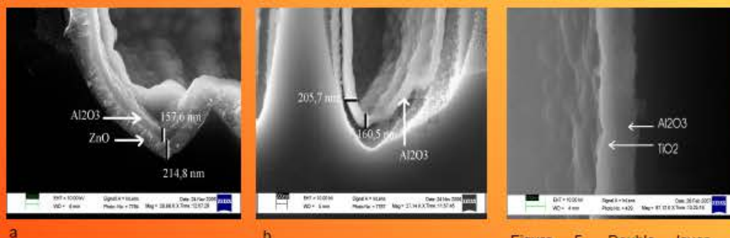

Figure 4. Multicoating at the bottom of the pore. Both Al_2O_3 and ZnO layers are visible and the interface between them is sharp (a). H_3PO_4 etching was done to emphasize the Al_2O_3 layer (b).

Figure 5. Double layer TiO_2/Al_2O_3 coating on pore wall.

Anodic alumina was used as a reference material. Commercial Anodisc alumina pores (aspect ratio 300:1) and in-house made alumina on silicon pores (8:1) were coated and studied in SEM.

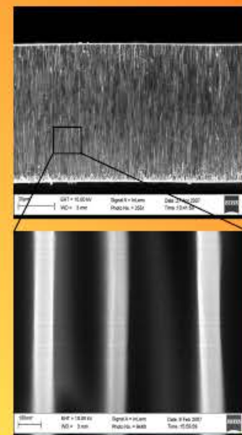

Figure 6. Cross section of anodic alumina membrane pores before ALD. Pore diameter is ca. 200 nm.

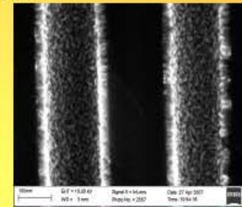

Figure 7. Cross section of anodic alumina membrane pores after ALD. Thickness of ZnO is ca. 30 nm.

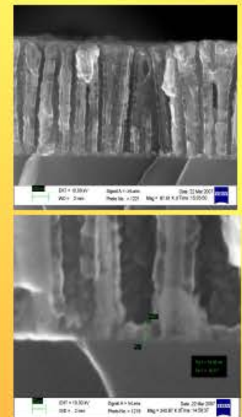

Figure 8. In-house made 500 µm thick anodic alumina with 60 nm pores coated with ZnO (a). Thickness of ZnO is ca. 20 nm (b).

Figure 40. Poster of Appendix I

Appendix II

The abstract of appendix II is presented below and the poster related to the abstract of appendix II is presented in Figure 41. The abstract and poster were presented at Nanotech Northern Europe Conference 2007 in Finland.

ALD layers for passivation and functionalization

of micro- and nano pores and membranes

Sari Sirviö [1], Lauri Sainiemi [1], K. Grigoras [1*], S. Franssila [1], V-M. Airaksinen [2]

[1] Micro and nanosciences laboratory, MICRONOVA, Department of Electrical and Communications Engineering, Helsinki University of Technology, P.O.Box 3500, FI-02015 TKK, Finland

[2] Micro and nanofabrication centre MINFAB, MICRONOVA, Department of Electrical and Communications Engineering, Helsinki University of Technology, P.O.Box 3500, FI-02015 TKK, Finland

Abstract

Atomic layer deposition (ALD) provides excellent uniformity, conformality and thickness control of the layer in the nanometer range. Additional advantage of this technique is a relatively low deposition temperature, what is quite important for polymer substrates and biochemical application. The range of the possible materials is widening.

The results of conformal coating of high aspect ration structures, including porous silicon and porous alumina membranes by ALD technique will be presented. Layers of aluminum oxide, zinc oxide and titanium oxide, several tens to several hundreds of nanometer thick, will be investigated. Optimization of ALD process parameters will be done for different type and size of the pores and channels. Several applications of such a functionalized structures will be shown.

ALD layers for passivation and functionalization of nanostructures

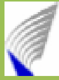

Sari Sirvio[1], Lauri Sainiemi[1], Sami Franssila[1], Veli-Matti Airaksinen[2], Kestas Grigoras[1]

[1]*Micro and Nanosciences laboratory, MICRONOVA, Dept. Of Electrical and Communications Engineering, Helsinki University of Technology, PO Box 3500, FI-02015 TKK, Finland*

[2]*Micro and Nanofabrication centre MINFAB, MICRONOVA, Dept. Of Electrical and Communications Engineering, Helsinki University of Technology, PO Box 3500, FI-02015 TKK, Finland*

ALD process

Atomic layer deposition (ALD) provides excellent uniformity, conformality and thickness control of the layer in the nanometer range. ALD utilizes self-saturating chemical reactions. During the first gas pulse the surface is coated with a molecular layer (a). Excess gas is purged away (b), and the second chemical is introduced (c). When the surface reaction is completed, the reactor is purged again (d). This cycle is repeated many times.

In this work, the results of conformal coating of high aspect ratio structures, including porous silicon, porous alumina membranes and micro-beads by ALD technique are presented. Layers of aluminum oxide, zinc oxide and titanium oxide were grown. Aluminum oxide was grown at 220°C using Trimethyl aluminum (TMA) and water as a precursors. Growth rate 0.9Å/cycle. Zinc oxide was grown at 220°C using diethylzinc (DEZ) and water. Growth rate 1.8 Å/cycle. Titanium dioxide was grown at 350°C using TiCl4 and water. Growth rate 0.45 Å/cycle. Several applications of such a structures are suggested.

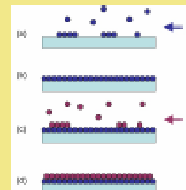

ALD cycle

ALD reactor TFS-500 (Beneq, Finland) in MICRONOVA

Coating of macroporous silicon

N-type 100-oriented silicon wafers have been electrochemically etched in HF:water:ethanol electrolyte. Almost 200 µm deep macropores, 1-2 µm in diameter, were obtained (aspect ratio ~100:1).

Double-layers of Al_2O_3 / ZnO or Ti_2O / Al_2O_3 were grown inside the pores. SEM reveals good conformality.

Applications: Alumina is interesting material in bioanalytical applications, and titania coating can suit for (photo)catalytic purposes.

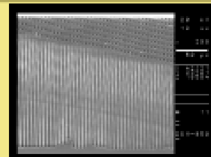

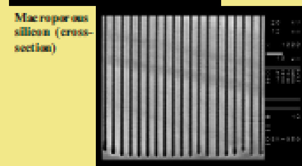

Macroporous silicon (cross-section)

Alumina/ZnO coating

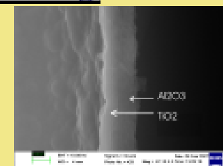

Titania/alumina coating

Coating of Anopore membranes

Commercially available 60 µm thick Anopore membranes (Whatman) with 200 nm pores have been used for conformality test (aspect ratio ~300:1). 30 nm thick ZnO layer was grown inside the pores using longer cycles (1s precursor pulse / 30s purge pulse). Growth temperature was reduced to 80°C because of the polypropylene ring supporting the membrane.

SEM studies reveal continuous coating, but layer thickness was not very uniform. Therefore, cycle parameters must be optimized in order to get better conformality.

Applications: Can be used to improve the catalytic activity of the large inner pore's surface.

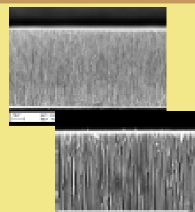

Cross-section of membrane

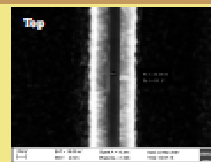

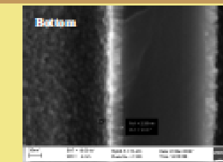

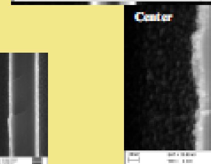

ZnO coating

Coating of polystyrene microspheres

Silicon wafer was covered with a monolayer of polystyrene micro-spheres (from water-based solution), 1 µm in diameter. Aluminum oxide layer was grown by ALD at quite low temperature (60°C)! Polystyrene was dissolved in acetone, to leave only alumina coating. SEM studies confirm successful layer growth at low temperature and conformal coating.

Experiments also with nano-spheres (100 nm in diameter) will follow.

Applications: High surface area sample treatment platform for bioanalysis.

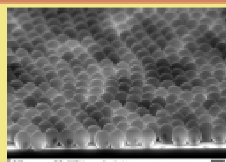

Polystyrene micro-spheres coated with alumina

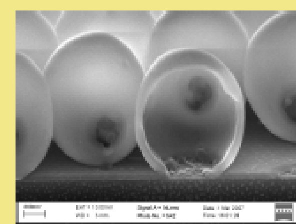

Hollow alumina microspheres (after dissolving of polystyrene)

Acknowledgment: Taja Nevanen from VTT is gratefully acknowledged for Anopore membrane samples and discussions

Figure 41. Poster of Appendix II

Appendix III

The abstract of appendix III is presented below and the poster related to the abstract of appendix III is presented as Figure 42. The abstract and poster were presented in ALD2008 Conferene in Belgium.

ELECTRICAL PROPERTIES OF CAPACITORS WITH ALD-GROWN Al_2O_3 AND Al_2O_3-TiO_2 NANOLAMINATE THIN FILM DIELECTRIC LAYERS

S.Sirviö, R.L.Puurunen, and H.Kattelus

VTT Technical Research Centre of Finland
Tietotie 3, Espoo, Finland
sari.sirvio@vtt.fi

The quality of the aluminium-titanium oxide nanolaminate dielectrics has been basis for successful manufacturing of electroluminescent displays during decades. Electrical properties of the insulator are, however, reported only to a limited extent [1, 2]. Measurement results for capacitance, dc leakage and breakdown strength in planar capacitors with ALD-grown Al_2O_3 and Al_2O_3-TiO_2 nanolaminate thin film dielectric layers are presented in this work. Their uniformity over the wafer is mapped. Also, possibilities for their use as energy storage in supercapacitors when fabricated over severe topography are discussed [3].

Capacitors with molybdenum as the bottom electrode, ALD thin film as the dielectric layer and bilayered Mo-Al as the top electrode were manufactured. Silicon dioxide was used for the interlevel dielectric and passivation. Two different kinds of dielectric films were used: films containing only Al_2O_3 and films containing Al_2O_3-TiO_2 nanolaminates with Al_2O_3 as the topmost layer. Five capacitors of different sizes were measured with surface areas from 0.25 mm^2 to 4 mm^2. The Al_2O_3 films were grown at 110 °C to 300 °C and the Al_2O_3 thickness varied from 20 nm to 60 nm. The Al_2O_3-TiO_2 nanolaminates were grown at 200 °C. In the nanolaminates, the thicknesses of the constituent Al_2O_3 layers ranged from 1 nm to 3 nm, while the TiO_2 layer was fixed at 3 nm. The volume fraction of TiO_2 in the films varied from 0.46 to 0.73. The number of Al_2O_3-TiO_2 nanolaminates layer was varied from 6 to 10, targeting to a constant overall film thickness of ~ 40nm.

The results of the electrical measurements were promising. The films were uniform and pinhole-free even when deposited at as low temperature as 110 °C, as observed in measurements of over 200 capacitors on a 150 mm wafer. The capacitance density and breakdown strength for 40 nm thick aluminium oxide insulator varied as a function of deposition temperature. With the deposition temperature increasing from 110 °C to 300 °C, the capacitance density decreased from 2.41 mF/m^2 to 2.02 mF/m^2 and the breakdown strength increased from 0.5 to 0.6 V/nm. The capacitance density did not depend fully linearly on the deposited film thickness, however, suggesting that the dielectric may have slightly eroded during the late device fabrication stages prior to top metallization. For the Al_2O_3-TiO_2 nanolaminates, the leakage current density increased significantly when the TiO_2 content was increased. However, the merit of the nanolaminates was that they tolerated heavy electrical stressing (power) prior to non-reversible failure.

The results show that fabricating capacitors using ALD thin films as the insulator is an excellent way to achieve high quality devices at low temperature. The low leakage current if aluminium

oxide promotes its use in high performance capacitors over large effective area while nanolaminates are able to short energetic peaks without failure.

[1]. Suntola, T. and Hyvärinen, J.,Ann. Rev. Mater.Sci. 15 (1985) 177-195
[2]. Chen, S.B. Lai, C.H. Chin, A. Hsieh, J.C. Liu, J. Highdensity MIM capacitors using Al_2O_3 and $AlTiO_x$ dielectrics, Electron Device Letters, IEEE, Apr 2002, Volyme: 23, Issue 4
[3]. F. Roozeboom, J. Klootwijk, J.F.C. Verhoevenm F.C. Can der Heuvel, W. Dekkers, S.B.S. Heil, J.L. Van Hemmen, M.C.M. van de Sanden, W.M.M. Kessels. ALD options for Si-integrated high-density capacitors in portable devices. ECS 210th meeting. Abstract 1105.

ELECTRICAL PROPERTIES OF CAPACITORS WITH ALD-GROWN Al_2O_3 AND Al_2O_3-TiO_2 NANOLAMINATE THIN FILM DIELECTRIC LAYERS

S. Sirviö, R.L. Puurunen, and H. Kattelus

INTRODUCTION

In this study we have focused on the electrical characterization of insulators deposited at low temperature. Capacitance, dc-leakage and breakdown strength were mesured for planar capacitors with ALD-grown Al_2O_3 and Al_2O_3-TiO_2 nanolaminate thin films dielectric layers. The deposition temperature was varied between 110 - 300°C.

CAPACITORS AND ALD THIN FILMS

The capacitors were of MIM type with molybdenum as the contacting electrode. Silicon dioxide was used for the interlevel dielectric and passivation.

The Al_2O_3 films were grown at 110°C to 300°C, and the Al_2O_3 thickness varied from 14 nm to 60 nm. The Al_2O_3-TiO_2 nanolaminates were grown at 200°C. In the nanolaminates, the thicknesses of the constituent Al_2O_3 layers ranged from 1 nm to 3 nm, while the TiO_2 layer thickness was fixed at 3 nm. The volume fraction of TiO_2 in the films varied from 0.46 to 0.73. The number of Al_2O_3-TiO_2 nanolaminate layers was varied from 6 to 10, targeting to a constant overall film thickness of ~ 40 nm.

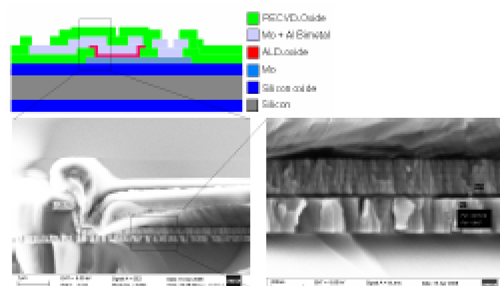

Figure 1. Schematic and SEM cross-section of the capacitor and close-up of the active area

RESULTS

CAPACITANCE

With the deposition temperature increasing from 110°C to 300°C, the capacitance density decreased from 2.42 nF/mm² to 2.00 nF/mm² when nominally 40 nm thick Al_2O_3 insulator was used. The reason for the decrease is assumed to be erosion of the insulator during photoresist development, being faster for films deposited at low temperature. For the same reason, the capacitance density did not appear to depend fully linearly on the deposited film thickness. Because accurate measurement of the insulator thickness in completed capacitors is tedious, we have estimated the thickness with the assumption that $\varepsilon_r \sim 8$ for Al_2O_3. The uncertainty of such estimation is assumed to be of the order of 10%.

Table 1. Al_2O_3 erodes in photoresist developer. Final insulator thickness is calculated from capacitance assuming permittivity of $\varepsilon_r = 8$.

Growth temperature	Theoretical thickness	Calculated thickness	Capacitance
110 °C	40 nm	29,3 nm	2,42 nF
200 °C	40 nm	32,9 nm	2,15 nF
300 °C	40 nm	35,4 nm	2 nF

Growth temperature	Theoretical thickness	Calculated thickness	Capacitance
200 °C	20 nm	14,4 nm	4,92 nF
200 °C	40 nm	32,9 nm	2,15 nF
200 °C	60 nm	51,0 nm	1,39 nF

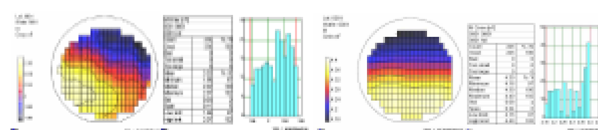

Figure 2. The uniformity of capacitance in capacitors with Al_2O_3 insulator(left) and with Al_2O_3-TiO_2 nanolaminate insulator (right).

DC LEAKAGE AND BREAKDOWN CHARACTERISTICS

Capacitors with ALD insulators deposited at low temperatures showed very good electrical characteristics. The leakage current densities were below 10 pA/mm² for aluminum oxide films deposited at 200°C at field strengths up to 3 MV/cm. Such aluminum oxide films, however, suffered from non-reversible dielectric breakdown in the field of 4.7 MV/cm.

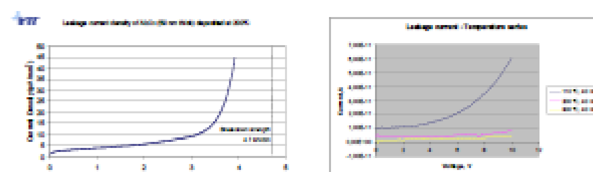

Figure 3. DC leakage of aluminum oxide films deposited at 200°C (left) and leakage characteristics for films deposited at different temperatures (right)

For the Al_2O_3-TiO_2 nanolaminates, the leakage current density increased significantly when the TiO_2 content was increased. However, the merit of the nanolaminates was that they tolerated heavy electrical stressing (power) prior to non-reversible breakdown.

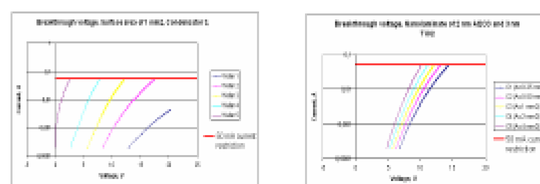

Figure 4. The leakage currents for Al_2O_3-TiO_2 nanolaminates of varying titanium content (left) and device area (right). The devices did not break down at current restriction conditions.

CONCLUSION

The results show that fabricating capacitors using ALD thin films as the insulator is an excellent way to achieve high quality devices at low temperature. The low leakage current of aluminium oxide promotes its use in high performance capacitors over large effective area while nanolaminates are able to short energetic peaks without failure.

VTT TECHNICAL RESEARCH CENTRE OF FINLAND
Visiting address: Tietotie 3 P.O. Box 1000
FIN-02044 VTT, Finland

Tel. +358 20 722 6638
Fax +358 20 722 7012
sari.sirvio@vtt.fi
www.vtt.fi

Figure 42. Poster of Appendix III